Dissertation zur Erlangung des Doktorgrades der Fakultät für Chemie und Pharmazie der Ludwig-Maximilians-Universität München

The use of novel polymeric vials for lyophilization of biopharmaceuticals and microwave-assisted freeze-drying

Nicole Härdter

aus

Stuttgart, Deutschland

2023

To my parents

Acknowledgements

First and foremost, I wish to express my sincere gratitude to my supervisor Professor Dr. Gerhard Winter. Thank you for giving me the opportunity to work on these exciting and multifaceted projects, and to immensely extend my scientific education in your group. I am very grateful for your valuable advice, your motivating encouragement, and support throughout the projects, your trust in my work, and the freedom you gave to me to follow my ideas. Thank you for the outstanding working atmosphere you created in your team and the numerous great social events. Finally, I want to thank you for the opportunity to present my work on several scientific conferences.

Secondly, I want to thank Dr. Raimund Geidobler and Dr. Ingo Presser from Boehringer Ingelheim GmbH & Co. KG for their interest in microwave-assisted freeze-drying, which made this project possible by funding. Thank you for insightful feedback and scientific expertise from both academic and industry perspective in our monthly meetings, the fruitful discussions and mentorship. I am very happy to continue working with you!

I am also grateful to Dr. Tim Menzen for his precious advice and scientific support with the polymer vials project. Thank you for the valuable discussions and feedback in our "Monday meetings" and your ideas on analytical challenges we faced.

Further, I want to thank Prof. Dr. Wolfgang Frieß for the interesting and valuable scientific input in the department seminar, and for being the co-referee of this thesis. Thanks also for creating such a warm atmosphere in the research groups.

I would like to thank Stephan Reuter, Dr. Alexander Tambovzev, Matthias Kopp, and Niklas Reinheimer from OPTIMA pharma GmbH for their support with the microwave-assisted freeze-dryer prototype, the efforts they have made in getting the best out of the iterative two-week experimental campaigns at the company's site, and the helpful technical and scientific discussions.

Many thanks are expressed to all the colleagues from AK Winter, AK Friess, and AK Merkel for the great time we had together at the institute and at the many scientific and social activities. Thank you also for always helping in finding solutions when problems

occurred. I would especially like to thank Dr. Dennis Krieg for his precious advice and helping hand in spite of our "cultural differences" between Swabians and Badeners. I also want to thank Prof. Dr. Hristo Svilenov for the support in our lab and scientific advice in my first months at the institute, and Dr. Andreas Stelzl for his support and advice with several analytical methods.

I am immensely grateful to Dr. Ruth Rieser and Dr. Sebastian Groël for their support and friendship, for always having a helping hand (especially with the seemingly endless TFF runs) and for our discussions about science. And also special thanks to Alice Hirschmann, for always providing me with enough of the "black gold" (coffee), encouraging me in stressful times and for your help throughout the years. I will never forget our lunches together, the "Sardinia breaks" which felt like vacation and the Heidelberger Melonenschnaps on several occasions!

Lastly, I would like to express my deepest gratitude to my parents, Sabine and Thomas, and my sister, Ann-Kristin, for their unconditional love, patience, and endless support. Without you, this would not have been possible! My heartfelt gratitude also goes to Thiemo. Your unwavering support and love are invaluable for me. Thank you for being my rock in times of turmoil.

Funding Acknowledgement

Table of Content

Chapter I   Current efforts in optimizing lyophilization

I.1 General Introduction

Since Muromonab was introduced to the market nearly four decades ago, significant efforts have been made towards the development of efficient and safe biopharmaceuticals, with over 160 commercial antibody formulations approved in the US and EU [1]. One of the key challenges in developing such drugs is selecting a formulation composition that stabilizes the protein throughout its intended shelf life upon administration to patients. As the route of application for all approved antibody drugs is via injection, they are preferentially formulated as a liquid or lyophilized if protein stability is insufficient in liquid [1,2]. However, even if freezing and drying stresses during the lyophilization process can be minimized by employing suitable stabilizers [3,4], long-term protein stability may still be limited in the solid [5]. It has been shown that for long-term storage in the dried state the retention of the proteins' native structure is crucial [6,7]. Therefore, rational choice of excipients fitting the characteristics of the specific active pharmaceutical ingredient (API) is of utmost importance. Due to the amorphous nature of freeze-dried biopharmaceuticals, there is still notable molecular mobility in the solid state, depending on the glass transition temperature (T_g) of the formulation [8]. Residual moisture is a critical quality attribute (CQA) that is directly linked to the global mobility in the cake, as it acts as a plasticizer [3]. Low amounts of residual moisture after freeze-drying, i.e., typically < 1%, reduce the susceptibility of the protein towards physical and chemical degradation such as aggregation, deamidation, browning reaction, and oxidation [5]. Nevertheless, even if optimum residual moisture content is achieved after lyophilization, degradation still occurs on a relevant time scale [9,10]. Several reviews are available, focusing on the various degradation pathways and possible influencing factors [5,8,9,11].

One major chemical degradation pathway is protein oxidation, both in liquid and lyophilized formulations [11]. It not only leads to changes in the primary structure of proteins but can also trigger aggregation by changing the higher-order structure. Consequently, immunogenicity may increase, and pharmacokinetics or binding and effector function can be altered up to complete loss of therapeutic function [11,12]. Proteins consist of multiple reactive amino acids that can undergo oxidation: methionine, cysteine, histidine, tyrosine, and tryptophan [11–14]. Several effects have been identified that foster oxidation of therapeutic proteins and detection of all potential oxidation promotive factors during drug product development remains a challenging task. Already during the production of

biopharmaceuticals in cell culture, the concentration of dissolved oxygen needs to be closely monitored to control oxidative modification [15–17]. Later, formulation and storage conditions also have a significant impact on the oxidation of protein pharmaceuticals. Generally, an increase in pH correlates with oxidation potential [13]. Besides the importance of the solid-state effective pH [18], several excipients contain sufficient levels of trace metal and peroxide impurities that foster oxidation [12,18]. The latter can be frequently found in polysorbate 20 and 80 [12,18], which are the most used surfactants [19]. The presence of metal ions is a common threat, as those impurities catalyze oxidation in various ways [13]. It must be mentioned that care must be taken with the freezing step during lyophilization, which is most critical regarding protein oxidation during the process, as A) in partially frozen systems, oxygen concentration is increased 1000 fold compared to the liquid at 0°C [11,13,20], and B) local formulation environment of the protein drastically changes due to cryoconcentration and potential pH changes, leading to adsorption at the ice-liquid interface and conformational changes [11,18,20]. Additionally, another factor when it comes to oxidation in lyophilizates is that oxygen solubility and permeability is increased in amorphous systems due to the higher mobility in those matrices compared to crystalline ones [18]. To minimize the presence of oxygen, vials are sealed in a nitrogen atmosphere at the end of the lyophilization process. However, stoichiometrically even 1% headspace oxygen may be sufficient to trigger complete oxidation of the drug product [8]. Depending on the extend of molecular mobility in the freeze-dried cake, another important oxidation route in the solid state can be photo-oxidation [18,21–24]. Photostability studies are carried out to understand susceptibility to light [25], and secondary packaging strategies (e.g., foil pouches) help to protect the drug product from light during long term storage [26,27]. Another possibility to protect the drug product from light would be the use of amber glass vials [28], but this in turn complicates visual inspection and oxidative reactions can be fostered due to leaching of incorporated heavy metals [29].

Due to the materials' transparency, inertness, durability and outstanding barrier properties, vials made of type I borosilicate glass are the most used primary packaging material [29,30]. Moreover, for use in lyophilization, high mechanical stability is required [31]. However, glass is a brittle material and already small flaws can lead to spalling or breakage, which is a severe failure during the drug product lifecycle [31–35]. Other pitfalls are posed by interaction of drug product with the glass material, causing contamination of the pharmaceutical with leachables and extractables, as well as surface delamination [29]. Those interactions may have negative effects on the quality of the protein drug and

immunogenicity [36]. The risk for leachables increases strongly at pH > 9, and silicon, sodium, and boron are the major extractables. While for lyophilized products the likelihood of interaction of the solid drug product with the packaging material is deemed low and thus also the risk for extractables and leachables, care has to be taken as the route of parenteral administration generally falls into the highest degree of concern categories of the USP [37].

Large volume, flexible plastic containers are commonly used for parenteral administration of i.v. medications. More recently, plastic vials and syringes for small volume injectables made from cyclic olefin polymer (COP) and cyclic olefin copolymer (COC) have been introduced to the market [29,38]. Those containers show glass-like transparency, good chemical resistance, and very low levels of inorganic extractables and metal ions, while being highly break resistant [38–40]. Sterilization can be conducted via radiation, ethylene oxide or autoclavation. Thus, cyclic olefin-based plastics are deemed ideal for vial systems, also when considering the inherent resistance to breakage when it comes to storage of new therapeutic modalities at subzero temperatures [38,41–44]. Production costs of high-quality polymer vials exceed the costs to produce glass vials; however, environmental impact is lower for the polymer vials [29,45]. The surface of containers made from polymers is only marginally charged due to the organically based plastic surface, which contrasts with the negatively charged surface of glass [39]. Several investigations found lower absorption propensity of proteins to COP material compared to glass [46,47], and adsorption of an IgG1 was mediated mainly by electrostatic interactions and therefore highly depended on pH and ionic strength of the formulation [48].

Nevertheless, even if moisture and gas barriers are significantly improved for COP and COC compared to other plastics (e.g., polypropylene, polystyrene), they cannot match those of glass [39]. This is particularly important with regard to lyophilizates, which are inherently moisture and oxygen sensitive. To obtain the necessary barrier function, secondary packaging such as an aluminum pouch can provide a remedy. By this, the major disadvantage for the use of polymeric vials for lyophilization can be overcome. The idea to face the inferior barrier properties of plastic containers by proper secondary packaging has already reached the market, e.g., in Japan, for prefilled polymer syringes a few years ago. It has been shown that protein oxidation can be impeded successfully when the syringes were stored in a blister containing an oxygen absorber [49,50]. Similarly, when pouches were filled with gaseous nitrogen, oxidation of therapeutic proteins was prevented [51]. Additionally, heat transfer in cyclic olefin polymer vials was shown to be very homogeneous [52], and uniform cake appearance was found after freeze-drying [39]. The aim of heat

transfer being homogeneous throughout the batch in the lyophilizer is difficult to achieve with traditional vial arrangement due to the so-called edge vial effect [53]. To offset differences in heat transfer, glass vials were nested in rack systems [54]. Likewise, the use of polymeric vials could counterbalance the edge vial effect since lower thermal conductivity ($\sim$0.2 W m^{-1} K^{-1} for COP versus $\sim$1.05 W m^{-1} K^{-1} for glass [55]) and reduced sensitivity to radiative heat transfer has been reported [52].

Maximizing heat and mass transfer during freeze-drying to speed up the typically lengthy process is a topic of ongoing interest. Thus, improvements are not only focusing on novel packaging materials and container designs [56], but also on machine, process, and formulation-related advances. Generally, the lyophilization process is a batch-process, posing additional challenges during drug product development and manufacturing [57–59]. It is highly time and energy consuming, and therefore optimization of the process in terms of time requirements and scale-up procedures is worthwhile [60–62]. Numerous new drying technologies and approaches are being developed [63–67]. Various attempts focus on formulation strategies, to enable fast and therefore aggressive drying without impairing cake appearance and particularly protein stability [68–71]. The use of organic solvents offers several advantages (e.g., increased sublimation rate, improved reconstitution characteristics, etc.), but also comes with a multitude of difficulties like safety concerns [72–76].

Shifting lyophilization processes from batch-mode to continuous manufacturing would drastically increase efficiency and operation flexibility [77]. Strong interest among large pharmaceutical companies [78] already led to progress, e.g., in solid oral dosage forms [79,80]. Plenty of machinery and approaches for bulk as well as unit-dose freeze-drying have been proposed and were reviewed recently [77]. Although continuous freeze-drying is already well-established in food industry, none of the proposed concepts has been applied successfully in the pharmaceutical industry due to deficits in control of indispensable parameters (i.e., sterility, dosage accuracy, product quality) [77].

Another technology that is already well-known from food industry is microwave-assisted freeze-drying (MFD) [81–83]. It has the potential to drastically shorten drying times of conventional freeze-drying (CFD) due to the (additional) application of microwave irradiation during the drying phase. The high-frequency electromagnetic waves specifically excite dielectric material and hereby enable instantaneous, volumetric, and selective heating, as well as rapid heat transfer [84,85]. Since freeze-drying is conducted under vacuum to drive the sublimation process, care must be taken about voltage breakdown stress when

microwave radiation is applied. Breakdown stress reaches a minimum at 1 mbar, and to the advantage of lyophilization, rises at lower pressures [86]. Over the past years, MFD gained more and more attention in the field of pharmaceuticals: After general applicability to monoclonal antibodies (mAbs) and a model vaccine was shown [87], comparable stability profiles were found for two IgG1-type mAbs following MFD and CFD [88,89]. Further studies on vaccines and proteins [90,91], and bacterial cells [92,93] were conducted. As indicated earlier, by interaction of the electromagnetic field with formulation components, energy is transferred during the process. Therefore, the efficiency of MFD is heavily material-dependent and changes within the process, as drying progresses [92,94,95]. Due to the inherent dielectric properties of water in comparison to ice ($\varepsilon'/\varepsilon'' = 77/13$ for water and $\varepsilon'/\varepsilon'' = 3.2/0.003$ for ice at 2.5 GHz) [86], microwaves interact with other formulations components than ice, i.e., the API, excipients and stabilizers, and the unfrozen water. The uniformity of the electromagnetic field, therefore, poses additional challenges as field homogeneity directly correlates with uniformity of drying [94]. Thus, the statistical electromagnetics theory was used to create an efficient and uniform field [91]. In [90], a first-principle model was proposed to study the mechanisms of microwave heating. Recently, mechanistic models were proposed that account for the different sources of heat transfer and may simulate microwave irradiation [96–98]. With this, further insights into the MFD technology and its optimization may be possible and move the technology forward towards commercial application.

I.2 Aim of the thesis

Lyophilization, a technique used for over a century in the medical field, is well-known for producing stable pharmaceuticals. Despite its long history, interest in understanding and optimizing the process from various angles remains strong. This thesis focuses on two different aspects regarding optimization of lyophilization.

In the first part, *Chapters II and III*, a secondary packaging for lyophilizates in polymer vials is developed and evaluated. While the stabilizing effect of secondary packaging for liquid formulations in plastic syringes has been demonstrated and oxidation was suppressed [49,50], no information on lyophilized powders in the novel containers was available. *Chapter II* investigates a secondary packaging combination, consisting of an aluminum pouch containing the vial, along with a combined oxygen and moisture absorber. Oxygen concentration in the pouch and in the headspace of the lyophilizates, residual moisture of the

freeze-dried cakes, and the chemical and physical stability of two monoclonal antibodies were determined over 12 months. The results were compared to polymeric vials without further packaging and commonly used glass vials. The packaging combination proved to be effective in minimizing antibody oxidation, with the amount of oxidized mAb being similar to that in glass vials. *Chapter III* presents further studies on the permeability of polymeric vials. Different packaging configurations were assessed that differed in headspace pressure as well as gas composition, and gaseous oxygen scavengers were compared with liquid ones. Oxygen concentration in the aluminum pouches and the headspaces of the vials was investigated for up to 10 months. The reduced pressure in the headspace typically applied for lyophilizates, proved to decelerate gas exchange, and hereby protects the drug product. The capability of the absorbers in actively removing significant amounts of oxygen from the headspaces of the vials was shown, and proved to be as efficient as a liquid oxygen scavenger.

One major disadvantage of the lyophilization process is its time and energy consumption. The overall aim is to shorten the drying time while maintaining drug product quality. In the second part, *Chapters IV and V*, studies on microwave-assisted freeze drying (MFD) are presented. Microwave radiation is applied to accelerate the conventional freeze drying (CFD) process. *Chapter IV* introduces a new MFD setup based on a common GMP lyophilizer. The machine is retrofitted with semiconductor microwave modules, allowing radiation to be added flexibly to the process. Solid-state properties, physical, and chemical stability of a mAb at a low concentration in various formulations were assessed following MFD. Stability studies were performed at 4°C, 25°C, and 40°C over 6 months, and protein stability was found to be comparable to CFD. *Chapter V* examines the effect of protein concentration in MFD. While protein stability for low-concentration protein formulations was the same following MFD and CFD, microwave radiation led to aggregate formation when protein concentration was increased. The chapter concludes with investigations into protein damage caused by microwave irradiation during drying.

Finally, *Chapter VI* summarizes the results and provides an outlook for the efficient and valuable use of polymeric vials and microwave-assisted freeze-drying.

I.3 References

1. Mieczkowski, C.A. The Evolution of Commercial Antibody Formulations. *J. Pharm. Sci.* **2023**, *112*, 1801–1810, doi:10.1016/j.xphs.2023.03.026.

2. Gervasi, V.; Dall Agnol, R.; Cullen, S.; McCoy, T.; Vucen, S.; Crean, A. Parenteral protein formulations: An overview of approved products within the European Union. *Eur. J. Pharm. Biopharm.* **2018**, *131*, 8–24, doi:10.1016/j.ejpb.2018.07.011.

3. Allmendinger, A.; Häuser, C.; Kumar, L.; Vollrath, I. Formulation Design for Freeze-Drying: Case Studies of Stabilization of Proteins. In *Principles and Practices of Lyophilization in Product Development and Manufacturing*; Jameel, F., Ed.; Springer International Publishing: Cham, 2023; pp. 83–101. ISBN 978-3-031-12634-5.

4. Costantino, H.R. Excipients for Use in Lyophilized Pharmaceutical Peptide, Protein, and other Bioproducts. In *Lyophilization of Biopharmaceuticals*; Costantino, H.R., Pikal, M.J., Eds.; American Association of Pharmaceutical Scientists, 2004; pp. 139–228. ISBN 0-9711767-6-0.

5. Wang, W. Lyophilization and development of solid protein pharmaceuticals. *Int. J. Pharm.* **2000**, *203*, 1–60, doi:10.1016/S0378-5173(00)00423-3.

6. Prestrelski, S.J.; Pikal, K.A.; Arakawa, T. Optimization of Lyophilization Conditions for Recombinant Human Interleukin-2 by Dried-State Conformational Analysis Using Fourier-Transform Infrared Spectroscopy. *Pharm. Res.* **1995**, *12*, 1250–1259, doi:10.1023/A:1016296801447.

7. Chang, B.S.; Beauvais, R.M.; Dong, A.; Carpenter, J.F. Physical Factors Affecting the Storage Stability of Freeze-Dried Interleukin-1 Receptor Antagonist: Glass Transition and Protein Conformation. *Arch. Biochem. Biophys.* **1996**, *331*, 249–258, doi:10.1006/abbi.1996.0305.

8. Chang, L.L.; Pikal, M.J. Mechanisms of protein stabilization in the solid state. *J. Pharm. Sci.* **2009**, *98*, 2886–2908, doi:10.1002/jps.21825.

9. Lai, M.C.; Topp, E.M. Solid-State Chemical Stability of Proteins and Peptides. *J. Pharm. Sci.* **1999**, *88*, 489–500, doi:10.1002/chin.199936308.

10. Pikal, M.J.; Dellerman, K.; Roy, M.L. Formulation and stability of freeze-dried proteins: effects of moisture and oxygen on the stability of freeze-dried formulations of human growth hormone. *Dev. Biol. Stand.* **1992**, *74*, 21–37; discussion 37-8.

11. Cleland, J.L.; Powell, M.F.; Shire, S.J. The development of stable protein formulations: a close look at protein aggregation, deamidation, and oxidation. *Crit. Rev. Ther. Drug Carrier Syst.* **1993**, *10*, 307–377.

12. Torosantucci, R.; Schöneich, C.; Jiskoot, W. Oxidation of Therapeutic Proteins and Peptides: Structural and Biological Consequences. *Pharm. Res.* **2014**, *31*, 541–553, doi:10.1007/s11095-013-1199-9.

13. Li, S.; Schöneich, C.; Borchardt, R.T. Chemical instability of protein pharmaceuticals: Mechanisms of oxidation and strategies for stabilization. *Biotechnol. Bioeng.* **1995**, *48*, 490–500, doi:10.1002/bit.260480511.

14. Luo, Q.; Joubert, M.K.; Stevenson, R.; Ketchem, R.R.; Narhi, L.O.; Wypych, J. Chemical modifications in therapeutic protein aggregates generated under different stress conditions. *J. Biol. Chem.* **2011**, *286*, 25134–25144, doi:10.1074/jbc.M110.160440.

15. SHACTER, E. QUANTIFICATION AND SIGNIFICANCE OF PROTEIN OXIDATION IN BIOLOGICAL SAMPLES*. *Drug Metab. Rev.* **2000**, *32*, 307–326, doi:10.1081/DMR-100102336.

16. Lin, A.A.; Miller, W.M. CHO cell responses to low oxygen: Regulation of oxygen consumption and sensitization to oxidative stress. *Biotechnol. Bioeng.* **1992**, *40*, 505–516, doi:10.1002/bit.260400409.

17. Mohammadian-Mosaabadi, J.; Naderi-Manesh, H.; Maghsoudi, N.; Khalilzadeh, R.; Shojaosadati, S.A.; Ebrahimi, M. Effect of oxidative stress on the production of recombinant human interferon-γ in

Escherichia coli. *Biotechnol. Appl. Biochem.* **2005**, *41*, 37–42, doi:10.1042/BA20030230.

18. Waterman, K.C.; Adami, R.C.; Alsante, K.M.; Hong, J.; Landis, M.S.; Lombardo, F.; Roberts, C.J. Stabilization of Pharmaceuticals to Oxidative Degradation. *Pharm. Dev. Technol.* **2002**, *7*, 1–32, doi:10.1081/PDT-120002237.

19. Jones, M.T.; Mahler, H.C.; Yadav, S.; Bindra, D.; Corvari, V.; Fesinmeyer, R.M.; Gupta, K.; Harmon, A.M.; Hinds, K.D.; Koulov, A.; et al. Considerations for the Use of Polysorbates in Biopharmaceuticals. *Pharm. Res.* **2018**, *35*, doi:10.1007/s11095-018-2430-5.

20. Authelin, J.-R.; Rodrigues, M.A.; Tchessalov, S.; Singh, S.K.; McCoy, T.; Wang, S.; Shalaev, E. Freezing of Biologicals Revisited: Scale, Stability, Excipients, and Degradation Stresses. *J. Pharm. Sci.* **2020**, *109*, 44–61, doi:10.1016/j.xphs.2019.10.062.

21. Kerwin, B.A.; Remmele, R.L. Protect from Light: Photodegradation and Protein Biologics. *J. Pharm. Sci.* **2007**, *96*, 1468–1479, doi:10.1002/jps.20815.

22. Sreedhara, A.; Yin, J.; Joyce, M.; Lau, K.; Wecksler, A.T.; Deperalta, G.; Yi, L.; Wang, Y.J.; Kabakoff, B.; Kishore, R.S.K. Effect of ambient light on IgG1 monoclonal antibodies during drug product processing and development. *Eur. J. Pharm. Biopharm.* **2016**, *100*, 38–46, doi:10.1016/j.ejpb.2015.12.003.

23. Schöneich, C. Photo-Degradation of Therapeutic Proteins: Mechanistic Aspects. *Pharm. Res.* **2020**, *37*, 45, doi:10.1007/s11095-020-2763-8.

24. Schöneich, C. Advanced Oxidation Processes in Pharmaceutical Formulations: Photo-Fenton Degradation of Peptides and Proteins. *Int. J. Mol. Sci.* **2022**, *23*, 8262, doi:10.3390/ijms23158262.

25. Stability Testing: Photostability Testing of New Drug Substances and Products Q1B Available online: https://database.ich.org/sites/default/files/Q1B Guideline.pdf (accessed on Nov 4, 2023).

26. Du, C.; Barnett, G.; Borwankar, A.; Lewandowski, A.; Singh, N.; Ghose, S.; Borys, M.; Li, Z.J. Protection of therapeutic antibodies from visible light induced degradation: Use safe light in manufacturing and storage. *Eur. J. Pharm. Biopharm.* **2018**, *127*, 37–43, doi:10.1016/j.ejpb.2018.02.007.

27. Janga, K.Y.; King, T.; Ji, N.; Sarabu, S.; Shadambikar, G.; Sawant, S.; Xu, P.; Repka, M.A.; Murthy, S.N. Photostability Issues in Pharmaceutical Dosage Forms and Photostabilization. *AAPS PharmSciTech* **2018**, *19*, 48–59, doi:10.1208/s12249-017-0869-z.

28. Henderson, O. Primary Container and Closure Selection for Biopharmaceuticals. In *Formulation and Process Development Strategies for Manufacturing Biopharmaceuticals*; Jameel, F., Hernshenson, S., Eds.; John Wiley & Sons, Inc.: Hoboken, NJ, USA, 2010; pp. 881–896 ISBN 9780470118122.

29. Sacha, G.A.; Saffell-Clemmer, W.; Abram, K.; Akers, M.J. Practical fundamentals of glass, rubber, and plastic sterile packaging systems. *Pharm. Dev. Technol.* **2010**, *15*, 6–34, doi:10.3109/10837450903511178.

30. Vitharana, S.; Stillahn, J.M.; Katayama, D.S.; Henry, C.S.; Manning, M.C. Application of Formulation Principles to Stability Issues Encountered During Processing, Manufacturing, and Storage of Drug Substance and Drug Product Protein Therapeutics. *J. Pharm. Sci.* **2023**, *112*, 2724–2751, doi:10.1016/j.xphs.2023.08.003.

31. Dietrich, C.; Maurer, F.; Roehl, H.; Frieß, W. Pharmaceutical packaging for lyophilization applications. In *Freeze-Drying/Lyophilization of Pharmaceutical and Biological Products: Third Edition*; Rey, L., May, J.C., Eds.; Informa Healthcare: London, UK, 2016; pp. 383–395. ISBN 9781439825754.

32. Gilead recalls remdesivir due to glass contamination Available online: https://www.pharmamanufacturing.com/production/aseptic-processing/news/11290014/gilead-recalls-remdesivir-due-to-glass-contamination (accessed on Oct 12, 2021).

33. Glass pieces trigger Merck recall Available online:

https://www.pharmamanufacturing.com/compliance/compliance-management/news/11290580/glass-pieces-trigger-merck-recall (accessed on Nov 4, 2023).

34. Teva recalls cancer drug after glass found in vial Available online: https://www.pharmamanufacturing.com/industry-news/news/11292082/teva-recalls-cancer-drug-after-glass-found-in-vial (accessed on Nov 4, 2023).

35. Li, G.G.; Cao, S.; Jiao, N.; Wen, Z.-Q. Classification of Glass Particles in Parenteral Product Vials by Visual, Microscopic, and Spectroscopic Methods. *PDA J. Pharm. Sci. Technol.* **2014**, *68*, 362–372, doi:10.5731/pdajpst.2014.00986.

36. Guidance for Industry, Immunogenicity Assessment for Therapeutic Protein Products Available online: https://www.fda.gov/media/85017/download (accessed on Nov 26, 2023).

37. <1664> ASSESSMENT OF DRUG PRODUCT LEACHABLES ASSOCIATED WITH PHARMACEUTICAL PACKAGING/DELIVERY SYSTEMS. In *United States Pharmacopeia*; 2023; GUID-080B9CD2-A445-44A2-A529-2CC7F86BCC64_3_en-US @2023 USPC.

38. Yoneda, S.; Torisu, T.; Uchiyama, S. Development of syringes and vials for delivery of biologics: current challenges and innovative solutions. *Expert Opin. Drug Deliv.* **2021**, *18*, 459–470, doi:10.1080/17425247.2021.1853699.

39. Waxman, L.; DeGrazio, F.L.; Vilivalam, V.D. Plastic packaging for parenteral drug delivery. In *Parenteral Medications, Fourth Edition*; Nema, S., Ludwig, J.D., Eds.; CRC Press: Boca Raton, USA, 2019; pp. 479–510. ISBN 9780429201400.

40. Zhang, Y.; Guo, J.; Zhang, K.; Ma, X.; Cao, D.; Bai, S.; Yuan, X.; Pan, L.; Sun, J.; Li, Y. Robust Ionic Cyclic Olefin Polymers with Excellent Transparency, Barrier Properties, and Antibacterial Properties. *Macromolecules* **2023**, *56*, 4371–4385, doi:10.1021/acs.macromol.3c00439.

41. Lyness, A.M.; Kraft, C.; Hashimdeen, S.; Rafiq, Q.A. Comparison of rigid polymer vials and flexible bags for cryopreservation of T cells. *Cytotherapy* **2020**, *22*, S148, doi:10.1016/j.jcyt.2020.03.301.

42. Kraft, C.; Glen, K.E.; Harriman, J.; Thomas, R.; Lyness, A.M. Evaluation of a novel cyclic olefin polymer container system for cryopreservation of adeno-associated virus. *Cytotherapy* **2020**, *22*, S147–S148, doi:10.1016/j.jcyt.2020.03.300.

43. Lee, M.; Keener, J.; Rodgers, G.M.; Adachi, R.Y. Novel polymer container systems for protein therapeutics and cell culturing. *Int. J. Polym. Mater. Polym. Biomater.* **2016**, *65*, 568–573, doi:10.1080/00914037.2016.1149845.

44. Woods, E.J.; Bagchi, A.; Goebel, W.S.; Vilivalam, V.D. Container system for enabling commercial production of cryopreserved cell therapy products. *Regen. Med.* **2010**, *5*, 659–667, doi:10.2217/rme.10.41.

45. Belboom, S.; Renzoni, R.; Verjans, B.; Léonard, A.; Germain, A. A life cycle assessment of injectable drug primary packaging: Comparing the traditional process in glass vials with the closed vial technology (polymer vials). *Int. J. Life Cycle Assess.* **2011**, *16*, 159–167, doi:10.1007/s11367-011-0248-z.

46. Qadry, S. Evaluation of CZ-resin vials for packaging protein-based parenteral formulations. *Int. J. Pharm.* **2003**, *252*, 207–212, doi:10.1016/S0378-5173(02)00641-5.

47. Eu, B.; Cairns, A.; Ding, G.; Cao, X.; Wen, Z.-Q. Direct Visualization of Protein Adsorption to Primary Containers by Gold Nanoparticles. *J. Pharm. Sci.* **2011**, *100*, 1663–1670, doi:10.1002/jps.22410.

48. Mathes, J.; Friess, W. Influence of pH and ionic strength on IgG adsorption to vials. *Eur. J. Pharm. Biopharm.* **2011**, *78*, 239–247, doi:10.1016/j.ejpb.2011.03.009.

49. Nakamura, K.; Abe, Y.; Kiminami, H.; Yamashita, A.; Iwasaki, K.; Suzuki, S.; Yoshino, K.; Dierick, W.; Constable, K. A Strategy for the Prevention of Protein Oxidation by Drug Product in Polymer-Based Syringes. *PDA J. Pharm. Sci. Technol.* **2015**, *69*, 88–95, doi:10.5731/pdajpst.2015.01009.

50. Masato, A.; Kiichi, F.; Uchiyama, S. Suppression of Methionine Oxidation of a Pharmaceutical Antibody Stored in a Polymer-Based Syringe. *J. Pharm. Sci.* **2016**, *105*, 623–629, doi:10.1002/jps.24675.

51. Werner, B.P.; Schöneich, C.; Winter, G. Silicone Oil-Free Polymer Syringes for the Storage of Therapeutic Proteins. *J. Pharm. Sci.* **2019**, *108*, 1148–1160, doi:10.1016/J.XPHS.2018.10.049.

52. Hibler, S.; Wagner, C.; Gieseler, H. Vial Freeze-Drying, part 1: New Insights into Heat Transfer Characteristics of Tubing and Molded Vials. *J. Pharm. Sci.* **2012**, *101*, 1189–1201, doi:10.1002/jps.23004.

53. Rambhatla, S.; Pikal, M.J. Heat and mass transfer scale-up issues during freeze-drying, I: Atypical radiation and the edge vial effect. *AAPS PharmSciTech* **2003**, *4*, 14, doi:10.1208/pt040214.

54. Daller, S.; Friess, W.; Schroeder, R. Energy Transfer in Vials Nested in a Rack System During Lyophilization. *Pharmaceutics* **2020**, *12*, 61, doi:10.3390/pharmaceutics12010061.

55. McAndrew, T.P.; Hostetler, D.; DeGrazio, F.L. Container and Reconstitution Systems for Lyophilized Drug Products. In *Lyophilization of Pharmaceuticals and Biologicals: New Technologies and Approaches*; Ward, K.R., Matejtschuk, P., Eds.; Springer New York: New York, NY, 2019; pp. 193–214. ISBN 978-1-4939-8928-7.

56. Kullmann, D.; Martinez, C.L.; Lümkemann, J.; Huwyler, J. Part I: Significant reduction of lyophilization process times by using novel matrix based scaffolds. *Eur. J. Pharm. Biopharm.* **2023**, *184*, 248–261, doi:10.1016/j.ejpb.2022.12.008.

57. Carpenter, J.F.; Pikal, M.J.; Chang, B.S.; Randolph, T.W. Rational Design of Stable Lyophilized Protein Formulations: Some Practical Advice. *Pharm. Res.* **1997**, *14*, 969–975, doi:10.1023/A:1012180707283.

58. Nail, S.L.; Jiang, S.; Chongprasert, S.; Knopp, S.A. Fundamentals of Freeze-Drying. In *Development and Manufacture of Protein Pharmaceuticals*; Nail, S.L., Akers, M.J., Eds.; Springer US: Boston, MA, 2002; pp. 281–360. ISBN 978-1-4615-0549-5.

59. Tang, X. (Charlie); Pikal, M.J. Design of Freeze-Drying Processes for Pharmaceuticals: Practical Advice. *Pharm. Res.* **2004**, *21*, 191–200, doi:10.1023/B:PHAM.0000016234.73023.75.

60. Patel, S.M.; Pikal, M.J. Lyophilization Process Design Space. *J. Pharm. Sci.* **2013**, *102*, 3883–3887, doi:10.1002/jps.23703.

61. Jameel, F.; Alexeenko, A.; Bhambhani, A.; Sacha, G.; Zhu, T.; Tchessalov, S.; Kumar, L.; Sharma, P.; Moussa, E.; Iyer, L.; et al. Recommended Best Practices for Lyophilization Validation—2021 Part I: Process Design and Modeling. *AAPS PharmSciTech* **2021**, *22*, 221, doi:10.1208/s12249-021-02086-8.

62. Cullen, S.; Walsh, E.; Gervasi, V.; Khamar, D.; McCoy, T.R. Technical transfer and commercialisation of lyophilised biopharmaceuticals — application of lyophiliser characterisation and comparability. *AAPS Open* **2022**, *8*, 14, doi:10.1186/s41120-022-00059-0.

63. Langford, A.; Bhatnagar, B.; Walters, R.; Tchessalov, S.; Ohtake, S. Drying technologies for biopharmaceutical applications: Recent developments and future direction. *Dry. Technol.* **2018**, *36*, 677–684, doi:10.1080/07373937.2017.1355318.

64. Sharma, A.; Khamar, D.; Cullen, S.; Hayden, A.; Hughes, H. Innovative Drying Technologies for Biopharmaceuticals. *Int. J. Pharm.* **2021**, *609*, 121115, doi:10.1016/j.ijpharm.2021.121115.

65. Emami, F.; Keihan Shokooh, M.; Mostafavi Yazdi, S.J. Recent progress in drying technologies for improving the stability and delivery efficiency of biopharmaceuticals. *J. Pharm. Investig.* **2023**, *53*, 35–57, doi:10.1007/s40005-022-00610-x.

66. Mehanna, M.M.; Abla, K.K. Recent advances in freeze-drying: variables, cycle optimization, and innovative techniques. *Pharm. Dev. Technol.* **2022**, *27*, 904–923, doi:10.1080/10837450.2022.2129385.

67. Hsein, H.; Auffray, J.; Noel, T.; Tchoreloff, P. Recent advances and persistent challenges in the design of freeze-drying process for monoclonal antibodies. *Pharm. Dev. Technol.* **2022**, *27*, 942–955, doi:10.1080/10837450.2022.2131818.

68. Horn, J.; Schanda, J.; Friess, W. Impact of fast and conservative freeze-drying on product quality of protein-mannitol-sucrose-glycerol lyophilizates. *Eur. J. Pharm. Biopharm.* **2018**, *127*, 342–354, doi:10.1016/j.ejpb.2018.03.003.

69. Haeuser, C.; Goldbach, P.; Huwyler, J.; Friess, W.; Allmendinger, A. Be Aggressive! Amorphous Excipients Enabling Single-Step Freeze-Drying of Monoclonal Antibody Formulations. *Pharmaceutics* **2019**, *11*, 616, doi:10.3390/pharmaceutics11110616.

70. Depaz, R.A.; Pansare, S.; Patel, S.M. Freeze-Drying above the Glass Transition Temperature in Amorphous Protein Formulations while Maintaining Product Quality and Improving Process Efficiency. *J. Pharm. Sci.* **2016**, *105*, 40–49, doi:10.1002/jps.24705.

71. Pansare, S.K.; Patel, S.M. Lyophilization Process Design and Development: A Single-Step Drying Approach. *J. Pharm. Sci.* **2019**, *108*, 1423–1433, doi:10.1016/j.xphs.2018.11.021.

72. Teagarden, D.L.; Baker, D.S. Practical aspects of lyophilization using non-aqueous co-solvent systems. *Eur. J. Pharm. Sci.* **2002**, *15*, 115–133, doi:10.1016/S0928-0987(01)00221-4.

73. Kasraian, K.; DeLuca, P.P. The Effect of Tertiary Butyl Alcohol on the Resistance of the Dry Product Layer During Primary Drying. *Pharm. Res.* **1995**, *12*, 491–495, doi: 10.1023/A:1016285425670.

74. Kunz, C.; Schuldt-Lieb, S.; Gieseler, H. Freeze-Drying From Organic Cosolvent Systems, Part 1: Thermal Analysis of Cosolvent-Based Placebo Formulations in the Frozen State. *J. Pharm. Sci.* **2018**, *107*, 887–896, doi:10.1016/j.xphs.2017.11.003.

75. Kunz, C.; Schuldt-Lieb, S.; Gieseler, H. Freeze-Drying From Organic Co-Solvent Systems, Part 2: Process Modifications to Reduce Residual Solvent Levels and Improve Product Quality Attributes. *J. Pharm. Sci.* **2019**, *108*, 399–415, doi:10.1016/j.xphs.2018.07.002.

76. Witschi, C.; Doelker, E. Residual solvents in pharmaceutical products: acceptable limits, influences on physicochemical properties, analytical methods and documented values. *Eur. J. Pharm. Biopharm.* **1997**, *43*, 215–242, doi:10.1016/S0939-6411(96)00037-9.

77. Pisano, R.; Arsiccio, A.; Capozzi, L.C.; Trout, B.L. Achieving continuous manufacturing in lyophilization: Technologies and approaches. *Eur. J. Pharm. Biopharm.* **2019**, *142*, 265–279, doi:10.1016/j.ejpb.2019.06.027.

78. Poechlauer, P.; Manley, J.; Broxterman, R.; Gregertsen, B.; Ridemark, M. Continuous processing in the manufacture of active pharmaceutical ingredients and finished dosage forms: An industry perspective. *Org. Process Res. Dev.* **2012**, *16*, 1586–1590, doi:10.1021/op300159y.

79. Heider, P.L.; Born, S.C.; Basak, S.; Benyahia, B.; Lakerveld, R.; Zhang, H.; Hogan, R.; Buchbinder, L.; Wolfe, A.; Mascia, S.; et al. Development of a multi-step synthesis and workup sequence for an integrated, continuous manufacturing process of a pharmaceutical. *Org. Process Res. Dev.* **2014**, *18*, 402–409, doi:10.1021/op400294z.

80. Mascia, S.; Heider, P.L.; Zhang, H.; Lakerveld, R.; Benyahia, B.; Barton, P.I.; Braatz, R.D.; Cooney, C.L.; Evans, J.M.B.; Jamison, T.F.; et al. End-to-end continuous manufacturing of pharmaceuticals: Integrated synthesis, purification, and final dosage formation. *Angew. Chemie - Int. Ed.* **2013**, *52*, 12359–12363, doi:10.1002/anie.201305429.

81. Guo, Q.; Sun, D.-W.; Cheng, J.-H.; Han, Z. Microwave processing techniques and their recent applications in the food industry. *Trends Food Sci. Technol.* **2017**, *67*, 236–247, doi:10.1016/J.TIFS.2017.07.007.

82. Chandrasekaran, S.; Ramanathan, S.; Basak, T. Microwave food processing—A review. *Food Res. Int.* **2013**, *52*, 243–261, doi:10.1016/J.FOODRES.2013.02.033.

83. Fan, K.; Zhang, M.; Mujumdar, A.S. Recent developments in high efficient freeze-drying of fruits and

vegetables assisted by microwave: A review. *Crit. Rev. Food Sci. Nutr.* **2019**, *59*, 1357–1366, doi:10.1080/10408398.2017.1420624.

84. Metaxas, A.C. Microwave heating. *Power Eng. J.* **1991**, *5*, 237–247, doi:10.1049/pe:19910047.

85. Clark, D.E.; Sutton, W.H. Microwave processing of materials. *Annu. Rev. Mater. Sci.* **1996**, *26*, 299–331, doi:10.1146/annurev.ms.26.080196.001503.

86. Meredith, R.J. Microwave interaction with dielectric materials. In *Engineers' handbook of industrial microwave heating*; The Institution of Electrical Engineers: London, UK, 1998; pp. 19–52. ISBN 0852969163.

87. Evans, R.K. Applications of Microwave Vacuum Drying and Lyospheres to Freeze-Drying of Vaccines and Biologics. In Proceedings of the CPPR: Freeze-Drying of Pharmaceuticals and Biologicals Conference; Garmisch-Partenkirchen, Germany, 23–26 September 2014.

88. Gitter, J.H.; Geidobler, R.; Presser, I.; Winter, G. Significant Drying Time Reduction Using Microwave-Assisted Freeze-Drying for a Monoclonal Antibody. *J. Pharm. Sci.* **2018**, *107*, 2538–2543, doi:10.1016/J.XPHS.2018.05.023.

89. Gitter, J.H.; Geidobler, R.; Presser, I.; Winter, G. Microwave-Assisted Freeze-Drying of Monoclonal Antibodies: Product Quality Aspects and Storage Stability. *Pharmaceutics* **2019**, *11*, 674, doi:10.3390/pharmaceutics11120674.

90. Bhambhani, A.; Stanbro, J.; Roth, D.; Sullivan, E.; Jones, M.; Evans, R.; Blue, J. Evaluation of Microwave Vacuum Drying as an Alternative to Freeze-Drying of Biologics and Vaccines: the Power of Simple Modeling to Identify a Mechanism for Faster Drying Times Achieved with Microwave. *AAPS PharmSciTech* **2021**, *22*, 52, doi:10.1208/s12249-020-01912-9.

91. Abdelraheem, A.; Tukra, R.; Kazarin, P.; Sinanis, M.D.; Topp, E.M.; Alexeenko, A.; Peroulis, D. Statistical electromagnetics for industrial pharmaceutical lyophilization. *PNAS Nexus* **2022**, *1*, 1–13, doi:10.1093/pnasnexus/pgac052.

92. Durance, T.; Noorbakhsh, R.; Sandberg, G.; Sáenz-Garza, N. Microwave Drying of Pharmaceuticals. In *Drying technologies for biotechnologies and pharmaceutical applications*; Ohtake, S., Izutsu, K.-I., Lechuga-Ballesteros, D., Eds.; Wiley-VCH Verlag GmbH & Co. KGaA: Weinheim, Germany, 2020; pp. 239–255. ISBN 9783527341122.

93. Ambros, S.; Bauer, S.A.W.; Shylkina, L.; Foerst, P.; Kulozik, U. Microwave-Vacuum Drying of Lactic Acid Bacteria: Influence of Process Parameters on Survival and Acidification Activity. *Food Bioprocess Technol.* **2016**, *9*, 1901–1911, doi:10.1007/s11947-016-1768-0.

94. Thostenson, E.T.; Chou, T.W. Microwave processing: fundamentals and applications. *Compos. Part A Appl. Sci. Manuf.* **1999**, *30*, 1055–1071, doi:10.1016/S1359-835X(99)00020-2.

95. Kelen, Á.; Ress, S.; Nagy, T.; Pallai, E.; Pintye-Hódi, K. Mapping of temperature distribution in pharmaceutical microwave vacuum drying. *Powder Technol.* **2006**, *162*, 133–137, doi:10.1016/j.powtec.2005.12.001.

96. Park, J.; Cho, J.H.; Braatz, R.D. Mathematical modeling and analysis of microwave-assisted freeze-drying in biopharmaceutical applications. *Comput. Chem. Eng.* **2021**, *153*, 107412, doi:10.1016/j.compchemeng.2021.107412.

97. Srisuma, P.; Barbastathis, G.; Braatz, R.D. Analytical solutions for the modeling, optimization, and control of microwave-assisted freeze drying. *Comput. Chem. Eng.* **2023**, *177*, 108318, doi:10.1016/j.compchemeng.2023.108318.

98. Srisuma, P.; Barbastathis, G.; Braatz, R.D. Mechanistic Modeling and Analysis of Thermal Radiation in Conventional, Microwave-assisted, and Hybrid Freeze Drying for Biopharmaceutical Manufacturing. *arXiv preprint arXiv:2308.02104* **2023**, doi:10.48550/arXiv.2308.02104.

Chapter II Minimizing Oxidation of Freeze-Dried Monoclonal Antibodies in Polymeric Vials Using a Smart Packaging Approach

This chapter is published as:

Author contributions:

N.H., T.M., and G.W. conceptualized the idea and planned the experiments. N.H. conducted the experiments and evaluated the data. N.H. wrote the manuscript. T.M. and G.W. provided scientific guidance, and reviewed and edited the manuscript.

The published article can be accessed online:

https://doi.org/10.3390/pharmaceutics13101695

Note from the authors:

The numbering of the subchapters, figures and tables was changed in comparison to the published version of the article, to fit the consecutive numbering of this thesis.

II.1 Abstract

Primary containers made of cyclic olefin polymer (COP) have recently gained attention since they may overcome several risks and shortcomings of glass containers as they exhibit a high break resistance, biocompatibility, and homogeneous heat transfer during lyophilization. On the downside, COP is more permeable for gases, which can lead to an ingress of oxygen into the container over time. Since oxidation is an important degradation pathway for monoclonal antibodies (mAbs), the continuous migration of oxygen into drug product containers should be avoided overall. To date, no long-term stability studies regarding lyophilizates in polymer vials have been published, potentially because of the unbearable gas permeability. In this study, we demonstrate that after lyophilization in COP

vials and storage of these vials in aluminum pouches together with combined oxygen and moisture absorbers ("smart packaging"), oxidation of two lyophilized therapeutic antibodies was as low as in glass vials due to the deoxygenated environment in the pouch. Nevertheless, active removal of oxygen from the primary container below the initial level over time during storage in such "smart" secondary packaging was not achieved. Furthermore, residual moisture was controlled. Overall, the smart packaging reveals a promising approach for long-term stability of biopharmaceuticals; in addition to COP's known benefits, stable, low oxygen and moisture levels as well as the protection from light and cushioning against mechanical shock by the secondary packaging preserve the sensitive products very well.

II.2 Introduction

Monoclonal antibodies (mAbs) are therapeutically highly relevant drugs [1]. Due to the complex structure of these molecules, chemical and physical degradation is frequently observed and therefore formulation of stable liquid dosage forms may be challenging [2–4]. Freeze-drying is a frequently employed technique to provide sufficient shelf life and improved stability during shipping for labile protein drugs [5,6]. Vials made of glass are the most common primary packaging for freeze-dried pharmaceuticals [7] due to the materials' inertness, transparency and excellent barrier properties against moisture and gases [8,9]. Nevertheless, concerns with glass like ion leaching, delamination and its susceptibility regarding breakage can affect safety and efficacy [7,10] and thus may lead to recalls [11]. More recently, vials made of cyclic olefin polymers and copolymers (COP and COC) have attracted attention as they have overcome the major drawbacks of glass by showing excellent chemical resistance [9] and low adsorption [7,12,13], while likewise providing a translucent and inert surface [7]. Moreover, an obvious benefit over glass is the great break resistance of the polymers, which therefore makes them favorable for recent cell and gene therapies as well [10,14–16]. Moreover, an environmental benefit using polymer over glass vials was found [17]. For more detailed information on plastic packaging, the reader is referred elsewhere [9].

It has been shown previously that lyophilization in cyclic olefins results in homogeneous heat transfer [18] and increased uniformity within the cakes [9]. The major disadvantage of

these polymeric materials is their permeability to gases, e.g., oxygen and water vapor [10], and therefore shelf life might be jeopardized. Particularly when it comes to biopharmaceuticals, which are prone to oxidation, contact with oxygen needs to be eliminated during storage. Since oxygen is constantly available in the ambient air, it can either damage biopharmaceuticals by directly oxidizing susceptible amino acids (e.g., methionine, cysteine) or by generating reactive oxygen species (ROS) [9]. Protein oxidation is one of the major degradation pathways and can lead to detrimental biological consequences, i.e., loss of potency, altered pharmacokinetics as well as unwanted immunogenicity [19–21]. Thus, vials are sealed under nitrogen atmosphere at the end of a lyophilization cycle. Moreover, residual moisture content of the lyophilizates throughout storage has to be taken into account, as it may directly deteriorate long-term stability of proteins as a potential reactant or by increasing molecular mobility as a plasticizer [22,23]. Hence, penetration of water vapor through the container walls of COP vials would increase the residual moisture of the lyophilized product and consequently result in reduced glass transition temperatures, eventually leading to a collapse of the cake [24].

To provide the necessary barrier function for cyclic olefin polymers, secondary packaging such as aluminum pouches may be utilized. This concept has already been introduced for packaging of biotech products in prefilled polymer syringes and has reached the market, e.g., in Japan, several years ago. Previous studies showed for liquid formulations that protein oxidation in COP syringes can be successfully suppressed when the syringes were stored in a blister pack containing an oxygen absorber [25,26]. Similarly, another approach investigated by Werner et al. prevented oxidation of therapeutic proteins by storage of COP syringes in nitrogen-filled aluminum pouches [27]. So far, lyophilizates in COP vials have not really been thought of as a relevant configuration, and the use of absorbers as enabling tools has not been considered in this context.

For the first time, in this study we evaluated the suitability of smart secondary packaging, including combined oxygen and moisture absorbers in aluminum pouches for lyophilizates of two relevant therapeutic monoclonal antibodies in COP vials. Oxygen levels in the headspaces, residual moisture of the lyophilizates as well as the chemical and physical stability of the mAbs were investigated at three different storage temperatures over the course of up to 12 months.

II.3 Materials and Methods

II.3.1 Monoclonal Antibodies and Chemicals

Two monoclonal IgG type 1 antibodies (mAbs) named LMU1 and LMU2 in the following were used in this study. The investigated model mAbs were selected because of their potential susceptibility to oxidation. L-histidine monohydrochloride monohydrate (99% purity) and L-histidine (cell culture reagent) were purchased from Alfa Aesar (Ward Hill, MA, USA). D(+)–trehalose dihydrate (97.0–102.0% purity) Ph. Eur., NF certified was purchased from VWR International (Radnor, PA, USA). EMPROVE® exp sucrose, EMPROVE® bio sodium chloride, EMSURE® sodium dihydrogen phosphate monohydrate, EMSURE® potassium dihydrogen phosphate, and EMSURE® sodium hydroxide solution 50% were purchased from Merck KGaA (Darmstadt, Germany). TWEEN® 20 Ph. Eur. certified, ammonium sulfate of BioXtra grade and acetic acid (≥99.8% purity) Ph. Eur. certified were purchased from Sigma-Aldrich (Steinheim, Germany). Super Refined™ Polysorbate 80-LQ-(MH) was purchased from Croda (Edison, NJ, USA). Di-sodium hydrogen phosphate dihydrate and potassium chloride were purchased from AppliChem GmbH (Darmstadt, Germany). For the preparation of all solutions, ultrapure water from an Arium® system of Sartorius Lab Instruments GmbH (Goettingen, Germany) was used.

II.3.2 Preparation of the Formulations

The bulk solutions of both mAbs were buffer exchanged to 20 mM (LMU1) or 10 mM (LMU2) histidine/histidine hydrochloride with pH 5.5 at 20 °C to 25 °C using Slide-A-Lyzer™ 10000 molecular weight cut-off dialysis cassettes (Thermo Fisher Scientific, Waltham, MA, USA). After extensive dialysis as described by Svilenov et al. [28], the final buffers contained either 20 mM histidine and 0.04% (w/v) polysorbate 20 for LMU1 or 10 mM histidine and 0.05% (w/v) polysorbate 80 for LMU2. The concentration of both antibodies was measured with a Nanodrop 2000 UV spectrophotometer (Thermo Fisher Scientific, Waltham, MA, USA). Stock solutions of the excipients were prepared in the respective histidine buffer and mixed with the dialyzed protein solution in a way that the final formulation contained 10 g/L mAb and either 7.2% trehalose and 0.04% (w/v) polysorbate 20 (LMU1) or 10% sucrose and 0.05% (w/v) polysorbate 80 (LMU2). Both formulations were sterile filtered using a 0.22 μm Sartolab® RF polyethersulfone vacuum filtration unit (Sartorius AG, Goettingen, Germany) prior to filling into the vials. Then, for each formulation, 2.5 mL were filled in 6R tubing vials either made from cyclic olefin polymer (COP Monolayer, Gerresheimer AG, Duesseldorf, Germany) or glass (Schott AG,

Mainz, Germany) and semi-stoppered with lyophilization stoppers (Flurotec® laminated rubber stoppers, West Pharmaceutical Services, Inc, Exton, PA, USA). The vials were arranged on a tray and surrounded by one row of shielding vials containing the respective placebo.

II.3.3 Freeze-Drying Process

Lyophilization was conducted using an FTS LyoStar™ 3 freeze-dryer (SP Scientific, Stone Ridge, NY, USA) following the same protocol for both formulations. Freezing was carried out as suggested by Tang et al. [5] with a few changes; once the shelf temperature (T_s) reached 5 °C and −5 °C subsequently, the respective temperatures were held for 45 min. The final freezing shelf temperature of −50 °C was held for 3 h. All cooling rates were 1 K/min. Primary drying was conducted at a shelf temperature of −20 °C (ramp 1 K/min) and a pressure of 90 µbar. The end of primary drying was determined by comparative pressure measurement between the thermal conductivity pressure gauge (Pirani) and the capacitance pressure gauge (MKS). T_s was then increased to 5 °C (ramp 0.15 K/min) and further to 30 °C (ramp 0.21 K/min) for secondary drying and held for 7 h at the aforementioned chamber pressure. After completion of the lyophilization cycle, the vials were stoppered under nitrogen atmosphere at 600 mbar and crimped with Flip-Off® seals (West Pharmaceutical Services, Inc, Exton, PA, USA).

II.3.4 Study Design

Subsequent to lyophilization, the vials were stored in three configurations as follows: configuration 1 (COP −A −P), COP vials stored without further secondary packaging; configuration 2 (COP +A +P), according to Figure II.1 each COP vial was single packed in an aluminum pouch (Floeter Verpackungsservice, Eberdingen, Germany) with one combined oxygen and moisture absorber (Pharmakeep®, Mitsubishi Gas Chemicals, Tokyo, Japan), where "A" stands for the absorber and the aluminum pouches are abbreviated "P" for more convenient reading, respectively. Sealing of the aluminum pouches was done at ambient conditions using a Polystar 245 (Rische + Herfurth GmbH, Hamburg, Germany). Furthermore, configuration 3 (glass) consisted of glass vials stored without secondary packaging. Samples from each configuration were stored under the exclusion of light at 4 °C, 25 °C and 40 °C for the desired time without controlling the relative humidity.
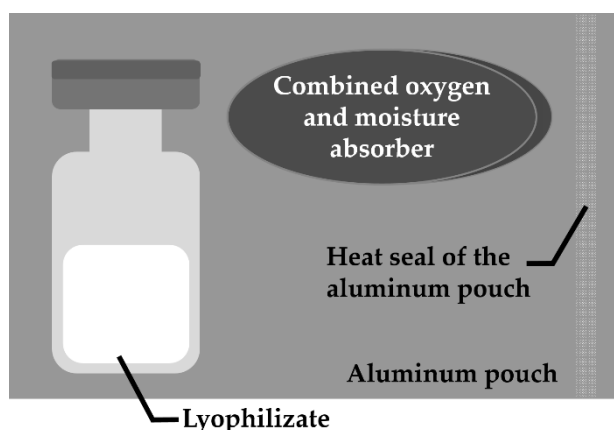
Figure II.1 Illustration of the smart packaging system with combined oxygen and moisture absorber. Each pouch was equipped with one absorber and one vial containing the lyophilizate and heat sealed under ambient conditions.

II.3.5 Oxygen Quantification

The oxygen concentration in the aluminum pouches and in the headspaces of the lyophilizates was measured by using a Microx 4 fiber optic oxygen meter (PreSens Precision Sensing GmbH, Regensburg, Germany). For the lyophilizates, the cap of the Flip-Off® seal was removed, and the needle-shielded sensor was introduced into the headspace by piercing the rubber stopper.

II.3.6 Karl–Fischer Titration

To determine the residual moisture content of the lyophilizates, coulometric Karl Fischer titration was used. The cakes were gently crushed under controlled humidity conditions in a glove box filled with pressurized air (relative humidity < 10%), and 30–50 mg of each cake was transferred into 2R vials and stoppered. Subsequently, the samples were placed in an oven (temperature 100 °C), and the extracted water was transferred to the coulometric titration cell with a dry carrier gas flow (Aqua 40.00 Vario plus, ECH Elektrochemie Halle GmbH, Halle (Saale), Germany). Knowing the weight of the sample, relative moisture content was calculated (w/w). Prior to analysis of the samples, equipment performance was verified by measuring the Apura® water standard oven 1% (Merck KGaA, Darmstadt, Germany) in triplicate.

II.3.7 Reconstitution of the Lyophilizates

Reconstitution of the lyophilized cakes was done by the addition of ultrapure water. For both formulations, the required volume was calculated to correspond to the volume of water removed during freeze-drying.

II.3.8 Hydrophobic Interaction Chromatography

The separation of oxidized species of LMU1 was performed on a Thermo Scientific™ Dionex™ UltiMate™ 3000 UHPLC system equipped with a VWD-3400RS UV/Vis absorbance detector using a MabPac HIC-20 column (4.6 × 250 mm), all from Thermo Fisher Scientific (Waltham, MA, USA). According to Baek et al. [29] the mobile phase A contained 2 M ammonium sulfate and 100 mM sodium phosphate, pH 7.0, whereas mobile phase B solely consisted of 100 mM sodium phosphate, pH 7.0. Prior to analysis, the samples were diluted to a mAb concentration of 5 g/L with mobile phase A, and 5 μL were injected. Starting with 60% B at a flow rate of 0.5 mL/min for 2 min, a linear gradient from 60% to 100% B in 28 min was then performed to separate the oxidation variants of LMU1. The elution of the samples was detected by absorption at 280 nm. The chromatograms were integrated using Chromeleon™ 7.2.7 (Thermo Fisher Scientific, Waltham, MA, USA). Because of the different extinction coefficients of the oxidized species, we used Equation 1 for the determination of the amount of fully oxidized mAb, adapted from Reference [30]:

$$\% \text{ Fully oxidized mAb} = 100 \times \frac{\text{Area}_{\text{oxidized}}}{\left(\text{Area}_{\text{oxidized}} + \frac{\text{Area}_{\text{initial}}}{\text{RF}_{\text{I/O}}}\right)} \tag{1}$$

$\text{RF}_{\text{I/O}}$ UV 280 nm: 1.49. For the calibration data see Figure II.S1 in the supplementary materials.

II.3.9 Protein A Chromatography

For the separation of oxidized species of LMU2, we used a Thermo Scientific™ Dionex™ UltiMate™ 3000 UHPLC system equipped with a VWD-3400RS UV/Vis absorbance detector and a POROS® A column (20 μm, 4.6 × 50 mm), all from Thermo Fisher Scientific (Waltham, MA, USA). The suitability of analytical protein A chromatography for the quantitative detection of oxidation was demonstrated by Loew et al. [31] more recently. Mobile phase A consisted of 10 mM phosphate-buffered saline with 2.7 mM potassium chloride and 134 mM sodium chloride, pH 7.4, whereas mobile phase B contained 100 mM acetic acid and 150 mM sodium chloride at pH 2.8. After an adsorption period of 5 min with 0% B at a flow rate of 2 mL/min, elution was performed in a linear gradient mode from 0% B to 36% B in 24 min. The injection volume was 10 μL. The elution of the samples was detected at 280 nm, and subsequently, the chromatograms were integrated using Chromeleon™ 7.2.7 (Thermo Fisher Scientific, Waltham, MA, USA). As for LMU1, the amount of fully oxidized mAb was determined with Equation (1), however using the main

peak heights instead of the peak areas ($RF_{I/O}$ UV 280 nm: 0.68). For the calibration data see Figure II.S2 in the supplementary materials.

II.3.10 Flow Imaging Microscopy

The formation of subvisible particles during storage in the different packaging configurations was analyzed with a FlowCam 8100 (Fluid Imaging Technologies, Inc., Scarborough, ME, USA) for both mAbs. The system was equipped with a 10× magnification flow cell (80 μm × 700 μm) and controlled by the VisualSpreadsheet® 4.7.6 software. At a flow rate of 0.15 mL/min, 150 μL sample was analyzed, and particle images were obtained at an auto image frame rate of 28 frames/s. The settings for particle identifications were 3 μm distance to the nearest neighbor and particle thresholds of 13 and 10 for dark and light pixels, respectively. The particle size was evaluated as the equivalent spherical diameter.

II.4 Results

II.4.1 Effect of the Absorber on the Oxygen Levels in the Pouches

We sealed the pouches for the smart packaging at ambient conditions to investigate the performance of the absorbers in a worst-case scenario. Within four weeks of storage, the oxygen levels in the pouches were strongly reduced from 20.1% right after sealing to less than 0.3% oxygen for both mAb formulations irrespective of the storage temperature (Figure II.2). Moreover, longer observations over the course of 3 months at elevated temperatures, i.e., 25 °C and 40 °C and over 12 months at 4 °C storage temperature revealed that the aforementioned reduction was long-lasting, since the oxygen levels remained below 0.3%.
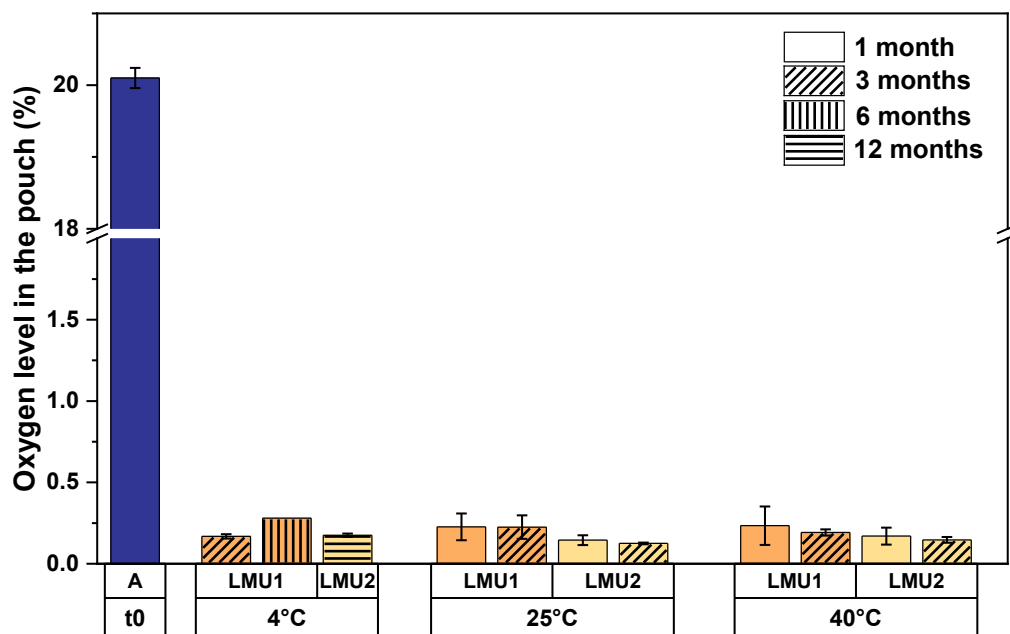
Figure II.2 Oxygen levels in the aluminum pouches stored at different temperatures for the respective time. Sealing was done at ambient conditions with a mean oxygen concentration of 20.1% (blue). The bars are means of six individual pouches; the error bars represent the standard deviation. A, ambient.

II.4.2 Effect of the Absorber on the Oxygen Levels in the Headspaces of the Lyophilizates

After lyophilization, oxygen levels in the headspaces were 6.73% ± 0.05% (COP) and 6.43% ± 0.08% (glass). If not depleted by an absorber, oxygen permeated into the COP vials from the oxygen-rich surrounding air (Figure II.3, COP −A −P). The longer the time a COP vial was exposed to ambient air and the higher the storage temperature, the more oxygen was found in the headspace. After 12 months at 4 °C, the oxygen level in the headspace of COP −A −P almost evened the atmospheric concentration with 17.3% ± 0.31% oxygen (Figure II.3A). Under accelerated storage conditions at elevated temperatures (Figure II.3B), we determined a quick increase in headspace oxygen within 1 month, which further ramped up to 13.80% ± 0.50% for LMU1 and 13.43% ± 0.93% for LMU2 at 25 °C. For the samples stored at 40 °C (Figure II.3C), the initial increase of oxygen in the headspace of COP −A −P was somewhat more pronounced (10.94% ± 0.43% for LMU1, 10.13% ± 0.28% for LMU2) over the course of 1 month. For LMU1, it then further increased to 15.80% ± 0.34%, while permeation was a little slower for LMU2, resulting in 11.53% ± 0.06% oxygen after 3 months.

For COP in the smart packaging (COP +A +P), headspace oxygen levels remained low comparable to those seen in glass, irrespective of the formulation. We even saw a slight decrease in headspace oxygen over time according to the storage temperature. After 3

months, the headspace oxygen level for LMU1 in COP +A +P at 4 °C was 6.87% ± 0.06%
(Figure II.3A); at 25 °C, we found 6.35% ± 0.33% (Figure II.3B), and 5.70% ± 0.11%
oxygen at 40 °C (Figure II.3C), respectively. Moreover, we observed a time-dependent effect
on headspace oxygen in the smart packaging as well. When we stored LMU2 in COP +A +P
at 4 °C (Figure II.3A), the headspace oxygen level was significantly reduced to 3.07% ±
1.93% after 12 months.

In the glass vials, headspace oxygen levels remained low for both formulations.
Nevertheless, with increasing storage temperature, i.e., 25 °C and 40 °C, we even saw a
slight increase in headspace oxygen for LMU1 over time. At 25 °C we found 6.75% ± 0.14%
(Figure II.3B) and 7.02% ± 0.13% (Figure II.3C) oxygen in the respective headspaces of
LMU1 after 3 months.
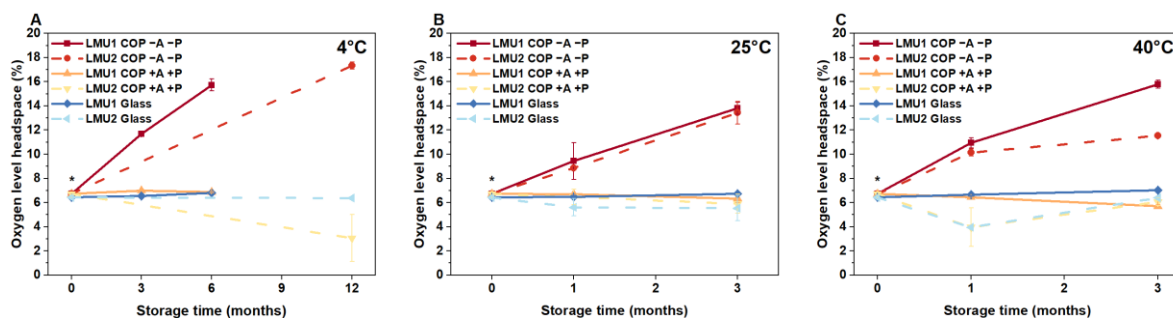
Figure II.3 Oxygen levels in the headspaces of the lyophilizates containing LMU1 and LMU2 measured
directly after freeze-drying and after storage up to 6 months (LMU1) and up to 12 months (LMU2) at 4 °C (A),
25 °C (B), and 40 °C (C). Asterisks (*) represent repeated experiment for LMU2 because occasionally
implausible initial data were obtained. The values are means (n = 6 for LMU1; n = 3 for LMU2) ± standard
deviation. COP, cyclic olefin polymer; A, absorber; P, pouch.

II.4.3 Effect of the Absorber on Residual Moisture Content of the Lyophilizates

After lyophilization, we observed slightly higher residual moisture contents in COP
(0.50% ± 0.04% for LMU1, 1.17% ± 0.05% for LMU2) compared to glass (0.38% ± 0.08%
for LMU1, 1.03% ± 0.07% for LMU2), as shown in Table II.1.

With regard to the polymer vials stored without any further packaging (COP −A −P), we
determined an increase in residual moisture for both formulations dependent on the storage
temperature and time of observation. Within 12 months at 4 °C, residual moisture content of
LMU2 samples increased to 1.71% ± 0.11%. At elevated temperatures, i.e., 25 °C and 40
°C, residual moisture was 1.74% ± 0.07% and 1.68% ± 0.01% after 3 months for LMU2,
respectively.

The smart packaging led to comparable changes in residual moisture over time as
observed for the glass vials (Figure II.4). At refrigerated temperatures (4 °C) residual

moisture content of COP +A +P was 1.30% ± 0.03% for LMU2 after 12 months (Figure II.4A). Within 3 months at 25 °C, residual moisture increased equally in COP +A +P and glass for LMU1 (0.81% ± 0.02% and 0.68% ± 0.02%, respectively), whereas we observed constant moisture levels in the smart packaging for LMU2 (1.21% ± 0.03%) (Figure II.4B). The same holds true for the samples stored at 40 °C over the course of 3 months; residual moisture content slightly increased to 0.84% ± 0.01% in COP +A +P for LMU1, whereas it remained constant at 1.23% ± 0.07% for LMU2 (Figure II.4C).

Similarly, we observed an increase in residual moisture for the glass vials depending on the storage temperature and time (Figure II.4). After 12 months at 4 °C, residual moisture content for LMU2 was 1.19% ± 0.15% (Figure II.4A) and at elevated temperatures, i.e., 25 °C and 40 °C, 1.28% ± 0.08% and 1.37% ± 0.03%, respectively (Figure II.4B,C).

Table II.1 Residual moisture results of the lyophilizates stored at different temperatures for the respective time.

Configuration		Residual Moisture, %						
		4 °C			**25 °C**		**40 °C**	
		0 m	3 m	6 m	1 m	3 m	1 m	3 m
LMU1	COP −A −P	0.50 ± 0.04	0.88 ± 0.04	0.92 ± 0.03	0.68 ± 0.00	1.13 ± 0.01	0.68 ± 0.02	1.02 ± 0.03
	COP +A +P	0.50 ± 0.04	0.78 ± 0.04	0.61 ± 0.02	0.57 ± 0.02	0.81 ± 0.02	0.66 ± 0.01	0.84 ± 0.01
	Glass	0.38 ± 0.08	0.65 ± 0.08	0.47 ± 0.03	0.48 ± 0.03	0.68 ± 0.02	0.54 ± 0.02	0.60 ± 0.06
		0 m	12 m		1 m	3 m	1 m	3 m
LMU2	COP −A −P	1.17 ± 0.05	1.71 ± 0.11		1.24 ± 0.11	1.74 ± 0.07	1.17 ± 0.04	1.68 ± 0.01
	COP +A +P	1.17 ± 0.05	1.30 ± 0.03		1.26 ± 0.09	1.21 ± 0.03	1.20 ± 0.06	1.23 ± 0.07
	Glass	1.03 ± 0.07	1.19 ± 0.15		1.06 ± 0.12	1.28 ± 0.08	1.20 ± 0.09	1.37 ± 0.03

The values are mean of three individual vials. The error represents the standard deviation of the mean. COP, cyclic olefin polymer; A, absorber; P, pouch; m, month.

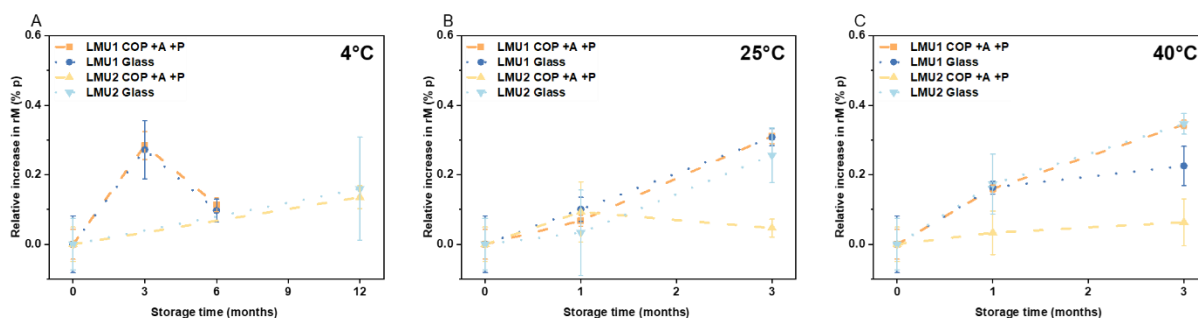**Figure II.4** Relative changes in the residual moisture content of the lyophilizates in the smart packaging (COP +A +P) and glass stored at (A) 4 °C, (B) 25 °C and (C) 40 °C up to 6 months (LMU1) and 12 months (LMU2). Residual moisture content directly after lyophilization was set to 0% p for all configurations. The values are means (n = 3) ± standard deviation. COP, cyclic olefin polymer; A, absorber; P, pouch, % p, percentage point.

II.4.4 Effect of the Smart Packaging on Protein Oxidation

After lyophilization, we determined 6.25% ± 0.08% (LMU1) and 5.60% ± 0.03% (LMU2) of fully oxidized mAb. When the COP vials were then stored at elevated storage temperatures without an absorber (COP −A −P), an increase in oxidation by 0.59% ± 0.11% for LMU1 and 0.14% ± 0.12% for LMU2 was observed at 25 °C after 3 months (Figure II.5A). Furthermore, after 3 months at 40 °C, the percentage of fully oxidized mAb increased by 1.27% ± 0.17% for LMU1 and 0.44% ± 0.07% for LMU2, respectively (Figure II.5B).

The smart packaging achieved similar amounts of oxidation in COP compared to glass. After storage at 25 °C for 3 months, no significant change in the amount of fully oxidized LMU2 was found in COP +A +P (−0.03% ± 0.04%). Only a slight increase in oxidation was observed after 3 months of storage at 40 °C for the respective antibody in the smart packaging (0.16% ± 0.12%). These overall changes within 3 months are comparable to the oxidation rates observed in glass (−0.01% ± 0.05% at 25 °C and 0.10% ± 0.04% at 40 °C). For LMU1, comparable changes in oxidation for the smart packaging and glass were found as well, even though the overall oxidation rate was increased for this antibody (0.99% ± 0.16% in COP +A +P and 0.88% ± 0.21% in glass after 3 months storage at 40 °C, respectively).
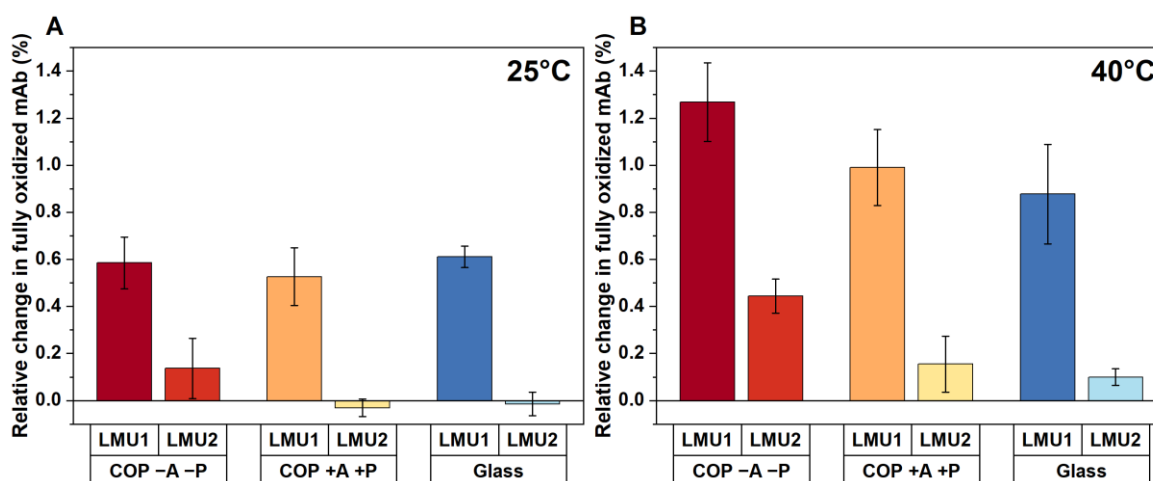
Figure II.5 Relative change in fully oxidized mAb determined by hydrophobic interaction chromatography (HIC) for LMU1 and analytical protein A chromatography (PA) for LMU2 after 3 months of storage at 25 °C (**A**) and 40 °C (**B**). The bars are means (n = 3) ± standard deviation. COP, cyclic olefin polymer; A, absorber; P, pouch.

II.4.5 Effect of the Vial Material on Particle Formation

For both formulations subvisible particle counts (SvP) were detected with flow imaging microscopy (data not shown). All particle concentrations (given in #/mL) are indicated

cumulatively. Directly after lyophilization, particle counts for LMU1 of 24 ± 14, 221 ± 123 and 3014 ± 748 for ≥ 25 μm, ≥ 10 μm and ≥ 1 μm were found for COP, respectively. For the samples in glass vials, we determined 4 ± 9, 53 ± 27, and 2148 ± 829 for ≥ 25 μm, ≥ 10 μm, and ≥ 1 μm, respectively. After 6 months of storage at refrigerated temperatures counts for particles ≥ 25 μm, ≥ 10 μm and ≥ 1 μm were close to the initial amounts with 6 ± 5, 168 ± 73, and 2997 ± 242 for the smart packaging and 5 ± 11, 31 ± 14, and 990 ± 103 for glass, respectively. The same is true if the samples of LMU1 were stored at 40 °C for 3 months; flow imaging microscopy revealed 31 ± 20, 396 ± 199, and 4656 ± 2172 particles ≥ 25 μm, ≥ 10 μm, and ≥ 1 μm for the smart packaging, and 4 ± 6, 60 ± 39, and 771 ± 457 for glass. We observed no significant difference regarding subvisible particles in the smart packaging versus COP $-A$ $-P$ for LMU1 (53 ± 51, 422 ± 243, and 4137 ± 1831 for particles ≥ 25 μm, ≥ 10 μm, and ≥ 1 μm) as well as for LMU2 after storage at 40 °C for 3 months.

Initially, particle counts for LMU2 after lyophilization were 31 ± 18, 2941 ± 911, and 20172 ± 4225 for particles ≥ 25 μm, ≥ 10 μm, and ≥ 1 μm for the smart packaging. In the glass vials we found 1 ± 3, 30 ± 18, and 465 ± 252 particles ≥ 25 μm, ≥ 10 μm, and ≥ 1 μm, respectively. After storage at 4 °C for 12 months, subvisible particle counts in COP $+A$ $+P$ decreased to 28 ± 11, 279 ± 33, and 4598 ± 824 for the aforementioned particle sizes. Similarly, particle numbers in the smart packaging decreased after 3 months of storage at 40 °C (32 ± 17, 291 ± 100, and 7376 ± 2324 for particles ≥ 25 μm, ≥ 10 μm, and ≥ 1 μm). No pronounced change in SvP was seen in glass vials after 3 months at 40 °C (15 ± 14, 48 ± 14, 456 ± 107, respectively).

II.5 Discussion

The aim of our study was to demonstrate that an appropriate secondary packaging for lyophilizates in COP vials provides constantly low oxygen and residual moisture levels. Consequently, protein oxidation in the primary container is comparable to glass vials due to the oxygen and moisture removing capability of an absorber in the package.

After sealing of the aluminum pouches, oxygen from the enclosed air was rapidly removed by the absorber (Figure II.2). With a concentration of less than 0.3% remaining oxygen, the cavity in the secondary packaging was practically deoxygenated. Moreover, we found unchangingly low oxygen levels in the pouch stored at 4 °C for one year, proving sealed aluminum pouches hold perfectly tight as well as the absorber's long-lasting

capability in removing oxygen. Hence, we think that there is no need for sealing the pouches under inert gases, which in turn increases production costs.

The amount of oxygen in the headspaces of the lyophilizates stored in COP vials without any further secondary packaging increased rapidly, as expected (Figure II.3). Due to the permeability of plastics to gases, Qadry et al. found a half-life duration of 15 days for oxygen to increase to 9.4% in CZ-resin COP vials [32]. Thus, less barrier properties to gases compared to glass as one of the major drawbacks of polymer vials was confirmed [10]. However, this supposed detriment was already successfully employed to advantage for liquid protein formulations, since dissolved oxygen was removed from polymer-based syringes by a deoxygenated packaging system and therefore oxidation could be prevented [25,26]. However, in the present study, we were not able to rapidly remove oxygen from the vials containing lyophilizates. Since the surrounding air in the pouch was successfully deoxygenated for the smart packaging, no further oxygen permeated into the vials and we observed constantly low oxygen amounts in the headspaces of COP +A +P, similar to glass. Compared to Nakamura et al., who observed no dissolved oxygen remaining in their liquid formulation in a COP syringe after 56 days in the deoxygenated packaging system [25], removal of oxygen seems to be less effective when it comes to lyophilized, i.e., solid formulations, enclosed in a vial. Of course, storage time and temperature have an effect on the diffusive exchange of gaseous oxygen from the lyophilizates, and we determined slightly lower oxygen amounts in the headspaces after storage for one year at 4 °C (Figure II.3A) and at elevated temperatures compared to glass (Figure II.3B,C). Nevertheless, an actual strong, practically relevant removal of oxygen from COP was not possible, and we are further evaluating the situation.

Remarkably homogeneous heat transfer was reported for polymeric vials during lyophilization, although the thermal conductivity is lower for COP ($\sim$0.2 W m^{-1} K^{-1}) compared to glass ($\sim$1.05 W m^{-1} K^{-1}) [18,33]. This leads to slightly higher initial residual moisture contents in COP compared to glass because less energy is transferred into the COP vial (Table II.1). As with oxygen, COP is permeable to water vapor [9,34]. Consequently, residual moisture significantly increased over time in COP $-$A $-$P due to the lack of a sufficient barrier. In contrast to that, residual moisture levels in the smart packaging (COP +A +P) only slightly increased over the course of 6 (LMU1) and 12 months (LMU2) of storage at 4 °C, very similarly to glass (Figure II.4A). Such a slight increase is frequently observed in lyophilizates, and equilibrium moisture level depends on product characteristics

according to Pikal et al. [35]. Moreover, regarding the residual moisture content at elevated storage temperatures, i.e., 25 °C and 40 °C, we again found very similar levels in the smart packaging compared to glass due to the dry air in the pouch (Figure II.4B,C). Accordingly, the moisture-absorbing capability is a useful synergistic effect when it comes to lyophilizates, since long-term protein stability generally decreases with increasing moisture content [23]. For LMU2, we even observed constant residual moisture levels in COP +A +P over storage and no increase over time at all. The possibility to remove moisture from lyophilizates in COP vials remains an option and needs to be studied with regard to different container stoppers (i.e., different brands, polymers, pretreatments, etc.).

Although chemical reactions are decelerated in lyophilizates because of the low water content, proteins undergo oxidation in the dried state as well [20,36]. In our study, we examined two clinically relevant antibodies to evaluate the actual profit of our smart packaging. One strategy to reduce oxidation is to reduce or exclude oxygen [37]. Hence, as a consequence of the consistently low and comparable headspace oxygen levels in COP +A +P and glass we found similar amounts of oxidation in both packaging configurations irrespective of the storage temperature (Figure II.5). Furthermore, with increasing levels of oxygen in the headspace (COP −A −P) the amount of fully oxidized mAb increases for both antibodies. Although the absolute changes in oxidation may appear low to moderate at first glance, more pronounced effects may be achieved in other, oxidation-sensitive systems. Note that the examined mAbs were already oxidized to a certain extend right from the start. Since protein oxidation is one of the major degradation pathways leading to altered conformation and biological activity [19,21], suppression of this degradation pathway is of utmost interest. Nevertheless, there is no superiority of COP +A +P over glass for the lyophilizates. With regard to the comparable headspace oxygen levels of the two configurations, similar degrees of oxidation are expectable.

Apart from chemical degradation, physical instabilities are also of relevance. As proteins are naturally interacting with surfaces, container materials have to be carefully selected [9,38,39]. We found low particle amounts for LMU1 throughout the study irrespective of the configuration, although subvisible particles ≥10 μm and ≥1 μm were slightly higher in COP compared to glass. Unexpectedly, subvisible particles of the order of ≥10 μm and ≥1 μm were found to be increased in COP directly after freeze-drying for LMU2. Particle counts then decreased over the course of 12 months at 4 °C to one fourth as well as within 3 months at 40 °C to one third of the starting value for particles ≥1 μm, respectively. Nevertheless, in

general we observe low cumulative particle amounts for both mAbs after storage for 3 months even at elevated temperatures (i.e., 25 °C and 40 °C). More recently, it has been reported that protein adsorption to cyclic olefin polymer is scarcely observed [12,13,40,41] and if so, it is mainly caused by the hydrophobic effect [42]. We assume that interaction of LMU2 with the hydrophobic surface of COP is the driving force for the increased subvisible particle counts after lyophilization since the mAb exhibits high hydrophobicity.

II.6 Conclusions

In conclusion, we presented a packaging approach for lyophilizates in COP vials (i.e., "smart packaging"), which disposes of permeability issues and renders stable, low headspace oxygen and residual moisture levels due to a combined oxygen and moisture absorber. Consequently, oxidation of two therapeutic monoclonal antibodies was found to be comparable to glass vials. Thus, the major drawback of cyclic olefin polymers regarding the use in the field of freeze-drying has been overcome. Possible concerns with respect to the suitability of cyclic olefin materials for lyophilization (e.g., conductivity issues) can be dispelled. Moreover, a low particle burden was observed after storage at elevated temperatures. The exceptional advantages of the smart packaging, such as the durable and inert polymer material, the tamper-evident closure of the pouch, as well as protection from light and cushioning against mechanical shock in the package optimally preserve sensitive biotech drugs. The numerous benefits of the packaging outweigh potential additional costs by far, particularly since to date secondary packaging of costly biopharmaceuticals is widely disregarded. Nevertheless, a drastic reduction of oxygen in the COP vials as seen for prefilled syringes [25,26] was not achieved. Further studies are needed to understand why the capability in removing oxygen from lyophilizates differs from liquid formulations in deoxygenated packaging concepts.

II.7 Supplementary Materials
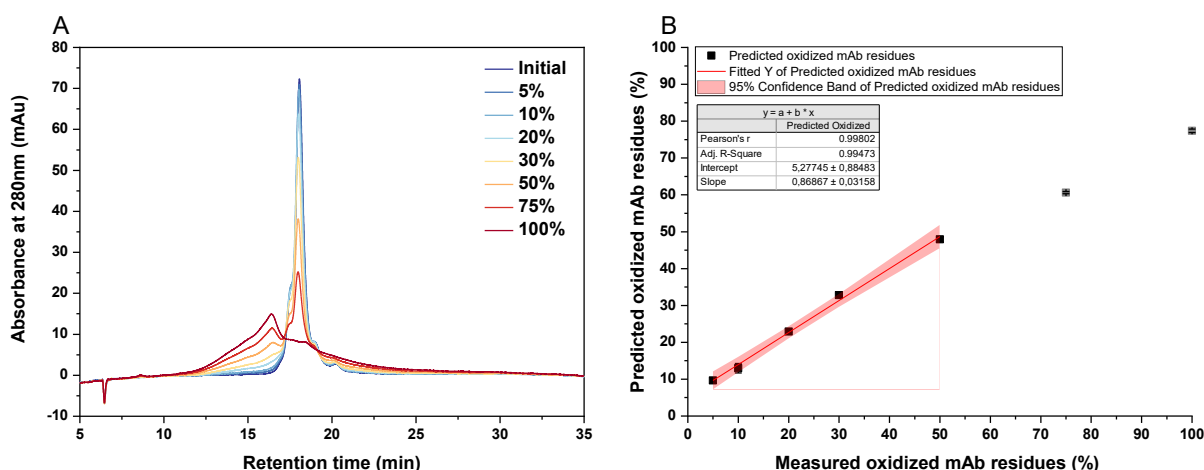
Figure II.S1 MAbPac HIC-20, 5 μm, 4.6 × 250 mm calibration data. (A) Hydrophobic interaction chromatography (HIC) chromatograms of the initial material and artificially oxidized mAb as well as the respective mixtures. (B) Percentage of fully oxidized mAb was determined experimentally and plotted against the theoretical amount of fully oxidized species. Calibration was performed in a linear range between 5% and 50% oxidized mAb residues. 75% and 100% were excluded.
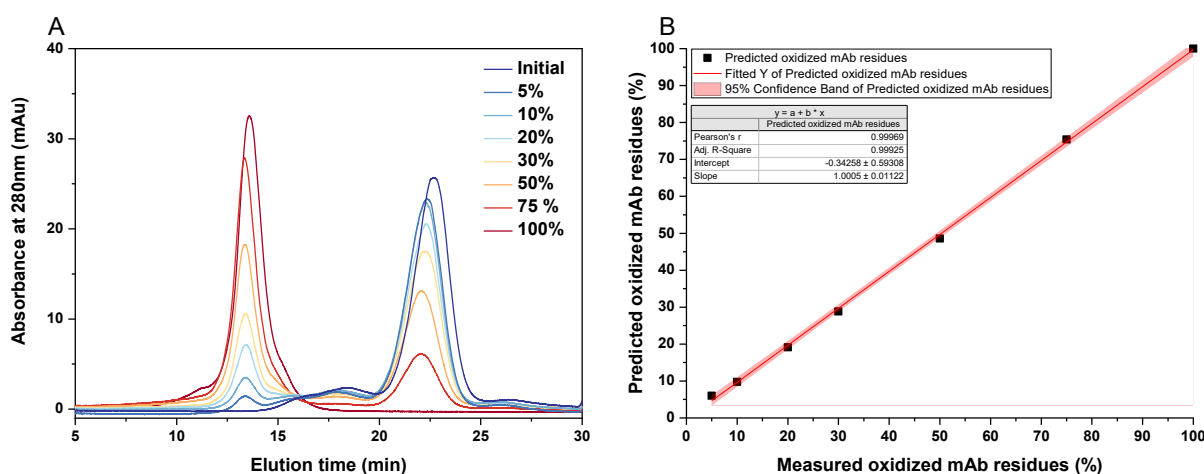
Figure II.S2 POROS® A, 20 μm, 4.6 × 50 mm calibration data. (A) Protein A chromatography chromatograms of the initial material and artificially oxidized mAb as well as the respective mixtures. (B) Percentage of fully oxidized mAb was determined experimentally and plotted against the theoretical amount of fully oxidized species. Calibration was performed in a linear range between 5% and 100% oxidized mAb residues.

II.8 Acknowledgements

II.9 References

1. BiopharmaDealmakers Moving up with the Monoclonals. Available online: https://www.nature.com/articles/d43747-020-00765-2 (accessed on 15 August 2021).

2. Uchiyama, S. Liquid formulation for antibody drugs. *Biochim. Biophys. Acta Proteins Proteom.* **2014**, *1844*, 2041–2052, doi:https://doi.org/10.1016/j.bbapap.2014.07.016.

3. Mahler, H.-C.; Müller, R.; Frieβ, W.; Delille, A.; Matheus, S. Induction and analysis of aggregates in a liquid IgG1-antibody formulation. *Eur. J. Pharm. Biopharm.* **2005**, *59*, 407–417, doi:https://doi.org/10.1016/j.ejpb.2004.12.004.

4. Gervasi, V.; Dall Agnol, R.; Cullen, S.; McCoy, T.; Vucen, S.; Crean, A. Parenteral protein formulations: An overview of approved products within the European Union. *Eur. J. Pharm. Biopharm.* **2018**, *131*, 8–24, doi:10.1016/j.ejpb.2018.07.011.

5. Tang, X. (Charlie); Pikal, M.J. Design of Freeze-Drying Processes for Pharmaceuticals: Practical Advice. *Pharm. Res.* **2004**, *21*, 191–200, doi:10.1023/B:PHAM.0000016234.73023.75.

6. Carpenter, J.F.; Pikal, M.J.; Chang, B.S.; Randolph, T.W. Rational Design of Stable Lyophilized Protein Formulations: Some Practical Advice. *Pharm. Res.* **1997**, *14*, 969–975, doi:10.1023/A:1012180707283.

7. Sacha, G.A.; Saffell-Clemmer, W.; Abram, K.; Akers, M.J. Practical fundamentals of glass, rubber, and plastic sterile packaging systems. *Pharm. Dev. Technol.* **2010**, *15*, 6–34, doi:10.3109/10837450903511178.

8. Dietrich, C.; Maurer, F.; Roehl, H.; Frieß, W.; Maurer, F.; Roehl, H.; Frieß, W. Pharmaceutical Packaging for Lyophilization Applications. In *Freeze-Drying/Lyophilization of Pharmaceutical and Biological Products*; Rey, L., Ed.; CRC Press: Boca Raton, FL, USA, 2010; pp. 283–395.

9. Waxman, L.; DeGrazio, F.L.; Vilivalam, V.D. Plastic packaging for parenteral drug delivery. In *Parenteral Medications, Fourth Edition*; CRC Press: Boca Raton, FL, USA, 2019; pp. 479–510 ISBN 9780429201400.

10. Yoneda, S.; Torisu, T.; Uchiyama, S. Development of syringes and vials for delivery of biologics: current challenges and innovative solutions. *Expert Opin. Drug Deliv.* **2021**, *18*, 459–470, doi:10.1080/17425247.2021.1853699.

11. Breakage and Particle Problems in Glass Vials and Syringes Spurring Industry Interest in Plastics. Available online: https://www.ipqpubs.com/2011/08/07/breakage-and-particle-problems-in-glass-vials-and-syringes-spurring-industry-interest-in-plastics/ (accessed on 8 August 2021).

12. Qadry, S.S.; Roshdy, T.H.; Char, H.; Del Terzo, S.; Tarantino, R.; Moschera, J. Evaluation of CZ-resin vials for packaging protein-based parenteral formulations. Int. J. Pharm. 2003, 252, 207–212, doi:https://doi.org/10.1016/S0378-5173(02)00641-5.

13. Mathes, J.; Friess, W. Influence of pH and ionic strength on IgG adsorption to vials. *Eur. J. Pharm. Biopharm.* **2011**, *78*, 239–247, doi:10.1016/j.ejpb.2011.03.009.

14. Lee, M.; Keener, J.; Rodgers, G.M.; Adachi, R.Y. Novel polymer container systems for protein therapeutics and cell culturing. *Int. J. Polym. Mater. Polym. Biomater.* **2016**, *65*, 568–573, doi:10.1080/00914037.2016.1149845.

15. Kraft, C.; Glen, K.E.; Harriman, J.; Thomas, R.; Lyness, A.M. Evaluation of a novel cyclic olefin polymer container system for cryopreservation of adeno-associated virus. *Cytotherapy* **2020**, *22*, S147–S148, doi:https://doi.org/10.1016/j.jcyt.2020.03.300.

16. Lyness, A.M.; Kraft, C.; Hashimdeen, S.; Rafiq, Q.A. Comparison of rigid polymer vials and flexible bags for cryopreservation of T cells. *Cytotherapy* **2020**, *22*, S148, doi:https://doi.org/10.1016/j.jcyt.2020.03.301.

17. Belboom, S.; Renzoni, R.; Verjans, B.; Léonard, A.; Germain, A. A life cycle assessment of injectable drug primary packaging: Comparing the traditional process in glass vials with the closed vial technology (polymer vials). *Int. J. Life Cycle Assess.* **2011**, *16*, 159–167, doi:10.1007/s11367-011-0248-z.

18. Hibler, S.; Wagner, C.; Gieseler, H. Vial Freeze-Drying, part 1: New Insights into Heat Transfer Characteristics of Tubing and Molded Vials. *J. Pharm. Sci.* **2012**, *101*, 1189–1201, doi:10.1002/jps.23004.

19. Cleland, J.L.; Powell, M.F.; Shire, S.J. The development of stable protein formulations: a close look at protein aggregation, deamidation, and oxidation. *Crit. Rev. Ther. Drug Carrier Syst.* **1993**, *10*, 307–377.

20. Li, S.; Schöneich, C.; Borchardt, R.T. Chemical instability of protein pharmaceuticals: Mechanisms of oxidation and strategies for stabilization. *Biotechnol. Bioeng.* **1995**, *48*, 490–500, doi:10.1002/bit.260480511.

21. Torosantucci, R.; Schöneich, C.; Jiskoot, W. Oxidation of Therapeutic Proteins and Peptides: Structural and Biological Consequences. *Pharm. Res.* **2014**, *31*, 541–553, doi:10.1007/s11095-013-1199-9.

22. Shalaev, E.Y.; Zografi, G. How Does Residual Water Affect the Solid-state Degradation of Drugs in the Amorphous State? *J. Pharm. Sci.* **1996**, *85*, 1137–1141, doi:https://doi.org/10.1021/js960257o.

23. Wang, W. Lyophilization and development of solid protein pharmaceuticals. *Int. J. Pharm.* **2000**, *203*, 1–60, doi:10.1016/S0378-5173(00)00423-3.

24. Oksanen, C.A.; Zografi, G. The Relationship Between the Glass Transition Temperature and Water Vapor Absorption by Poly(vinylpyrrolidone). *Pharm. Res.* **1990**, *7*, 654–657, doi:10.1023/A:1015834715152.

25. Nakamura, K.; Abe, Y.; Kiminami, H.; Yamashita, A.; Iwasaki, K.; Suzuki, S.; Yoshino, K.; Dierick, W.; Constable, K. A Strategy for the Prevention of Protein Oxidation by Drug Product in Polymer-Based Syringes. *PDA J. Pharm. Sci. Technol.* **2015**, *69*, 88–95, doi:10.5731/pdajpst.2015.01009.

26. Masato, A.; Kiichi, F.; Uchiyama, S. Suppression of Methionine Oxidation of a Pharmaceutical Antibody Stored in a Polymer-Based Syringe. *J. Pharm. Sci.* **2016**, *105*, 623–629, doi:10.1002/jps.24675.

27. Werner, B.P.; Schöneich, C.; Winter, G. Silicone Oil-Free Polymer Syringes for the Storage of Therapeutic Proteins. *J. Pharm. Sci.* **2019**, *108*, 1148–1160, doi:10.1016/J.XPHS.2018.10.049.

28. Svilenov, H.; Gentiluomo, L.; Friess, W.; Roessner, D.; Winter, G. A New Approach to Study the Physical Stability of Monoclonal Antibody Formulations—Dilution From a Denaturant. *J. Pharm. Sci.* **2018**, *107*, 3007–3013, doi:10.1016/j.xphs.2018.08.004.

29. Baek, J.; Liu, X. *Separation of Monoclonal Antibody (mAb) Oxidation Variants on a High-Resolution HIC Column*; Thermo Fisher Scientific: Sunnyvale, CA, USA; Available online: https://tools.thermofisher.com/content/sfs/brochures/AN-21069-LC-MAbPac-HIC-20-Oxidized-mAb-Separation-AN21069-EN.pdf (accessed on 27 March 2020).

30. Yang, H.; Koza, S.; Chen, W. *Anion-Exchange Chromatography for Determining Empty and Full Capsid Contents in Adeno-Associated Virus;* Waters Corporation: Milford, MA, USA, 2019; Available online: https://www.waters.com/content/dam/waters/en/app-notes/2020/720006825/720006825-zh.pdf (accessed on 26 November 2020).

31. Loew, C.; Knoblich, C.; Fichtl, J.; Alt, N.; Diepold, K.; Bulau, P.; Goldbach, P.; Adler, M.; Mahler, H.-C.; Grauschopf, U. Analytical Protein A Chromatography as a Quantitative Tool for the Screening of Methionine Oxidation in Monoclonal Antibodies. *J. Pharm. Sci.* **2012**, *101*, 4248–4257, doi:10.1002/jps.23286.

32. Qadry, S..; Roshdy, T..; Knox, D..; Phillips, E.. Model development for O2 and N2 permeation rates through CZ-resin vials. *Int. J. Pharm.* **1999**, *188*, 173–179, doi:10.1016/S0378-5173(99)00220-3.

33. McAndrew, T.P.; Hostetler, D.; DeGrazio, F.L. Container and Reconstitution Systems for Lyophilized Drug Products. In *Lyophilization of Pharmaceuticals and Biologicals: New Technologies and Approaches*; Ward, K.R., Matejtschuk, P., Eds.; Springer: New York, NY, USA, 2019; pp. 193–214 ISBN 978-1-4939-8928-7.

34. Presser, I. Innovative Online Messverfahren zur Optimierung von Gefriertrocknungsprozessen, Dissertation zur Erlangung des Doktorgrades, Fakultät für Chemie und Pharmazie, Ludwig-Maximilians-Universität München, München, Germany, 2003.

35. Pikal, M.J.; Shah, S. Moisture transfer from stopper to product and resulting stability implications. *Dev. Biol. Stand.* **1992**, *74*, 165-77; discussion 177-9.

36. Kenkare, U.W.; Richards, F.M. The histidyl residues in ribonuclease-S. Photooxidation in solution and in single crystals; the iodination of histidine-12. *J. Biol. Chem.* **1966**, *241*, 3197–3206, doi:10.1016/S0021-9258(18)96515-4.

37. Fujimoto, S.; Nakagawa, T.; Ishimitsu, S.; Ohara, A. On the Mechanism of Inactivation of Papain by Bisulfite. *Chem. Pharm. Bull.* **1983**, *31*, 992–1000, doi:10.1248/cpb.31.992.

38. Mahler, H.-C.; Friess, W.; Grauschopf, U.; Kiese, S. Protein aggregation: Pathways, induction factors and analysis. *J. Pharm. Sci.* **2009**, *98*, 2909–2934, doi:10.1002/jps.21566.

39. Perevozchikova, T.; Nanda, H.; Nesta, D.P.; Roberts, C.J. Protein adsorption, desorption, and aggregation mediated by solid-liquid interfaces. *J. Pharm. Sci.* **2015**, *104*, 1946–1959, doi:10.1002/jps.24429.

40. Fujita, R.; Nagatoishi, S.; Adachi, S.; Nishioka, H.; Ninomiya, H.; Kaya, T.; Takai, M.; Arakawa, T.; Tsumoto, K. Control of Protein Adsorption to Cyclo Olefin Polymer by the Hofmeister Effect. *J. Pharm. Sci.* **2019**, *108*, 1686–1691, doi:10.1016/j.xphs.2018.12.023.

41. Eu, B.; Cairns, A.; Ding, G.; Cao, X.; Wen, Z.-Q. Direct Visualization of Protein Adsorption to Primary Containers by Gold Nanoparticles. *J. Pharm. Sci.* **2011**, *100*, 1663–1670, doi:https://doi.org/10.1002/jps.22410.

42. Yoneda, S.; Maruno, T.; Mori, A.; Hioki, A.; Nishiumi, H.; Okada, R.; Murakami, M.; Zekun, W.; Fukuhara, A.; Itagaki, N.; et al. Influence of protein adsorption on aggregation in prefilled syringes. *J. Pharm. Sci.* **2021**, doi:10.1016/j.xphs.2021.07.007.

Chapter III   Further Studies on Gas Permeability of Polymer Vials for Lyophilizates

III.1 Introduction

In chapter II, a packaging approach for lyophilizates in polymer vials was presented, which reduced oxidation of two monoclonal IgG1 antibodies to a minimum, similar to the level in glass vials. Nevertheless, the barrier properties and associated capability of absorbers in actually removing oxygen from the headspaces of the lyophilizates are not fully understood. Hence, this chapter focuses on the technical details of removing oxygen from the vials.

It has been shown before that by selecting a suitable secondary packaging for primary containers made of polymeric materials, oxidation can be successfully suppressed [1–4]. The studies examined liquid formulations in COP syringes and were either stored in aluminum pouches filled with nitrogen [1,4] or comprised of an oxygen absorber in a blister pack [2,3]. However, container closure and other characteristics of prefilled syringes (PFS) differ in several aspects from vials containing a lyophilizate, irrespective of the material they are composed of. While the vial is typically closed with a rubber stopper and sealed with a crimp cap, PFS comprise of multiple sealing areas, i.e., the injection needle and the syringe barrel [5]. The potential for escape of gases from the needle lumen [6] and through rubber materials in needle shields [7,8], as well as due to inappropriate plunger selection or movement [5,9] has been described. Thus, the vial configuration is typically considered less vulnerable to gas permeation compared to syringes, when comparing containers made of the same material.

Apart from that, vials are typically stoppered in a nitrogen atmosphere in the freeze dryer at the end of the lyophilization process. Consequently, oxygen concentration is already minimized right from the start of shelf life. In contrast, PFS are typically filled and sealed at atmospheric conditions, and filling in a nitrogen atmosphere [10] is rather an exceptional case. Besides, dissolved oxygen has been identified as one of the main root causes for protein oxidation in liquid formulations, next to radical generation by sterilization using irradiation [2,3,11,12]. On the contrary, the levels of dissolved oxygen in lyophilized drug products are expected to be extremely low due to the low residual moisture levels in the lyophilized drug product. As a result, product properties differ significantly when comparing PFS and vials containing a lyophilizate, even if the primary containers are composed of the same material, and therefore transfer of study results from one format to the other has to be done carefully.

Moreover, limited literature is available on permeability of primary containers for pharmaceuticals made of cyclic olefin polymers (COP) and copolymers (COC). It has been shown for cyclic olefin copolymer (COC) that permeability coefficients are strongly dependent on the chemical structure of the polymer, i.e., backbone constituents [13]. In [14], a model was developed for CZ® resin vials made of a high-quality COP, which describes the permeation of oxygen and nitrogen, assuming the vials contain a liquid fill. The authors found that the permeability of oxygen through the CZ® resin material is significantly higher compared to nitrogen. However, permeation behavior might differ when comparing a liquid formulation and a lyophilizate in a vial, as the liquid system shows three interfaces in total, i.e., the liquid-gas interface, the gas-solid interface at the inner wall of the vial, and the liquid-solid interface. In comparison, the lyophilizate system consists of only the gas-solid interface, assuming that residual moisture is very low [15], and the gap between the cake and the vial wall is also accessible for gases through the porous structure of the lyophilizate, and even more if the cake detached from the inner vial wall [16].

In this study, the permeability of COP vials containing a lyophilizate was investigated. The effect of headspace pressure was assessed, and the capability of the Pharmakeep® absorbers in controlling oxygen in the smart packaging was reaffirmed. Moreover, it was shown that oxygen can be actively removed from the headspace of the vial, as previously described for liquid formulations [1,2,4]. Additionally, the gas exchange from inside the vial to the exterior was found to be efficient for the smart packaging with an absorber, and permeability was not improved when an oxygen scavenging liquid was surrounding the vial in the pouch.

III.2 Materials and Methods

III.2.1 Chemicals

L-histidine monohydrochloride monohydrate (99% purity) and L-histidine (cell culture reagent) were purchased from Alfa Aesar (Ward Hill, MA, USA). D(+)-trehalose dihydrate (97.0–102.0% purity) Ph. Eur., NF certified was purchased from VWR International (Radnor, PA, USA). TWEEN® 20 Ph. Eur. certified, sodium sulfite BioUltra grade, and Cobalt standard for ASS were purchased from Sigma-Aldrich (Steinheim, Germany). Ultrapure water was collected from an Arium® system of Sartorius Lab Instruments GmbH (Goettingen, Germany).

III.2.2 Preparation of the Formulations

The experiments were carried out with a placebo formulation. Stock solutions of the excipients were prepared in 20 mM histidine buffer and mixed so that the final formulation contained 210 mM trehalose and 0.04% polysorbate 20 (*w/V*) at pH 5.5. Prior to filling the vials, the formulation was sterile filtered using a 0.22 µm Sartolab® RF polyethersulfone vacuum filtration unit (Sartorius AG, Goettingen, Germany). 6R tubing vials made from cyclic olefin polymer (COP Monolayer, Gerresheimer AG, Duesseldorf, Germany) were filled with 2.5 mL of the formulation, resulting in circa 188 mg of dried cake following the drying process. Subsequently, the vials were semi-stoppered with lyophilization stoppers (Flurotec® laminated rubber stoppers, West Pharmaceutical Services, Inc, Exton, PA, USA).

III.2.3 Lyophilization Process

The lyophilization process was performed four times to generate different starting conditions regarding the gas composition and pressure in the vial headspaces. It was either conducted on an FTS LyoStar™ 3 freeze-dryer (SP Scientific, Stone Ridge, NY, USA) or on a Christ ε2-6D (Martin Christ, Osterode am Harz, Germany) laboratory-scale freeze-dryer. The freezing step was carried out as suggested in [15], with prolonged time intervals for the shelf cooling steps at 5°C and -5°C, i.e., 45 minutes. The final freezing temperature of -50°C was held for 3 hours to ensure complete freezing. Set points for primary drying were a shelf temperature of -20°C at 67 mTorr. Comparative pressure measurement was applied to determine the end of the primary drying step (Pirani/capacitance difference of 5%). Next, the shelf temperature was increased to 5°C (ramp 0.15 K/min) and subsequently 30°C (ramp 0.21 K/min) for secondary drying. After 7 hours at this setpoint, the lyophilization process was completed and the vials were stoppered inside the chamber. For this, different protocols were applied: A) vials were stoppered in a nitrogen atmosphere at 600 mbar or 1000 mbar, and B) the chamber was vented with compressed air and vials were stoppered at 800 mbar or 1000 mbar. Following this, the vials were crimped with Flip-Off® seals (West Pharmaceutical Services, Inc, Exton, PA, USA).

III.2.4 Study Design

The study was carried out in three parts. In part I, vials that were stoppered under nitrogen at 600 mbar and 1000 mbar were processed as follows: COP vials were either stored without secondary packaging (COP-A-P), or sealed in aluminum pouches (Floeter Verpackungsservice, Eberdingen, Germany) with one (COP+A+P) or four (COP+4A+P) absorbers (Pharmakeep®, Mitsubishi Gas Chemicals, Tokyo, Japan) enclosed. The pouches

were heat sealed and contained a volume of approximately 80 mL of ambient air. The absorbers used were combined oxygen and moisture absorbers, so that the air within the smart packaging was also dehumidified for the storage of the moisture-sensitive cakes.

In part II of the study, the samples that were stoppered at 800 mbar in a compressed air environment were stored either without secondary packaging (COP-A-P) or with one (COP+A+P) or four (COP+4A+P) absorbers. Additionally, the vials stoppered at 1000 mbar under compressed air were sealed in aluminum pouches with one absorber (COP+A+P). For more convenient reading, the above-mentioned abbreviations are used in the following text, where "A" stands for absorber, and "P" is a shortcut for aluminum pouch.

In part III, the vials stoppered at 600 mbar in a nitrogen atmosphere were sealed in aluminum pouches containing either "oxygen-rich" or "oxygen-free" ultrapure water. The former was produced by blowing air into the water while it was simultaneously stirred. The deoxygenated water was prepared by dissolving sodium sulfite and cobalt nitrate in highly purified water, followed by shaking according to [17]. Prior to filling the water into the pouches, oxygen concentrations were controlled.

For all studies, the samples were stored at 4°C, 25°C, and 40°C for the desired time without controlling relative humidity.

III.2.5 Oxygen Quantification

The oxygen concentration in the air enclosed in the aluminum pouches, in the water sealed within the pouches, and in the headspaces of the lyophilizates was assessed using a Microx 4 fiber optic oxygen meter (PreSens Precision Sensing GmbH, Regensburg, Germany). Firstly, measurements were conducted in the pouches, and after removal of the vial from the secondary packaging, oxygen levels within the headspaces were immediately measured. For this, the plastic cap of the Flip-Off® seal was removed, and the needle-shielded oxygen sensor was introduced into the headspace through the rubber stopper.

III.2.6 Karl–Fischer Titration

The residual moisture content of the lyophilizates was determined by using coulometric Karl–Fischer titration. In a glove box filled with pressurized air (relative humidity < 10%), the cakes were gently crushed and approximately 70 mg of each cake was transferred into 2R vials. The water was extracted by heating up the sample in the device's oven (temperature setpoint 100°C) and transferred to the coulometric titration cell with a dry carrier gas flow (Aqua 40.00 Vario plus, ECH Elektrochemie Halle GmbH, Halle (Saale), Germany). Relative moisture content was calculated (*m/m*). Prior to sample analysis, the Apura® water

standard oven 1% (Merck KGaA, Darmstadt, Germany) was measured in duplicate to ensure the correct performance of the device.

III.3 Results & Discussion

III.3.1 Effect of the Pressure Inside the Vial (part I)

Vials are typically sealed under nitrogen at reduced pressure following the lyophilization process to optimize protein stability and ensure container closure integrity by better holding the stopper in place. To investigate whether the vacuum inside the vial has a regressive effect on gas permeation through the vial wall, vials were stoppered under nitrogen at atmospheric pressure. Additionally, to study the role of absorbers' capacity for the smart packaging, it was equipped with one and four absorbers, respectively.

The aluminum pouches were sealed at ambient conditions, to test the absorbers' ability in capturing oxygen in a worst-case scenario. Starting from 20.8% in the pouches right after sealing, oxygen was quickly reduced to less than 0.5% within one week at all storage temperatures (Figure III.1). Moreover, four absorbers did not perform better compared to one absorber in the respective pouches. Keeping in mind the intended volume of enclosed air is very important when it comes to the choice of an absorber type and number. In this study, around 80 mL of air were enclosed in each aluminum pouch. Thus, with a specified capacity of 20 mL oxygen for a Pharmakeep® absorber, circa 20% of the absorbers' capacity remained unused in the tightly sealed aluminum pouches, serving as a safety margin throughout the study. Increasing the number of absorbers did not improve the oxygen removal from the pouches, at least within a time frame of one week. However, if the volume of air would be increased in other configurations, the limit of capacity of the used absorbers has to be carefully evaluated.
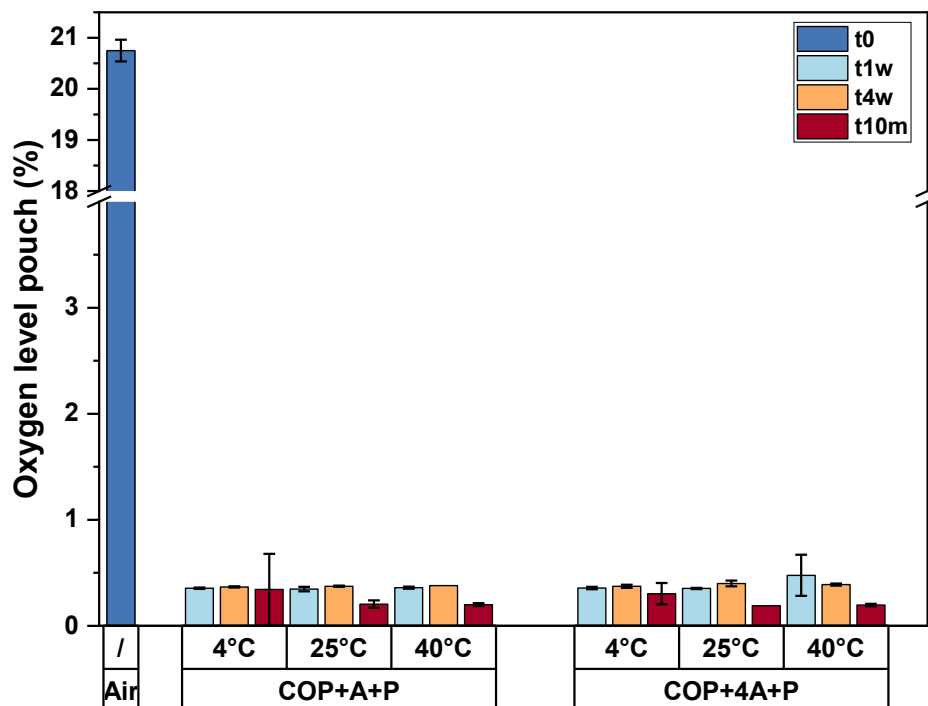
Figure III.1 Oxygen levels in the aluminum pouches. After sealing at room air (dark blue, t0), pouches with one absorber (COP+A+P) and four absorbers enclosed (COP+4A+P) were stored at 4 °C, 25 °C, and 40 °C. The bars are means of three individual pouches; the error bars represent the standard deviation. COP, cyclic olefin polymer; A, absorber; P, pouch.

The oxygen level in the headspaces of COP vials was $0.56\% \pm 0.01\%$ after stoppering in a nitrogen atmosphere following the freeze-drying cycle (t0, Figure III.2). When stored without a secondary packaging (COP-A-P), oxygen quickly permeated into the vial (COP-A-P, Figure III.2). Oxygen levels in the headspaces correlated well with storage time and temperature: After 10 months, $12.93\% \pm 0.15\%$ oxygen were found in samples stored at 4 °C, and almost equaled atmospheric concentration after storage at 40 °C ($18.83\% \pm 0.06\%$). Based on the data it appears that oxygen ingress is almost linear in the first weeks (e.g., 0.56% per week at 40 °C) and then decelerates towards equilibrium. This is consistent with the findings in [14], as the driving force for permeation is the difference in partial pressure on both sides of the membrane. When oxygen permeates into the vial, the driving force is reduced until oxygen partial pressure inside the vial equals the outside. According to [11] oxygen concentration increases exponentially inside the vial headspace and can be expressed as a function of time using Eq. 1.

$$C_i = C_o(1 - e^{-Kt}) \qquad (1)$$

where: C_i is the oxygen concentration in the vial headspace, C_o is the concentration of oxygen outside the vial (atmospheric), and K represents the rate constant.

In the smart packaging, headspace oxygen is well controlled throughout the study (COP+A+P and COP+4A+P, Figure III.2). Looking at the data from the first week, it appears that a small amount of oxygen permeates into the vial in the configuration with one absorber at 25 °C and 40 °C (COP+A+P, light blue bar). This effect is not seen in the configuration with four absorbers (COP+4A+P). However, after four weeks, headspace oxygen is stabilized and low in all configurations, i.e., $\leq 1.2\%$, and was further reduced within 10 months (yellow and red bars, COP+A+P and COP+4A+P).
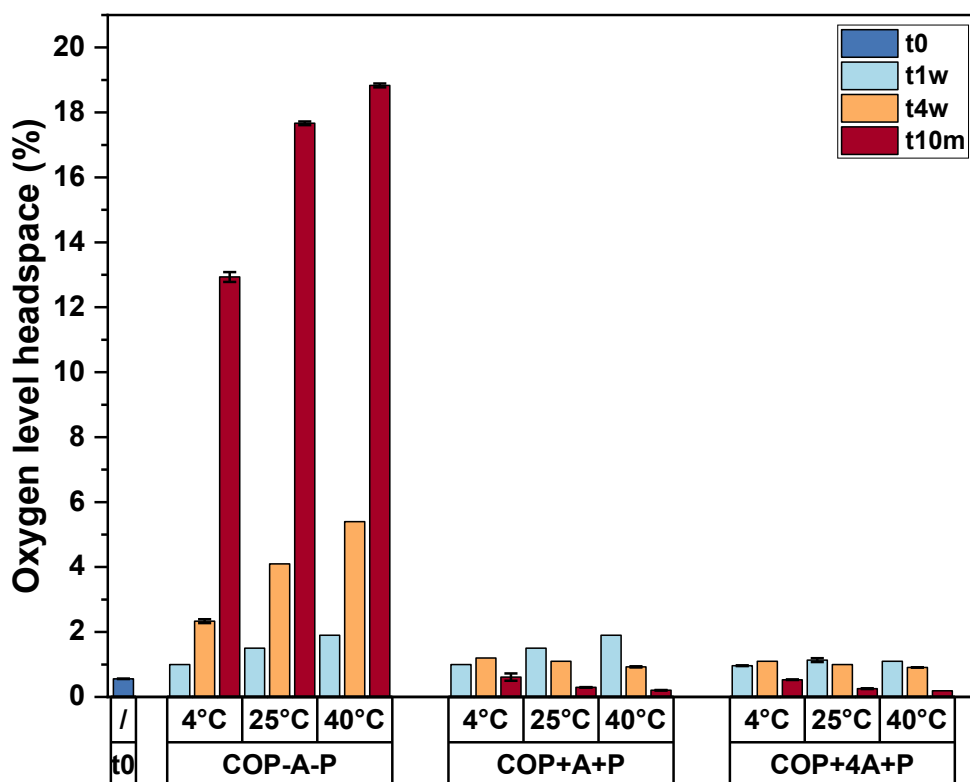
Figure III.2 Oxygen concentrations in the headspaces of the vials throughout the stability study. Vials were stoppered in a nitrogen atmosphere at 1000 mbar and subsequently stored at 4 °C, 25 °C, and 40 °C for 10 months. The bars are means of three individual vials; the error bars represent the standard deviation. COP, cyclic olefin polymer; A, absorber; P, pouch.

Next, to investigate the effect of the pressure within the vial on gas diffusion, oxygen levels in the headspaces after stoppering at two different pressures were compared. Data from samples stoppered at 600 mbar and 1000 mbar and stored at 25 °C, and 40 °C for four weeks were collected (Table III.1). While the oxygen levels directly after stoppering were comparable (t0, Table III.1), a trend towards slightly higher headspace oxygen levels in vials stoppered at atmospheric pressure was observable after four weeks for both, the positive control (COP-A-P) and the smart packaging (COP+A+P). However, the net increase in

oxygen concentration was by far higher when COP vials were stored without a secondary packaging. Consequently, gas exchange appears to be easier when vials are stoppered at atmospheric pressure. Given that gas permeability through the vial/stopper/flip-off cap system is almost zero, permeation of gases in COP vials is mainly through the polymer matrix. The diffusion through polymers resembles diffusion through a liquid solution and is therefore directed from the side of higher partial pressure to the low-pressure side [18]. If the vials were sealed under vacuum at 600 mbar in the experiment, gas exchange of nitrogen from the region of higher partial pressure inside the vial to the outside is impeded by the overall vacuum within the vial, and by this the nitrogen permeation to the vial outside and exchange with oxygen is slowed down. When the vials were stoppered at atmospheric pressure, permeation is not impeded by a vacuum and thus gas exchange is without hindrance. Oxygen that is not captured by an absorber diffuses into the vial. As a consequence, stoppering under vacuum seems to pose an additional safety attribute for maintaining drug product quality after lyophilization in COP vials.

Table III.1 Oxygen concentrations in the headspaces following lyophilization (t0) and after four weeks at the respective storage temperatures. Vials were stoppered in a nitrogen atmosphere at either 600 mbar or 1000 mbar. The values are the mean of three individual vials. The error represents the standard deviation of the mean. COP, cyclic olefin polymer; A, absorber; P, pouch.

		Headspace oxygen %			
	t0	COP-A-P		COP+A+P	
		25 °C	40 °C	25 °C	40 °C
600 mbar	0.64 ± 0.03	3.34 ± 0.15	4.85 ± 0.43	0.66 ± 0.05	0.36 ± 0.05
1000 mbar	0.56 ± 0.01	4.10 ± 0.00	5.40 ± 0.00	1.1 ± 0.00	0.93 ± 0.02

In [19] COP vials were likewise stoppered in a nitrogen atmosphere and subsequently stored in an oxygen rich environment ($\geq 75\%$ oxygen) to evaluate permeability of the material. The oxygen level was many times higher after storage for four weeks at 40°C ($40.68\% \pm 0.17\%$) compared to this study. However, such high oxygen concentrations surrounding the vial represent an artificial environment, while the above-mentioned data from this study can give guidance on permeation behavior in a more realistic storage setup.

III.3.2 Removal of Oxygen from the Headspaces (Part II)

In a further experiment, the ability to remove oxygen from the vial headspace within the smart packaging was evaluated. For this, the lyophilizer was flushed with compressed air instead of nitrogen following the lyophilization process. The advantage of using compressed air over ambient air is its low moisture content (i.e., circa 5% relative humidity). By using

the former, one can avoid collapse of the lyophilizates during storage due to increased residual moisture levels. The vials were then either stoppered at 800 mbar or at atmospheric pressure (1000 mbar) and sealed in aluminum pouches with one or four absorbers (800 mbar headspace pressure) or one absorber (1000 mbar headspace pressure), respectively (Figure III.3).
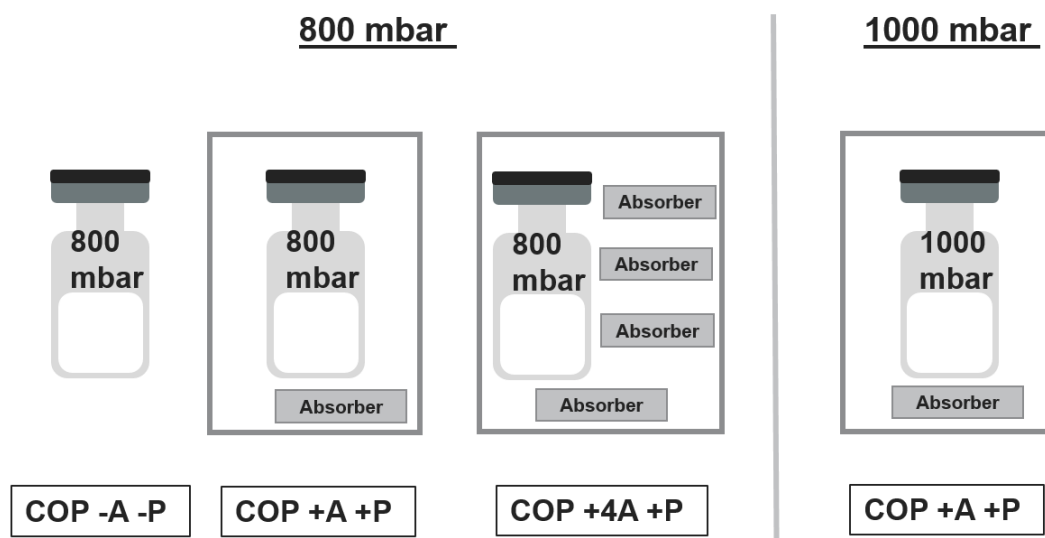
Figure III.3 Schematic overview of the configurations investigated in the study. Vials were sealed at either 800 mbar or 1000 mbar in pressurized air. In case of the smart packaging the aluminum pouches were equipped with one or four combined oxygen and moisture absorbers. The grey rectangle represents the aluminum pouch. COP, cyclic olefin polymer; A, absorber; P, pouch.

The aluminum pouches were again sealed at ambient conditions to test the packaging configurations in a worst-case scenario. Oxygen level of ambient air in the pouches was 20.7% right after sealing (t0, Figure III.4). Irrespective of the vial configuration and absorber amount, oxygen was reduced to < 0.4% within four weeks at all storage temperatures (Figure III.4). Already after one week of storage the absorber captured almost all the oxygen enclosed in the pouch, only for the vials stoppered at atmospheric pressure and stored at 4°C slightly higher values were found after one week (1.4% ± 0.3%, Figure III.4B).
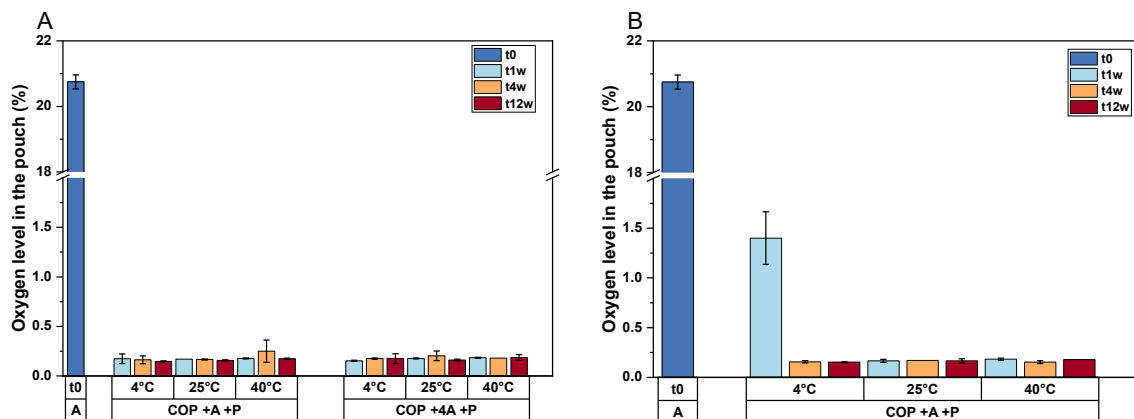
Figure III.4 Oxygen levels in the aluminum pouches. The pouches contained one (COP+A+P) or four (COP+4A+P) Pharmakeep® absorbers and a vial that was stoppered in a compressed air environment at (A) 800 mbar and (B) 1000 mbar. After sealing of the pouches at room air conditions (dark blue, t0), pouches were stored at 4 °C, 25 °C, and 40 °C. The bars are means of three individual pouches; the error bars represent the standard deviation. COP, cyclic olefin polymer; A, absorber; P, pouch.

The oxygen levels in the headspaces of the vials equaled atmospheric concentration after stoppering under compressed air (t0, Figure III.5). If the vials were stored without secondary packaging (COP-A-P), oxygen concentration was constantly high at room air level throughout the study due to the gas exchange with surrounding ambient air.

When the vials were stoppered at 800 mbar and stored within the aluminum pouch with one (COP+A+P) and four absorbers (COP+4A+P), respectively, oxygen was quickly removed from the headspaces. Reduction in headspace oxygen correlated with storage temperature and significantly reduced levels were found after four weeks at all storage temperatures. The configuration with four absorbers did not perform better compared to the pouches equipped with one absorber, and similar, strongly reduced oxygen levels were found after 3 months at 40 °C (8.45% ± 0.15% for COP+A+P and 8.73% ± 0.01% for COP+4A+P). When vials were stoppered at 1000 mbar, the reduction in headspace oxygen was even more pronounced, as only approximately 20% of the initial oxygen concentration is found in the headspace after 3 months at 40°C (4.63% ± 0.1%).
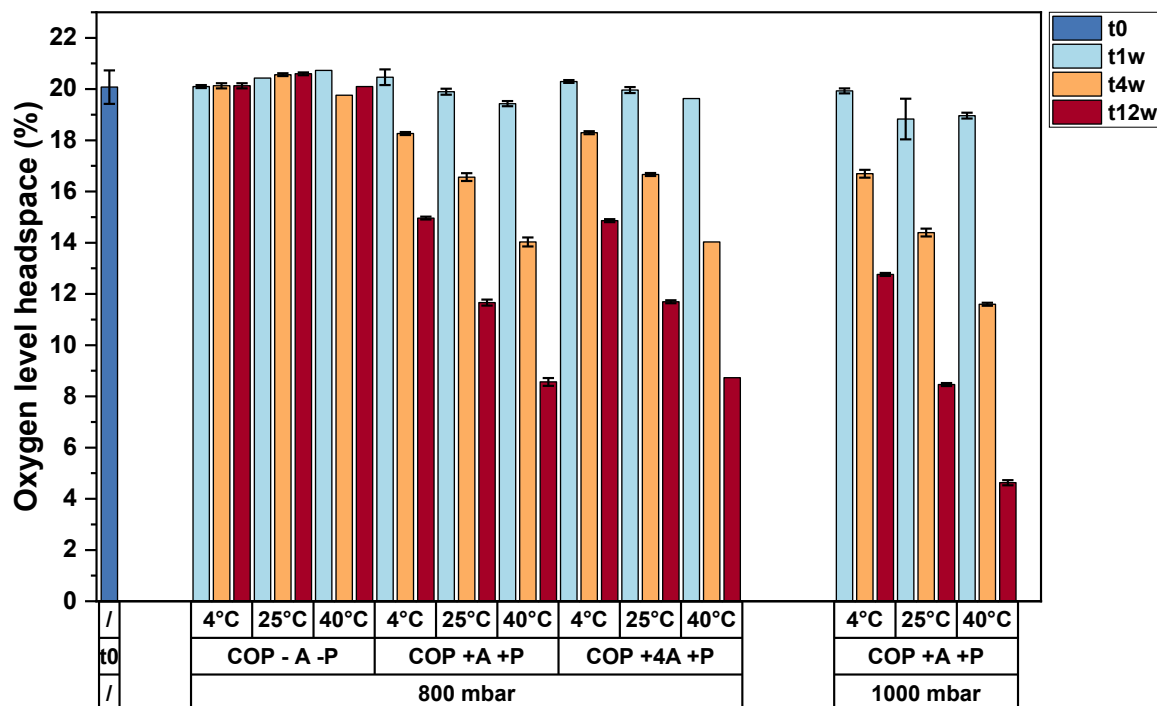
Figure III.5 Oxygen concentrations in the headspaces after stoppering in a compressed air environment and subsequent storage at 4 °C, 25 °C, and 40 °C for up to 12 weeks. Vials were stoppered either at 800 mbar or at 1000 mbar. The bars are means of three individual vials; the error bars represent the standard deviation. COP, cyclic olefin polymer; A, absorber; P, pouch.

Considering the results of the study three implications can be made: Firstly, oxygen can be actively removed from the vial headspace by using oxygen absorbers, as shown for liquid formulations in prefilled syringes [2]. Secondly, if the absorbers' capacity is chosen properly with regard to the intended volume of the pouch, permeation rate is solely affected by the storage temperature. With increasing temperature, permeability increases presumably due to the increased mobility of the gas. And thirdly, as likewise observed in the aforementioned study (Table III.1), vacuum inside the headspace decelerates gas permeation from inside the vial to the outside and by that gas exchange.

Next, in Table III.2, data for the COP vials were compared to previously published results from studies with prefilled COP syringes stored in different secondary packaging configurations [1,2,4]. The studies investigated the concentration of dissolved oxygen within the solution in the prefilled syringes. In [2] a quite similar approach to this study was taken: a blister package was equipped with an oxygen sensor, while in [1,4] aluminum pouches were flushed with nitrogen prior to sealing. In all studies, oxygen concentration equaled

atmospheric concentration at the start of the study. After 12 weeks of storage at 25°C oxygen levels in the primary packaging differed across the studies.

However, direct comparison of gaseous oxygen concentrations in the headspace with dissolved oxygen in solution is difficult, as dissolved oxygen in the liquid is in balance with the oxygen concentration in the entrapped air between the liquid and the rubber plunger stopper, dependent on the surrounding temperature. In [1] all trapped air was removed during the stoppering process, while in [2,4] a specific air headspace remained between the liquid and the stopper. Qadry et al. [14] assumed that gas permeation from inside the vial to the outside occurs only at the solid–gas interface in a vial containing a liquid. Consequently, as headspace volumes differed in the studies with COP syringes, different oxygen concentrations were found after a certain time interval, with the lowest reduction in [1] where no headspace was present. If a certain air volume was kept between the liquid and the plunger, oxygen presumably permeated from the syringe headspace into the secondary packaging and by this, oxygen from the liquid is shuttling into the gaseous phase and a new intermediate equilibrium is established. In lyophilizates almost no dissolved oxygen is present, as residual moisture is very low (i.e., typically < 0.5% [15]). In this study, residual moisture after lyophilization was $0.68\% \pm 0.01\%$ (m/m). Each vial contained roughly 200 mg of lyophilized powder. Considering an oxygen solubility of 9.1 mg/L in pure water at 20°C [20], approximately 0.06 ppm oxygen were present in the residual moisture of the cake. Consequently, solubilized oxygen can be neglected in lyophilizates with low moisture levels and gas exchange may occur through the whole vial body except for the stopper area, provided that there is no gas permeation through the stopper.

Thus, the surface area available for gas exchange also plays an important role when comparing different packaging materials. When increasing available surface area of a container made of a certain material, gas exchange may increase. In this study, the surface area of the COP vial was calculated using its body and neck height and diameter, respectively. The inner surface area of the vials used was 2.14×10^3 mm^2. For the prefilled syringes in [4] an inner surface area of 0.90×10^3 mm^2 was calculated, while according to the given fill volume the available headspace area was approximately 0.11×10^3 mm^2. Calculations for [1,2] were not possible considering the published data. However, although the inner surface area of the vial is more than twice the surface area of the prefilled syringe, stronger reduction of oxygen was observed for the prefilled syringes (Table III.2, [4]). Another reason for this observation was considered to be the wall thickness of the containers,

but this parameter was quite comparable for both container types (1.8 mm for the prefilled syringe and 1.5 mm for the vial). Lastly, the observed differences in oxygen removal across the studies may be attributable to the container closure integrity of the primary packaging formats. For the container closure combination investigated in this study, the dye ingress test was passed according to the European Pharmacopoeia [21]. Given that there is no gas diffusion through the stopper in the vial, quite substantial oxygen amounts were removed from the vial compared to the different syringe configurations, which are typically more prone to gas exchange due to multiple sealing areas.

Table III.2 Comparison of published data on COP syringes in secondary packaging systems with the COP vial data from this study. Oxygen data from [2] and [4] were derived from figures and converted from mg/L to % oxygen assuming the measurement was carried out at 20°C at atmospheric pressure. In [1] all entrapped air was removed during the stoppering.

			Nakamura et al. [2]	Stelzl [4]	Werner et al. [1]	This study
Primary container			COP syringe			COP vial
Secondary packaging			Blister package with oxygen absorber	Aluminum pouch with gaseous nitrogen		Aluminum pouch with combined oxygen and moisture absorber
Oxygen measured			Dissolved oxygen in solution			Gaseous oxygen in the headspace
Mean oxygen concentration in solution (%)	At the start of the stability study	mg/L	9.0	8.2	8.3*	N/A
		%	20.8*	19.1*	19.2	
	After 12 weeks at 25°C	mg/L	0.0	1.2	6.8*	N/A
		%	0.0*	2.8*	15.7	
Approximate reduction (%)			20.8	16.3	3.5	
Mean oxygen concentration in the headspace (%)	At the start of the stability study		N/A			20.1
	After 12 weeks at 25°C		N/A			8.5
Approximate reduction (%)						11.6

* Calculated values.

III.3.3 Effect of Different Forms of Matter on Diffusion (Part III)

In a third experiment it was investigated, whether there is a difference in gas permeability of the COP material when a liquid phase is adjacent to the vial (i.e., a vial in an aluminum pouch filled with a liquid), compared to a gaseous phase (i.e., a vial in the pouch with enclosed air and an oxygen absorber). The configuration was studied, as it is analogous to prefilled syringes containing a liquid formulation and stored in pouches with nitrogen gas enclosed. For this purpose, the vials were sealed in pouches that were filled with deoxygenated water and oxygen rich water, respectively.

The oxygen-rich water contained 21.3% oxygen directly after sealing of the pouches and was slightly reduced within storage (17.7% ± 0.7% after 10 months at 40°C), as oxygen from the water permeated into the headspace of the vial (Figure III.6). Corresponding increase in headspace oxygen correlated with storage temperature and time, and almost equaled the oxygen concentration in the liquid after 10 months at 40°C (15.4% ± 0.7%). This is slightly lower compared to vials stoppered at 1000 mbar and stored at ambient air without a secondary packaging (18.8% ± 0.05% after 10 months at 40°C, see Figure III.2.) However, as oxygen concentration in the water reduces as equilibration with the vial headspace takes place, the partial pressure of oxygen decreases and with it the driving force for gas permeation. Besides, no distinct difference in gas permeability was observed within the first week of storage when a liquid phase was adjacent to the polymer matrix compared to a gaseous phase (1.3% ± 0.2% when the vials were stored at 40°C in oxygen rich water, 1.9% ± 0.0% when stored at 40°C without secondary packaging). Consequently, permeability of the polymer material is not depending on the phase of matter adjacent to it (i.e., liquid or gaseous).

The deoxygenated water was almost oxygen free at the start of the stability study and oxygen levels remained low within 10 months of storage, due to the low permeability and tight sealing of the aluminum pouches (Figure III.6). Similar to the storage of the lyophilizate in the smart packaging with an oxygen absorber, oxygen levels in the headspace were low and well controlled.
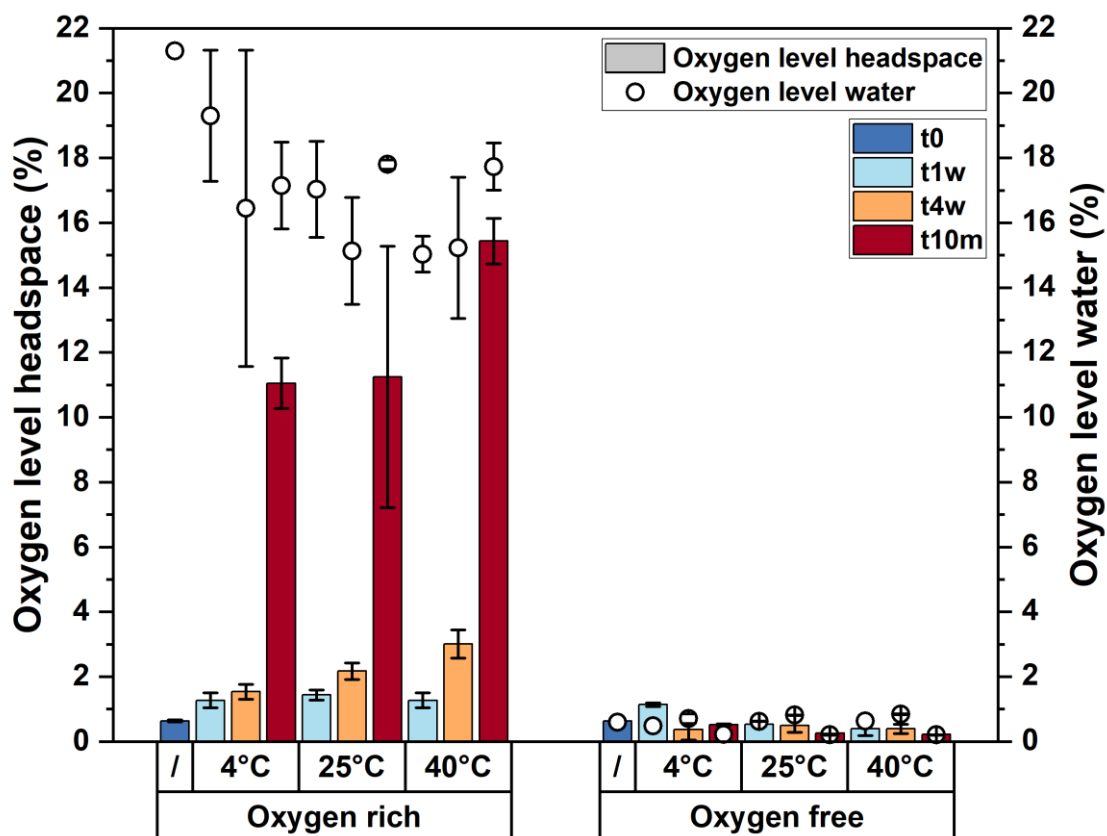
Figure III.6 Oxygen levels in the headspaces of the vials and in the water the pouches were filled with. Samples were stoppered in a nitrogen atmosphere at 600 mbar following the lyophilization process and stored in oxygen-rich or oxygen-free water, respectively. The values are means of three individual samples. The error represents the standard deviation of the mean.

III.4 Conclusion

The aim of this study was to investigate permeability of COP vials in the context of lyophilization. It was found that gas permeation is not only depended on the partial pressure of the gas on both sides of the vial wall (i.e., interior and exterior), the absolute pressure inside the headspace also impacted permeability. With lower pressure in the vial headspace, gas exchange was slowed down. Since vials are typically stoppered under vacuum in a nitrogen atmosphere following the lyophilization process, this helps to protect the final product from oxygen ingress. Comparable to other studies [1,2,4] with liquid formulations in COP syringes, it was possible to remove oxygen from the vial headspace by an absorber. Thus, if oxygen would accidentally get into the headspace following the freeze-drying process, it can be removed by the absorber. This poses a safety aspect when the smart packaging is used for drug products in COP vials. However, reduction of headspace oxygen was slower compared to some studies with prefilled syringes, which may be attributable to

the tightness of the vial-stopper system compared to syringes with multiple sealing areas. Besides, there was no difference in the gas exchange through the COP vial if a liquid is adjacent to the material compared to a gaseous phase. Consequently, the use of absorbers is a suitable and convenient approach for overcoming permeability issues that hamper the use of polymer vials in lyophilization, and helps to protect drug product quality, as shown for liquid formulations in COP syringes [2,3].

III.5 Acknowledgements

III.6 References

1. Werner, B.P.; Schöneich, C.; Winter, G. Silicone Oil-Free Polymer Syringes for the Storage of Therapeutic Proteins. *J. Pharm. Sci.* **2019**, *108*, 1148–1160, doi:10.1016/J.XPHS.2018.10.049.

2. Nakamura, K.; Abe, Y.; Kiminami, H.; Yamashita, A.; Iwasaki, K.; Suzuki, S.; Yoshino, K.; Dierick, W.; Constable, K. A Strategy for the Prevention of Protein Oxidation by Drug Product in Polymer-Based Syringes. *PDA J. Pharm. Sci. Technol.* **2015**, *69*, 88–95, doi:10.5731/pdajpst.2015.01009.

3. Masato, A.; Kiichi, F.; Uchiyama, S. Suppression of Methionine Oxidation of a Pharmaceutical Antibody Stored in a Polymer-Based Syringe. *J. Pharm. Sci.* **2016**, *105*, 623–629, doi:10.1002/jps.24675.

4. Stelzl, A. Subcutaneous delivery of high concentrated mAb-formulations using novel application systems, Ph.D. Thesis, Ludwig-Maximilians-Universität, München, Germany, 2021.

5. Peláez, S.S.; Mahler, H.C.; Matter, A.; Koulov, A.; Singh, S.K.; Germershaus, O.; Mathaes, R. Container Closure Integrity Testing of Prefilled Syringes. *J. Pharm. Sci.* **2018**, *107*, 2091–2097, doi:10.1016/j.xphs.2018.03.025.

6. Scheler, S.; Knappke, S.; Schulz, M.; Zuern, A. Needle clogging of protein solutions in prefilled syringes: A two-stage process with various determinants. *Eur. J. Pharm. Biopharm.* **2022**, *176*, 188–198, doi:10.1016/j.ejpb.2022.05.009.

7. De Bardi, M.; Müller, R.; Grünzweig, C.; Mannes, D.; Rigollet, M.; Bamberg, F.; Jung, T.A.; Yang, K. Clogging in staked-in needle pre-filled syringes (SIN-PFS): Influence of water vapor transmission through the needle shield. *Eur. J. Pharm. Biopharm.* **2018**, *127*, 104–111, doi:10.1016/j.ejpb.2018.02.016.

8. Thakare, V.; Mayr, B.; Artenjak, A.; Nianios, D.; Sest, M.; Müller, M.; Maltsev, O. V.; Nowicki, K.; Mischo, A.; Ehrenstrasser, C.; et al. Investigation of drug product and container-closure interactions: A case study of diluent containing prefilled syringe. *Eur. J. Pharm. Biopharm.* **2019**, *140*, 67–77, doi:10.1016/j.ejpb.2019.04.018.

9. Sacha, G.; Rogers, J.A.; Miller, R.L. Pre-filled syringes: a review of the history, manufacturing and challenges. *Pharm. Dev. Technol.* **2015**, *20*, 1–11, doi:10.3109/10837450.2014.982825.

10. Larmené- Beld, K.H.M.; van Berkel, S.; Wijnsma, R.; Taxis, K.; Frijlink, H.W. Prefilled Cyclic Olefin Sterilized Syringes of Norepinephrine Injection Solution Do Not Need to Be Stabilized by Antioxidants. *AAPS PharmSciTech* **2020**, *21*, 247, doi:10.1208/s12249-020-01784-z.

11.   Yoneda, S.; Torisu, T.; Uchiyama, S. Development of syringes and vials for delivery of biologics: current challenges and innovative solutions. *Expert Opin. Drug Deliv.* **2021**, *18*, 459–470, doi:10.1080/17425247.2021.1853699.

12.   Nakamura, K.; Yoshino, K.; Okihara, H.; Yoshimoto, T.; Iwasaki, K.; Abe, Y.; Yoshimoto, T.; Suzuki, S. Advantage of plastic prefilled syringes in the biopharmaceutical product. Available online: https://www.researchgate.net/profile/Keisuke-Yoshino-2/publication/271518798_Advantage_of_plastic_prefilled_syringes_in_the_biopharmaceutical_product/links/54cabf100cf2517b75600aeb/Advantage-of-plastic-prefilled-syringes-in-the-biopharmaceutical-product.p (accessed on Oct 24, 2023).

13.   Hu, C.C.; Lee, K.R.; Ruaan, R.C.; Jean, Y.C.; Lai, J.Y. Gas separation properties in cyclic olefin copolymer membrane studied by positron annihilation, sorption, and gas permeation. *J. Memb. Sci.* **2006**, *274*, 192–199, doi:10.1016/j.memsci.2005.05.034.

14.   Qadry, S.S.; Roshdy, T.H.; Knox, D.E.; Phillips, E.M. Model development for O2 and N2 permeation rates through CZ-resin vials. *Int. J. Pharm.* **1999**, *188*, 173–179, doi:10.1016/S0378-5173(99)00220-3.

15.   Tang, X. (Charlie); Pikal, M.J. Design of Freeze-Drying Processes for Pharmaceuticals: Practical Advice. *Pharm. Res.* **2004**, *21*, 191–200, doi:10.1023/B:PHAM.0000016234.73023.75.

16.   Patel, S.M.; Nail, S.L.; Pikal, M.J.; Geidobler, R.; Winter, G.; Hawe, A.; Davagnino, J.; Rambhatla Gupta, S. Lyophilized Drug Product Cake Appearance: What Is Acceptable? *J. Pharm. Sci.* **2017**, *106*, 1706–1721, doi:10.1016/J.XPHS.2017.03.014.

17.   PreSens Precision Sensing GmbH How can I prepare the calibration solutions cal0 and cal100 for oxygen sensors? Available online: https://www.presens.de/support-services/faqs/question/how-can-i-prepare-the-calibration-solutions-cal0-and-cal100-for-oxygen-sensors-35 (accessed on Oct 29, 2021).

18.   Treybal, R.E. Diffusion in Solids. In *Mass-Transfer Operations*; McGraw-Hill, 1980; pp. 93–94.

19.   Werner, B.P. Filtration and novel polymeric containers for the improved quality of biotech drug products. PhD Thesis, Ludwig-Maximilians-Universität, München, Germany, 2017.

20.   Battino, R.; Rettich, T.R.; Tominaga, T. The Solubility of Oxygen and Ozone in Liquids. *J. Phys. Chem. Ref. Data* **1983**, *12*, 163–178, doi:10.1063/1.555680.

21.   3.2.9. RUBBER CLOSURES FOR CONTAINERS FOT AQUEOUS PARENTERAL PREPARATIONS FOR POWDERS AND FOR FREEZE-DRIED POWDERS. In *Eur. Pharmacopoeia 7.0,* 2011, 374–376.

Chapter IV Accelerated Production of Biopharmaceuticals via Microwave-Assisted Freeze-Drying (MFD)

This chapter is published as:

Author contributions:

N.H., R.G., I.P. and G.W. conceptualized the idea and planned the experiments. N.H. conducted the experiments and evaluated the data. N.H. wrote the manuscript. R.G., I.P. and G.W. provided scientific guidance, and reviewed and edited the manuscript.

The published article can be accessed online:

https://doi.org/10.3390/pharmaceutics15051342

Note from the authors:

The numbering of the subchapters, figures and tables was changed in comparison to the published version of the article, to fit the consecutive numbering of this thesis.

IV.1 Abstract

Recently, attention has been drawn to microwave-assisted freeze-drying (MFD), as it drastically reduces the typically long drying times of biopharmaceuticals in conventional freeze-drying (CFD). Nevertheless, previously described prototype machines lack important attributes such as in-chamber freezing and stoppering, not allowing for the performance of representative vial freeze-drying processes. In this study, we present a new technical MFD setup, designed with GMP processes in mind. It is based on a standard lyophilizer equipped with flat semiconductor microwave modules. The idea was to enable the retrofitting of standard freeze-dryers with a microwave option, which would reduce the hurdles of implementation. We aimed to collect process data with respect to the speed, settings, and controllability of the MFD processes. Moreover, we studied the performance of six monoclonal antibody (mAb) formulations in terms of quality after drying and stability after

storage for 6 months. We found drying processes to be drastically shortened and well controllable and observed no signs of plasma discharge. The characterization of the lyophilizates revealed an elegant cake appearance and remarkably good stability in the mAb after MFD. Furthermore, overall storage stability was good, even when residual moisture was increased due to high concentrations of glass-forming excipients. A direct comparison of stability data following MFD and CFD demonstrated similar stability profiles. We conclude that the new machine design is highly advantageous, enabling the fast-drying of excipient-dominated, low-concentrated mAb formulations in compliance with modern manufacturing technology.

Keywords: microwave; freeze-drying; lyophilization; monoclonal antibody; excipients; stability

IV.2 Introduction

To date, almost half of biopharmaceutical products are marketed in the form of dry, solid formulations [1], as they are not sufficiently stable in aqueous formulations over the intended shelf life [2,3]. Conventional freeze-drying (CFD), also known as lyophilization, is a well-established method of preserving sensitive protein drugs but comes with long process times and high energy consumption [3,4]. With emerging patient-centered drug manufacturing in the biopharmaceutical industry [5], small batch sizes create an increasing need for time-saving technologies and flexibility. Hence, numerous new drying technologies and approaches are being developed to speed up the lengthy process [1,6–9].

In this paper, we are neither focused on a particular formulation attempt to enable aggressive freeze drying [10–12], nor on the use of organic solvents [13–15] or continuous processes [16,17] but rather on a new solution to introduce sublimation energy faster and more effectively using microwaves. Due to the nature of microwave radiation, energy is directly transferred to the lyophilizates, resulting in volumetric heating [18]. This contrasts with CFD, where energy is delivered mainly through convection [19] and only partly through conduction and radiation. For more information on the basic principles of microwave-assisted freeze-drying (MFD), the reader is referred to [20]. While MFD is already widely used for quality foods [21,22], only a few studies have been published addressing its applications in bacterial cells [20,23]; vaccines and proteins [24,25]; and, specifically, monoclonal antibodies (mAbs) [26,27]. A few years back, Evans et al. first

introduced the technology in the field of pharmaceuticals and demonstrated its applicability to mAbs and a model vaccine [28]. Following this, Gitter et al. evaluated the stability of two monoclonal IgG1-type antibodies and found comparable stability profiles following MFD and CFD [26,27]. More recently, Bhambhani et al. proposed a first-principle model investigating the principles of microwave-assisted freeze-drying of proteins and a vaccine [24]. Furthermore, a mechanistic model was proposed by Park et al. [29]. In [25], the statistical electromagnetics theory was used to create efficient and uniform heating for myoglobin samples. Nevertheless, these previously described machines come with several drawbacks: (1) Samples have to be frozen externally and subsequently transferred to the microwave dryer because shelf-freezing within the cabinet is not feasible. (2) In-chamber stoppering after lyophilization is not possible with prototypes, meaning that vials have to be stoppered by hand at atmospheric pressure. In [25], an auxiliary chamber was inserted into a lab-scale freeze-dryer, and it remains an open question whether the vials are in direct shelf contact during freezing and if machine-stoppering the vials inside this chamber is possible. However, these features are indispensable for implementation in a GMP environment. There is a definite need for much better-controlled processes (i.e., the loading of the vials using proven systems or freezing and stoppering within the chamber) to avoid external side effects such as particulate entry, temperature variations, water absorption until container closure, and associated increased residual moisture contents.

This work addresses the challenges identified and presents a new setup for microwave-assisted freeze-drying (MFD), which combines the advantages of a regular GMP lyophilizer with flat and scalable microwave radiation sources. The results of our investigation display the new setup and its performance in two aspects: (A) Process data were collected with respect to microwave settings, drying speed, and controllability. (B) The quality of the dried products after drying and their stability after storage were assessed. Accordingly, we examined six different formulations of a monoclonal antibody (mAb) in the new drying setup. The antibody was formulated in a generic and low concentration in the presence of a typical histidine buffer and a commonly used surfactant (i.e., polysorbate 20). To study the effect of the solid content, we added different sugar types, namely, sucrose and trehalose, in two concentrations. Moreover, we investigated the dryability of non-standard matrices in MFD using 2-hydroxypropyl-beta-cyclodextrin (HP-β-CD) and arginine phosphate. Finally, we compared the stability profiles of the samples following the two drying protocols, i.e., MFD and CFD. The solid-state properties of the lyophilizates, as

well as the physical and chemical stability of the mAb, were investigated at 4 °C, 25 °C, and 40 °C over the course of 6 months.

The new microwave-assisted freeze-drying (MFD) setup meets the requirements of modern manufacturing technology and is based on a typical laboratory-scale freeze-dryer with stainless steel shelves allowing for temperature control via silicon oil circulation. Chamber geometry, condenser, and cooling and vacuum systems represent the regular state of the art. Therefore, freezing, drying with and without microwave radiation, and stoppering under a partial vacuum can be conducted easily. Furthermore, neither the microwave source nor the product is rotated in this MFD setup: a phase shift is applied repeatedly to avoid the formation of cold and hot spots. With this work, we aim to provide a proof of concept for this new technology setup, but further process optimization is beyond the scope of the study.

IV.3 Materials and Methods

IV.3.1 Monoclonal Antibody and Chemicals

A monoclonal IgG type 1 antibody (mAb) was used in the study. L-histidine monohydrochloride monohydrate (99% purity) and L-histidine (cell culture reagent) were purchased from Alfa Aesar (Ward Hill, MA, USA). D(+)-trehalose dihydrate (97.0–102.0% purity) Ph. Eur., NF certified, was purchased from VWR International (Radnor, PA, USA). EMPROVE® exp sucrose, EMPROVE® exp di-sodium hydrogen phosphate dihydrate, EMPROVE® bio sodium chloride, and EMSURE® ortho-phosphoric acid (85%) were purchased from Merck KGaA (Darmstadt, Germany). Trizma® base and Trizma® hydrochloride (both in BioXtra grade), (2-Hydroxypropyl)-β-cyclodextrin produced by Wacker Chemie AG, L-arginine BioUltra (≥99.5%), and sodium azide (≥99.5%) were purchased from Sigma Aldrich (Burlington, MA, USA). Sodium dihydrogen phosphate dihydrate (99%) was purchased from Grüssing GmbH (Filsum, Germany). Super Refined™ Polysorbate 20-LQ-(MH) was purchased from Croda (Edison, NJ, USA). For the preparation of all solutions, ultrapure water from an Arium® system from Sartorius Lab Instruments GmbH (Goettingen, Germany) was used.

IV.3.2 Preparation of the Formulations

The first experiments were carried out with 8% (*w/v*) and 10% (*w/v*) sucrose placebo formulations. Next, we continued with six verum formulations (Table IV.1). The bulk solution of the mAb was dialyzed and concentrated using a Minimate™ Tangential Flow Filtration (TFF) capsule (MWCO 30 kDa; Pall Corporation, New York, NY, USA). After

extensive dialysis using a 7-fold excess of 10 mM of histidine buffer (pH 5.5), the final buffer consisted of 10 mM of histidine and 0.04% (*w/v*) polysorbate 20. The concentration of the mAb was determined with a Nanodrop 2000 UV spectrophotometer (Thermo Fisher Scientific, Waltham, MA, USA) at 280 nm, using the molar extinction coefficient. Stock solutions of the excipients were prepared with 10 mM of histidine buffer and mixed with the protein solution according to the intended composition (Table IV.1). Then, all formulations were sterile-filtered using 0.22 μm Sartolab® RF polyethersulfone vacuum filtration units (Sartorius AG, Goettingen, Germany). For each formulation, 63 10R FIOLAX vials (MGlas AG, Muennerstadt, Germany) were filled with 5 mL of the respective solutions and semi-stoppered with lyophilization stoppers (Flurotec® laminated rubber stoppers, West Pharmaceutical Services, Inc, Exton, PA, USA).

Table IV.1 Investigated formulations with the corresponding drying times as well as the relative monomer yield (RMY) and relative amount of high-molecular-weight species (HMWS) after the storage of the respective mAb formulations.

Formulation Number	Protein Conc. (g/L)	Sucrose (%)	Trehalose (%)	HP-β-CD (%)	Arginine Phosphate (%)	PS 20 (%)	Drying Time (h)	RMY after 6 Months at 40 °C (%)	HMWS after 6 Months at 4 °C (%)	HMWS after 6 Months at 40 °C (%)
F1	10	8.0				0.04	28.5	102.4 ± 0.5	0.40 ± 0.03	0.51 ± 0.01
F2	10	16.0				0.04	26.4	75.5 ± 0.2	0.37 ± 0.01	21.07 ± 0.08
F3	10		8.0			0.04	29.1	102.9 ± 0 8	0.52 ± 0.00	0.73 ± 0.01
F4	10		16.0			0.04	26.9	104.7 ± 0.2	0.58 ± 0.01	0.64 ± 0.01
F5	10	2.4		5.6		0.04	29.9	103.2 ± 0.3	0.70 ± 0.07	1.09 ± 0.02
F6	10				8.0	0.04	31.5	101.1 ± 0.9	1.56 ± 0.11	3.34 ± 0.06

The values are means (*n* = 3) ± standard deviation. HP-β-CD, (2-Hydroxypropyl)-β-cyclodextrin; PS 20, polysorbate 20.

IV.3.3 Freeze-Drying Process

A laboratory-scale freeze-dryer by OPTIMA Pharma GmbH (Schwäbisch Hall, Germany) equipped with flat, emitting semiconductor microwave modules was used for all lyophilization runs. Due to the experimental nature of the new technical setup, the experiments had to be carried out in the technical workshop of the machine manufacturer. The vials were arranged in a hexagonal array (180 mm × 190 mm) in the middle of a shelf (486 mm × 440 mm) of the freeze-dryer. The microwave modules were mounted below the shelf above the vials (antenna area approximately 26 cm × 26 cm) and showed high mechanical stability to enable the stoppering of the vials after drying. Freezing to a final shelf temperature of −50 °C was carried out as suggested by Tang et al. [4]. Primary drying

was conducted at a shelf temperature of −15 °C and then increased to 30 °C for secondary drying and held for 6 h (chamber pressure, 50 µbar; all ramps, 1 K/min). For MFD, 2 × 90 W (2.43–2.48 GHz) was applied during drying. For this purpose, microwave radiation was started as soon as the intended vacuum for primary drying was established (to decrease the risk of local plasma emergence [30]) and ran continuously until the shelf temperature reached 0 °C to not overheat the samples. The most commonly used temperature sensors, i.e., thermocouples and resistance temperature detectors [31], malfunction in electromagnetic environments. For this reason, fiber-optic temperature sensors (Weidmann Technologies Deutschland GmbH, Dresden, Germany) were employed for product temperature recording for both MFD and CFD. To monitor the drying process, a mass spectrometer (Pfeiffer Vacuum GmbH, Asslar, Germany) was used in addition to comparative pressure measurement via a Pirani and MKS Baratron gauge. After the completion of the drying process, vials were stoppered under a partial vacuum in a nitrogen atmosphere and crimped with Flip-Off® seals (West Pharmaceutical Services, Inc., Exton, PA, USA).

IV.3.4 Karl–Fischer Titration

Coulometric Karl–Fischer titration was used to determine the residual moisture content (rM) of the lyophilizates of F1–F6. Under controlled humidity conditions (relative humidity < 10%), the cakes were gently crushed, and 40–70 mg of each cake was transferred into 2R vials. Afterward, the samples were placed in an oven (temperature 100 °C), and the extracted water was transferred to the coulometric titration cell with a dry carrier gas flow (Aqua 40.00 Vario Plus, ECH Elektrochemie Halle GmbH, Halle (Saale), Germany). Relative moisture content was calculated (%, *w/w*). Prior to sample analysis, equipment performance was verified by measuring the Apura® water standard oven 1% (Merck KGaA, Darmstadt, Germany) in triplicate.

IV.3.5 Frequency Modulated Spectroscopy (FMS)

A Lighthouse FMS-1400T (Lighthouse Instruments, Charlottesville, VA, USA) was used to perform a 100% headspace moisture analysis after lyophilization. Samples were kept refrigerated and subsequently equilibrated at room temperature for at least 3 h before analysis. Headspace moisture data are provided as partial pressures in mbar. Nitrogen was used as a buffer gas to remove background noise due to ambient air moisture, and samples were equilibrated in the device for 15 s before the measurements were started. Before sample

analysis, a system suitability test was conducted using five standards covering an appropriate moisture range.

IV.3.6 Brunauer–Emmet–Teller (BET) Krypton Gas Adsorption

The specific surface area was determined according to Brunauer–Emmet–Teller (BET) using krypton gas adsorption in a liquid nitrogen bath at 77 K (Autosorb 1, Quantachrome, Boynton Beach, FL, USA). At least 100 mg of the gently crushed samples was used to fill the 9 mm sample cells under controlled humidity conditions (relative humidity < 10%). An outgassing step was performed for at least 2 h at room temperature prior to analysis. Gas adsorption was determined for 11 measuring points, covering a relative pressure ratio of 0.05–0.30. The specific surface area was determined using the multipoint BET method fit in the Autosorb 1.55 software.

IV.3.7 Scanning Electron Microscopy (SEM)

The morphology of the freeze-dried cakes was analyzed via scanning electron microscopy (SEM) using a Helios NanoLab G3 UC (FEI, Hillsboro, OR, USA) at an acceleration voltage of 2 kV. Fragments of the top and bottom layers of the lyophilizates were extracted in a glove box (relative humidity < 10%). Subsequently, the samples were sputtered with carbon (10 nm layer thickness) using a CCU-010 HV sputterer (Safematic GmbH, Zizers, Switzerland). Images were taken at 175-fold magnification.

IV.3.8 Micro-Computed Tomography (μ-CT)

Noninvasive 3-dimensional micro-computed tomography (μCT) using a Skyscan 1273 X-ray microtomograph (Bruker, Billerica, MA, USA) was used to obtain global information on the cake structure. The lyophilizates were measured without further processing at an acceleration voltage of 70 kV and a beam current of 114 μA. The image pixel size is 6.5 μm/voxel. To reduce beam hardening effects related to the vial geometry, a flat field acquisition in the headspace of the vials was carried out prior to each measurement. An exposure time of 345 ms with 6 averages per projection was applied. The samples were rotated over 360° with a step size of 0.15°. Image reconstruction and analysis were carried out using the NRecon 1.7.5.1 and CTAnalyzer 1.20.8.0 software, respectively.

IV.3.9 X-ray Powder Diffractometry (XRPD)

An ARL EQUINOX X-ray diffractometer (Thermo Fisher Scientific, Waltham, MA, USA) was used to determine the solid state of the lyophilized samples. The device operated with Cu-Kα_1 and Cu-Kα_2 radiation (λ = 0.15417 nm) at 40 kV and 0.5 mA. Detection was

carried out with a curved counting wire detector with flowing counting gas (angular range, 110° 2-θ); the radiation source was a microfocus X-ray tube with mirror optics. Prior to analysis, the lyophilized cakes were gently ground into powder and placed on brass sample holders. Adhesive tape was used to seal the sample holders immediately after sample mounting to protect the moisture-sensitive powders from the surrounding air. Powder diffraction scans were conducted in a 2-θ range of 5° to 45° (0.03° steps).

IV.3.10 Reconstitution of the Lyophilizates

Reconstitution of the lyophilizates was performed by adding ultrapure water. The required volume was calculated individually for all formulations to match the volume of water removed during freeze-drying.

IV.3.11 Size Exclusion Chromatography (SEC)

For the quantification of monomer yield and protein aggregates, we used a Thermo Scientific™ Dionex™ UltiMate™ 3000 UHPLC system equipped with a VWD-3400RS UV/Vis absorbance detector, all from Thermo Fisher Scientific (Waltham, MA, USA), and a TSKgel G3000SWxl, 7.8 × 300 mm, 5 µm column (Tosoh Bioscience, Tokyo, Japan). The running buffer was composed of 100 mM of sodium phosphate, 300 mM of sodium chloride, and 0.05% (*w/v*) sodium azide, pH 7.0. Separation was performed at a flow rate of 1 mL/min, and 10 µL was injected. The elution of the reconstituted lyophilizates was detected by absorption at 280 nm, and, subsequently, the chromatograms were integrated using Chromeleon™ 7.2.7 (Thermo Fisher Scientific, Waltham, MA, USA). The relative monomer yield was calculated in relation to the amount of monomer prior to freeze-drying the respective formulations. The relative amount of high-molecular-weight species (HMWS) was calculated according to Svilenov et al. [32].

IV.3.12 Cation Exchange Chromatography (CEX)

The chemical stability of the mAb was analyzed using a Thermo Scientific™ Dionex™ UltiMate™ 3000 UHPLC system equipped with a VWD-3400RS UV/Vis absorbance detector and a ProPac™ WCX-10G BioLC™ analytical column (4 × 250 mm) equipped with a ProPac™ WCX-10G BioLC™ guard column (4 × 50 mm), all from Thermo Fisher Scientific (Waltham, MA, USA). Mobile phase A consisted of 20 mM TRIS (pH 8.0), whereas mobile phase B contained 20 mM of TRIS and 300 mM of sodium chloride (pH 8.0). Elution was performed in a linear salt gradient mode from 0% B to 20% B in 30 min with a flow rate of 1 mL/min. Before analysis, the samples were diluted to a mAb

concentration of 0.1 g/L with mobile phase A, and the injection volume was 100 µL. Elution was detected at 280 nm, and the integration of the chromatograms was performed with Chromeleon™ 7.2.7 (Thermo Fisher Scientific, Waltham, MA, USA). The peak areas were divided into three components: the main peak, acidic variants corresponding to every peak eluting before the main peak, and basic variants corresponding to every peak eluting after the main peak.

IV.3.13 Flow Imaging Microscopy

The formation of subvisible particles was analyzed with a FlowCam 8100 (Fluid Imaging Technologies, Inc., Scarborough, ME, USA). The device was equipped with a 10 × magnification flow cell (80 µm × 700 µm) and operated using the VisualSpreadsheet® 4.7.6 software. A 150 µL sample was analyzed at a flow rate of 0.15 mL/min, and particle images were taken at an auto image frame rate of 28 frames/s. Settings specified for particle identifications were at a 3 µm distance to the nearest neighbor and particle thresholds of 13 and 10 for dark and light pixels, respectively. The size of the particles was reported as the equivalent spherical diameter.

IV.4 Results and Discussion

IV.4.1 Effects of Microwave Assistance on the Freeze-Drying Process

The first and most obvious effect of MFD is its potential to drastically reduce drying times. With microwave assistance, a 10% (m/V) sucrose formulation was dried within approximately 27 h, while it took about 44 h to dry it in a conventional manner. For both MFD and CFD, the vials were arranged in a similar setup on the shelf (Figure IV.1).
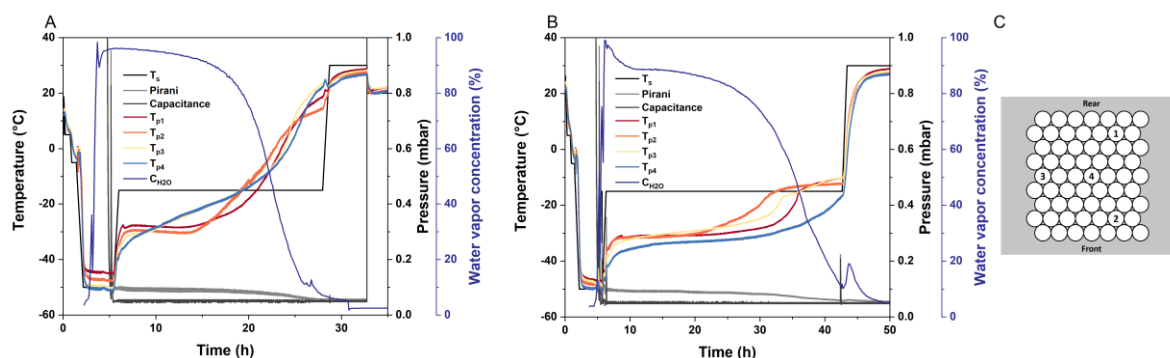
Figure IV.1 Readouts of the drying processes of a 10% (m/V) sucrose formulation. T_s represents the shelf temperature; the chamber pressure is monitored via a Pirani gauge (Pirani) and an MKS Baratron gauge (Capacitance); T_p is the readout of the fiber optic temperature sensors; and the water vapor concentration (C_{H2O}) during drying is recorded with a mass spectrometer. (**A**) Microwave-assisted freeze-drying was conducted at 2.43 GHz–2.48 GHz and 180 W. (**B**) Conventional freeze-drying was performed using the same lyophilizer. (**C**) Position of the four fiber optic temperature probes and arrangement of the vial package on the shelf.

A second interesting effect is the distribution of heat in MFD. When comparing the temperature profiles of MFD and CFD, a drastic difference can be found: the typically observed edge effect is reversed in MFD, and center vials temporarily run equal to or warmer than edge vials (Figure IV.1A,B). After MFD, the residual moisture of the center vials was significantly lower (headspace moisture, 1.72 mbar ± 0.29 mbar) than in the edge vials (headspace moisture, 2.23 mbar ± 0.29 mbar), $p < 0.05$ (Figure IV.S1). For more information on non-destructive headspace moisture analysis, allowing for other subsequent analytics on the very same sample vial, the reader is referred to [33]. Furthermore, a distinct spread between the product temperature readings toward the end of primary drying, as observed for CFD, is not found in MFD. Likewise, we observed slightly lower residual moisture levels in the center vials (1.41% ± 0.12%) compared with the edge vials (1.57% ± 0.13%) following CFD due to cooling radiation effects from the chamber walls, when the shelf temperature is increased during secondary drying ($n = 7$, [34]. The edge vial effect caused by differences in heat transfer during primary drying in CFD is an important issue that needs to be taken into account during cycle development as well as in scale-up, and this often leads to long, conservative drying cycles [34,35]. As our data indicated, this limitation can be overcome due to better energy distribution in MFD. It is in accordance with findings from Bhambhani et al., who found no constraint in energy input due to vial heat transfer, K_v, when MFD is used [24]. The equalization of heat transfer in the center and corner vials is a promising effect and needs to be evaluated further to identify optimal frequencies and phase settings.

Thirdly, another peculiarity of MFD can be observed when looking at the process phases. When the shelf temperature is increased for secondary drying, the increased pressure reading from the Pirani gauge and water vapor concentration detected by mass spectrometry indicate a fair amount of residual water in the vials at that point in CFD (Figure IV.1B). These high levels cannot be found in MFD (Figure IV.1A). We, therefore, assume that separated primary and secondary drying does not exist in MFD. Moreover, the dielectric properties of frozen and liquid water are very different [36–38]. While ice shows a low dielectric loss factor [20], microwaves probably excite the highly polarizable unfrozen water [29]. This allows for faster and more robust drying processes since the glass transition temperature of the freeze concentrate thereby increases as the drying process progresses. The strength of MFD technology is often described as having the potential to increase heat transfer via volumetric heating and, therefore, overcome the bottleneck of CFD in heat transfer [20,24]. Apart from that, efforts toward robust formulations enabling fast and aggressive CFD have been made

[10,12,39,40]. However, the aggressive drying of low-concentration protein formulations lacking crystalline bulking agents results in a poor macroscopic appearance [12,39,41]. Therefore, we particularly see the strength of MFD technology, among other things, in the fact that the processing of "difficult-to-dry" formulations, i.e., low T_g' and T_c, combined with high filling volumes, can be conducted very fast as a result of increasing T_g' during drying.

IV.4.2 Effects of the Excipients and Solute Concentration

To better understand how MFD processes work, we next aimed to examine the effect of solute concentration using two sugars, namely, sucrose and trehalose (Table IV.1, F1–F4), which are two of the most prominent stabilizers in the field of lyophilization [42]. While F1 and F3 with 8% (m/V) sugar represent commonly used concentrations for protein stabilization, 16% (m/V) sugar containing the formulations F2 and F4 are considered to be particularly difficult to dry using CFD. The reason for this is that high solute concentrations lead to increased mass transfer resistance, especially when combined with high filling volumes, which constitute a worst-case scenario, resulting in long drying times in CFD. Here, we observed that this relationship is different in MFD: despite the fact that higher dry-layer resistances in the cakes must be overcome, an increased solute content enhances dielectric heating. With MFD, F1 was dried within 28.5 h, while it took 55.7 h without microwaves (CFD) when the same protocol was applied. An increase in sugar concentration by factor two resulted in even shorter microwave-assisted drying times (26.4 h for F2) due to the lower amount of water that needed to be removed. The same is true for trehalose-based formulations F3 and F4 (29.1 h and 26.9 h drying time with MFD, respectively). The ability to enhance microwave absorption efficiency due to a higher solute concentration is in accordance with recently published work [24]. Furthermore, the amount of unfrozen water depends strongly on the composition of the formulation and correlates with the concentration of amorphous solutes [43,44]. Accordingly, MFD efficacy further increases with an increasing quantity of highly polarizable unfrozen water being excitable in F2 and F4 compared with F1 and F3.

To further study the effects of excipients, we investigated stabilizers that are less frequently used than disaccharides in the new MFD setup. More recently, the addition of cyclic oligosaccharide 2-hydroxypropyl-beta-cyclodextrin (HP-β-CD) was shown to provide stable formulations of monoclonal antibodies following aggressive CFD protocols [10,11]. Due to the high T_g' and T_c of such formulations [45,46], elegant cakes were obtained while

HP-β-CD remained fully amorphous [47]. The first results from our group in a different MFD setup also indicated the applicability of HP-β-CD for MFD [26]. In this study, a binary mixture of HP-β-CD and sucrose was used (Table IV.1, F5), as proposed by Haeuser et al. [10]. The drying time with MFD was 29.9 h, and we believe that this can be even further reduced by applying higher shelf temperatures.

Since dipole rotation/vibration is a major mechanism in most biological materials resulting in heating due to microwave radiation [20], we were interested in studying an arginine-based formulation (Table IV.1, F6). Due to its pK_a of 13.8 [48], arginine is positively charged in acidic, neutral, and most basic formulation conditions [49]. The drying time of arginine-based formulation F6 (Table IV.1) was 31.5 h and thus did not differ much from the disaccharide-based formulations.

IV.4.3 Solid State Properties of the Lyophilizates

The obtained cakes looked elegant on a macroscopic scale. Only for F2 was shrinkage in the cakes observed. On a microscopic scale, a cellular pore structure was found with scanning electron microscopy (SEM) for F3–F6, whereas F1 and F2 appeared to be microcollapsed (Figures IV.2 and IV.S2). However, due to the low T_g' values of the sucrose formulations, microcollapse may not be avoided with fast and aggressive drying [11]. This phenomenon is not related to the application of microwaves, and we likewise observed a microcollapsed structure for F1 after CFD [34]. Apart from that, the top and bottom showed a similar structure in SEM, even when sugar-rich formulations were dried. These findings align well with a micro-computed tomography (μCT) analysis of F1–F4, which revealed very similar pore size distribution for the respective pairs, i.e., 8% and 16% sugar (Figure IV.S3). For the sucrose containing formulations F1 and F2, pore size was found to be shifted toward larger pores due to the aforementioned microcollapse. Furthermore, the specific surface area (SSA) indicated that the porous cake structures were retained throughout the stability study, except for F2 after 6 months at 40°C, where further shrinkage appeared (Figure IV.3, bars). This is in good agreement with the residual moisture, which was low in all formulations after MFD (Figure IV.3, symbols) and remained constant over the course of 6 months except for fluctuations in the sucrose-rich formulation (F2). We, therefore, assume that, with F2, even the MFD technology is stretched to its limits, whereas the trehalose-rich formulation F4 showed no limitations. Furthermore, we used X-ray powder diffractometry (XRPD) to study the structural patterns of the lyophilizates. All formulations were fully amorphous after MFD (Figure IV.S4) and storage at 40 °C for 6 months (exc. F2; [51].
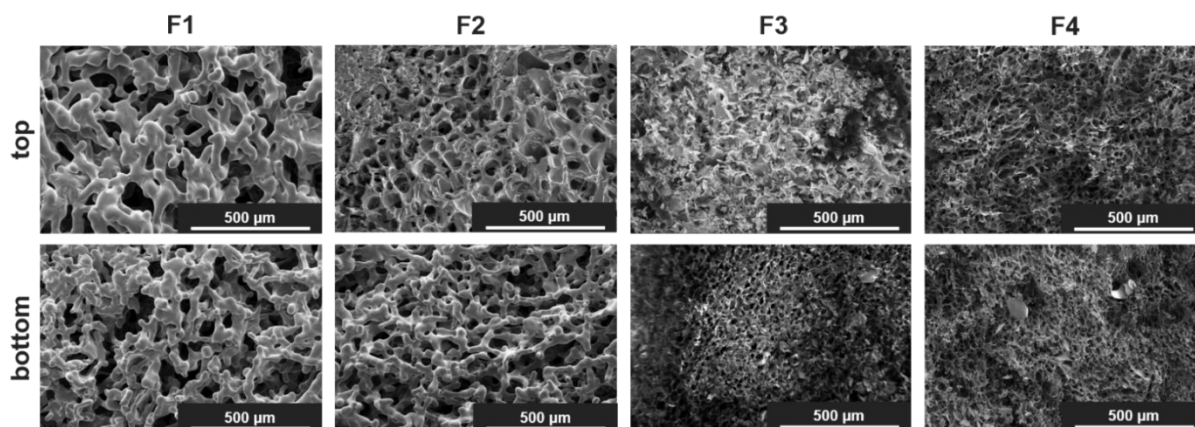
Figure IV.2 Representative SEM pictures from the top and bottom of the cakes after MFD at 175-fold magnification.
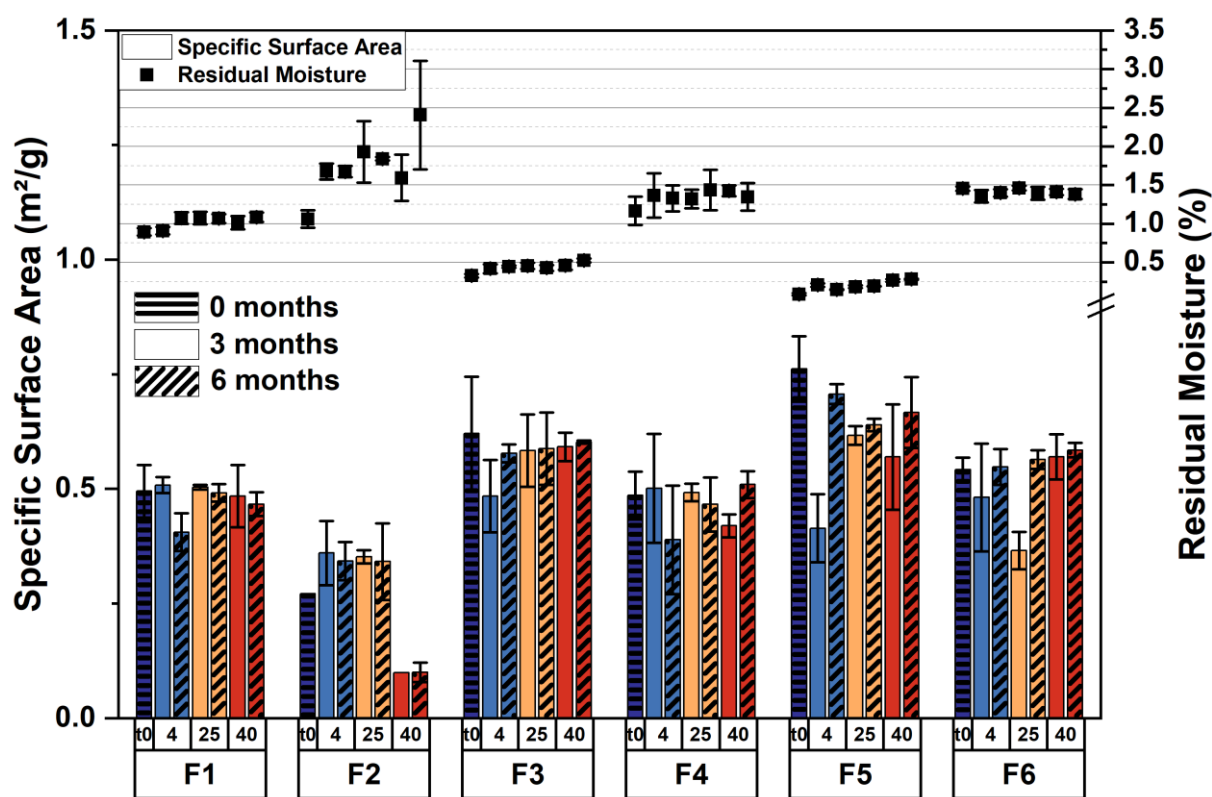
Figure IV.3 Solid-state properties of lyophilized formulations. Specific surface area (bars) and the respective residual moisture data (symbols) were obtained directly after lyophilization and during the stability study over the course of 6 months. The values are means (n = 2 for SSA; n = 3 for rM) ± standard deviation. Storage temperatures: 4, 25, and 40 °C.

IV.4.4 Storage Stability of the Formulations

Physical and chemical protein stability was determined after MFD and after storage at 4 °C, 25 °C, and 40 °C over the course of 6 months, respectively. It is important to emphasize that all formulations demonstrated remarkably good stability directly after MFD, which is not self-evident with regard to the aggressive drying conditions. The relative monomer yield

remained constant within 6 months of storage for all formulations (Tables IV.1 and IV.S1–S3), except for F2, which was stored at 40 °C (75.5 % ± 0.2% after 6 months). This can be explained by the low glass transition temperature (T_g) of the sugar-rich formulation (51.4 °C ± 2.1 °C). The excipients also had an impact on the formation of high-molecular-weight species (HMWS), i.e., soluble protein aggregates, during storage. The relative number of soluble aggregates was low for all formulations stored at 4 °C and 25 °C (Tables IV.1, IV.S1, and IV.S2). With 21.07% ± 0.08%, the highest number of aggregates was detected for F2 after storage for 6 months at 40 °C, while the mAb was preserved very well in F1, F3, and F4 at this temperature (Tables IV.1 and IV.S3). A slight increase in HMWS was observed for F5 (1.09% ± 0.02%) and F6 (3.34% ± 0.06%) after 6 months at 40 °C (Table IV.1).

The formation of larger, insoluble aggregates (≥25 μm and ≥10 μm) was low for F1–F5 after MFD and storage (Figure IV.S5). In F6, the formation of aggregates was induced during drying, resulting in higher particle counts right from the start of the stability study (Figure IV.S5). Although the ability of arginine salts to prevent protein aggregation has been published before and was confirmed in recent studies [49,50], we observed that, in the presence of microwave irradiation, its protective effect seems to be diminished, probably due to strong ion–dipole interactions between the microwave field and arginine salts, resulting in increased local heating. Further studies are needed to investigate whether this effect is also observed in other proteins and what effect other charged molecules or amino acids in MFD have. The number of subvisible particles (≥1 μm) was found to be at a relatively high level throughout the study but within the range of placebo formulations.

The chemical stability of the mAb was assessed with weak cation exchange (CEX) chromatography (Table IV.2). Directly after MFD, the relative number of acidic, i.e., deamidated, and basic species was found to be within the standard deviation of the liquid bulk [51]. Although a microcollapsed structure was observed for F1 and F2, only slight chemical changes were detected after storage for 6 months at 4 °C and 25 °C, respectively. After 6 months at 40 °C, acidic variants did not change significantly, and basic variants increased slightly from 13.7% ± 0.3% after lyophilization to 15.5% ± 0.3% for F1. For F2, acidic variants increased from 25.8% ± 0.1% to 30.5% ± 1.6%, and basic variants changed from 13.1% ± 0.3% to 20.9% ± 0.7% at 40 °C storage temperature. For the trehalose-based formulations, F3 and F4, the relative number of acidic species differs little from the amount directly after MFD, even when stored at 40 °C (F3, 26.0% ± 0.1% after MFD and 28.3% ± 1.0% after 6 months; F4, 24.3% ± 0.6% and 28.1% ± 2.4%), indicating very robust chemical stability over time. We observed somewhat more pronounced changes in the basic species

of F3 (14.5% ± 0.3% after MFD, 20.5% ± 0.6% after storage at 40 °C) and F4 (11.0% ± 0.6% after MFD, 18.2% ± 1.4% after storage at 40 °C). However, chemical changes are in the same range for F3 and F4, suggesting that the mAb is equally well stabilized, and high trehalose concentrations do not limit MFD. Formulations F5 and F6 appeared less stabilizing at higher storage temperatures, i.e., at 25 °C and 40 °C. The relative number of acidic variants of F5 increased from 27.8% ± 0.1% to 32.9% ± 0.8% at 40 °C, and basic variants increased from 11.6% ± 0.6% to 25.7% ± 1.8%. The arginine phosphate that contained formulation F6 showed a noticeable increase in both acidic (27.2% ± 1.0% after MFD and 43.7% ± 0.2% after storage at 40 °C) and basic species (11.8% ± 1.9% and 21.4% ± 0.3%).

Table IV.2 Relative number of acidic and basic variants after MFD and storage at the respective temperatures over the course of 6 months for all formulations.

Formulation Number	Acidic Variants (%)				Basic Variants (%)			
	0 m	6 m			0 m	6 m		
		4 °C	25 °C	40 °C		4 °C	25 °C	40 °C
F1	24.5 ± 0.6	26.9 ± 1.5	24.9 ± 1.6	25.7 ± 1.4	13.7 ± 0.3	14.6 ± 0.2	13.7 ± 1.0	15.5 ± 0.3
F2	25.8 ± 0.1	27.1 ± 1.4	26.1 ± 2.6	30.5 ± 1.6	13.1 ± 0.3	13.0 ± 0.6	13.4 ± 0.5	20.9 ± 0.7
F3	26.0 ± 0.1	25.5 ± 1.0	26.6 ± 0.6	28.3 ± 1.0	14.5 ± 0.3	13.2 ± 0.2	15.1 ± 0.5	20.5 ± 0.6
F4	24.3 ± 0.6	26.6 ± 2.2	26.3 ± 2.9	28.1 ± 2.4	11.0 ± 0.6	13.5 ± 0.4	14.2 ± 0.4	18.2 ± 1.4
F5	27.8 ± 0.1	29.8 ± 0.3	31.0 ± 0.5	32.9 ± 0.8	11.6 ± 0.6	13.5 ± 1.2	16.3 ± 0.5	25.7 ± 1.8
F6	27.2 ± 1.0	29.0 ± 1.1	31.2 ± 0.4	43.7 ± 0.2	11.8 ± 1.9	12.1 ± 0.4	16.4 ± 0.5	21.4 ± 0.3

The values are means ($n = 3$) ± standard deviation. m, month.

Since sugar-rich formulations are typically difficult to dry in CFD, we directed particular attention to the storage stability of these formulations following MFD and compared it with lower amounts of the same disaccharide. We, therefore, deliberately refrained from simultaneously increasing the mAb concentration, as the robustness of the lyophilization process correlates with the protein concentration [39]. Accordingly, we tested the most prominent used disaccharides, sucrose and trehalose, in two concentrations. The results of this study showed good storage stability for F1–F4, with the sucrose-rich formulation, F2, reaching its limits at the highest storage temperature, i.e., 40 °C. In comparison with sucrose, trehalose exhibits higher glass transition temperatures (T_g) [51]. In the present study, trehalose-based formulation F3, and even trehalose-rich formulation F4, showed good overall mAb stability and appeared to be a promising approach for the fast and efficient drying of proteins with MFD. The high T_g value is also an attribute making cyclodextrins a valuable alternative, with HP-β-CD already being approved in parenteral products [47]. Although the mAb was preserved slightly better in "disaccharide-only" formulations, the

authors conclude that the use of an HP-β-CD/sucrose mixture in the described MFD setup is technically possible. Further investigations to find the best excipient ratios are beyond the scope of this study. With regard to the aggressive drying conditions, phosphate was chosen as an arginine counter ion for F6, as it exhibits higher glass transition temperatures compared with others [52]. However, Stärtzel et al. found an increased propensity for the aggregation of an IgG1 mAb in sucrose/arginine phosphate mixtures [53]. After MFD and subsequent storage, we likewise observed protein aggregation and less chemical stability in the protein in F6 compared with other formulations in this study. Consequently, the investigated formulation F6 needs to be optimized further to stabilize the mAb used in this study.

IV.4.5 Comparison of the Protein Storage Stability following MFD and CFD

To investigate the impact of microwave radiation on degradation, we lyophilized formulation F1 conventionally. The formulation was chosen because it represents a generic composition of a low-concentrated mAb formulation. After freeze-drying, we observed slightly lower residual moisture contents after MFD (0.89% ± 0.05%) compared with CFD (1.10% ± 0.23%), as shown in Figure IV.4A. Only a slight increase in rM was observed over the course of 6 months at 4 °C, 25 °C, and 40 °C (Figure IV.4A, circles). Although the drying time was reduced by approximately half for MFD, the specific surface area was found to be comparable for the two technologies after lyophilization and subsequent storage (Figure IV.4A, rectangles), indicating the comparable pore structure of the cakes.
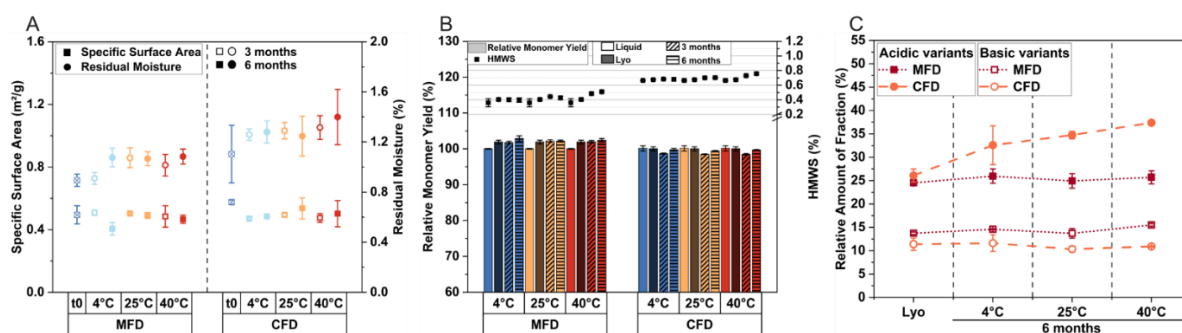
Figure IV.4 Direct comparison of MFD and CFD: solid-state properties and protein stability for F1 after lyophilization and storage at the respective temperatures over the course of 6 months. In (**A**), the specific surface area (rectangles) and residual moisture (circles) are shown. Relative monomer yield and relative number of high-molecular-weight species (HMWS) are depicted in (**B**). In (**C**), the relative number of acidic and basic variants is shown. All values are means (n = 3) ± standard deviation.

We then compared protein stability following MFD and CFD. The mAb was well preserved, irrespective of the drying procedure. The relative monomer yield remained constant at all storage temperatures (Figure IV.4B, bars). With an increasing storage

temperature, the formation of HMWS increased slightly for MFD ($0.36\% \pm 0.06\%$ after lyophilization and $0.51\% \pm 0.01\%$ after 6 months at 40 °C), as well as for CFD ($0.67\% \pm 0.01\%$ after lyophilization and $0.76\% \pm 0.02\%$ after 6 months at 40 °C); see Figure IV.4B (symbols).

The quantity of both acidic and basic species was similar following MFD and CFD, respectively (Figure IV.4C). After MFD, the relative number of acidic species was $24.5\% \pm 0.6\%$ and $13.7\% \pm 0.3\%$ for basic species. Following CFD, $26.1\% \pm 1.4\%$ acidic and $11.4\% \pm 1.3\%$ basic species were found. After storage for 6 months at 40 °C, the relative number of basic species changed slightly for MFD ($15.5\% \pm 0.3\%$) and did not vary significantly for CFD ($10.9\% \pm 0.1\%$). The formation of acidic variants during storage at 40 °C was not observed for the MFD sample population ($25.7\% \pm 1.4\%$ after 6 months), while an increase was observed for conventionally dried samples ($37.4\% \pm 0.5\%$ after 6 months at 40 °C). We assume that the overall slightly higher number of HMWS and increased number of acidic variants following CFD compared with MFD is attributable to slightly higher residual moisture levels in CFD samples [54–56]. Therefore, we conclude comparable mAb storage stability, which is in good accordance with previous work [26,27].

IV.5 Conclusion

In this study, we explored the application of a novel microwave-assisted freeze-drying setup for the lyophilization of biopharmaceutical formulations. Our work is valuable and relevant, as up to now, a machine setup that is in line with GMP requirements has been missing. Besides drastically reducing drying times, we found that the edge vial effect was inversed. Consequently, energy input is mainly driven by microwave radiation, and the technology has the potential to offset conventionally observed disparities in heat transfer. Moreover, we propose simultaneous primary and secondary drying in MFD, which allows for rather aggressive but still robust drying conditions due to the increase in the glass transition temperature as drying progresses. We studied various representative antibody formulations and showed their applicability in the new MFD setup. The charged amino acid system showed inferior capability in stabilizing the antibody, and it needs to be investigated further. Similar stability profiles were found with MFD vs. CFD for a generic antibody formulation over the course of 6 months, despite drastically shortened drying times for MFD. To underline the operationality of the setup, a representative mAb used worldwide was chosen for the study. By virtue of its unique technical setup, utilizing a GMP lyophilizer

with small, flat, and even microwave modules, microwave radiation can be added to the process flexibly and on demand. We believe that the presented setup and data offer a significant advance in the time- and cost-saving manufacturing of essential medicines and represent a crucial step toward the application of the MFD technology to the pharmaceutical industries.
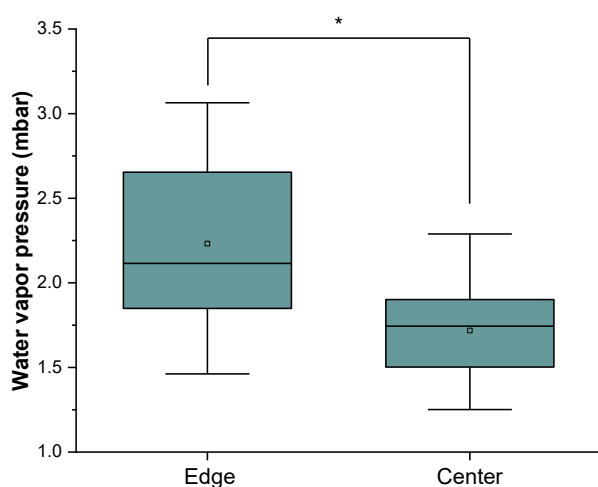
IV.6 Supplementary Materials

Figure IV.S1 Headspace moisture data of MFD samples determined with frequency modulated spectroscopy. The formulation contained 8% (m/V) sucrose, 0.04% polysorbate 20 in 10 mM histidine buffer. Values are means (n = 27 for edge vials, n = 32 for center vials) ± standard deviation. Asterisk (*) indicates statistical significance, $p < 0.05$.

Table IV.S1 Storage stability of the mAb following MFD. Relative monomer yield (RMY) and relative amount of high molecular weight species (HMWS) after storage at 4°C of the respective mAb formulations.

Formulation number	0 m		3 m		6 m	
	RMY, %	HMWS, %	RMY, %	HMWS, %	RMY, %	HMWS, %
F1	101.9 ± 0.5	0.40 ± 0.02	101.8 ± 0.4	0.40 ± 0.03	102.9 ± 0.8	0.40 ± 0.03
F2	105.5 ± 0.1	0.38 ± 0.00	105.6 ± 0.3	0.38 ± 0.00	105.8 ± 0.3	0.37 ± 0.01
F3	102.6 ± 0.3	0.46 ± 0.02	102.2 ± 0.1	0.45 ± 0.06	102.6 ± 0.1	0.52 ± 0.00
F4	104.7 ± 0.6	0.57 ± 0.01	104.9 ± 0.1	0.63 ± 0.00	104.6 ± 0.2	0.58 ± 0.01
F5	103.7 ± 0.6	0.51 ± 0.03	102.0 ± 0.2	0.62 ± 0.02	103.0 ± 0.2	0.70 ± 0.07
F6	99.3 ± 0.6	1.54 ± 0.11	101.2 ± 0.8	1.52 ± 0.17	102.4 ± 1.9	1.56 ± 0.11

The values are means (n = 3) ± standard deviation.

Table IV.S2 Storage stability of the mAb following MFD. Relative monomer yield (RMY) and relative amount of high molecular weight species (HMWS) after storage at 25°C of the respective mAb formulations.

Formulation number	0 m		3 m		6 m	
	RMY, %	HMWS, %	RMY, %	HMWS, %	RMY, %	HMWS, %
F1	101.9 ± 0.5	0.40 ± 0.02	102.2 ± 0.4	0.44 ± 0.01	102.2 ± 0.3	0.43 ± 0.02
F2	105.5 ± 0.1	0.38 ± 0.00	105.5 ± 0.7	0.39 ± 0.01	105.9 ± 0.8	0.50 ± 0.21
F3	102.6 ± 0.3	0.46 ± 0.02	102.3 ± 0.3	0.54 ± 0.01	102.9 ± 0.2	0.62 ± 0.01
F4	104.7 ± 0.6	0.57 ± 0.01	104.9 ± 0.2	0.63 ± 0.01	104.7 ± 0.1	0.61 ± 0.01
F5	103.7 ± 0.6	0.51 ± 0.03	102.6 ± 1.4	0.73 ± 0.01	103.1 ± 0.2	0.88 ± 0.02
F6	99.3 ± 0.6	1.54 ± 0.11	101.0 ± 1.4	2.09 ± 0.05	101.5 ± 0.6	2.21 ± 0.08

The values are means (n = 3) ± standard deviation.

Table IV.S3 Storage stability of the mAb following MFD. Relative monomer yield (RMY) and relative amount of high molecular weight species (HMWS) after storage at 40°C of the respective mAb formulations.

Formulation number	0 m		3 m		6 m	
	RMY, %	HMWS, %	RMY, %	HMWS, %	RMY, %	HMWS, %
F1	101.9 ± 0.5	0.40 ± 0.02	102.0 ± 0.4	0.48 ± 0.02	102.4 ± 0.5	0.51 ± 0.01
F2	105.5 ± 0.1	0.38 ± 0.00	82.1 ± 1.0	23.27 ± 1.63	75.5 ± 0.2	21.07 ± 0.08
F3	102.6 ± 0.3	0.46 ± 0.02	102.8 ± 0.2	0.62 ± 0.01	102.9 ± 0.8	0.73 ± 0.01
F4	104.7 ± 0.6	0.57 ± 0.01	104.7 ± 0.1	0.67 ± 0.02	104.7 ± 0.2	0.64 ± 0.01
F5	103.7 ± 0.6	0.51 ± 0.03	102.3 ± 0.3	0.93 ± 0.01	103.3 ± 0.3	1.09 ± 0.02
F6	99.3 ± 0.6	1.54 ± 0.11	99.9 ± 0.2	2.93 ± 0.10	101.1 ± 0.9	3.34 ± 0.06

The values are means (n = 3) ± standard deviation.
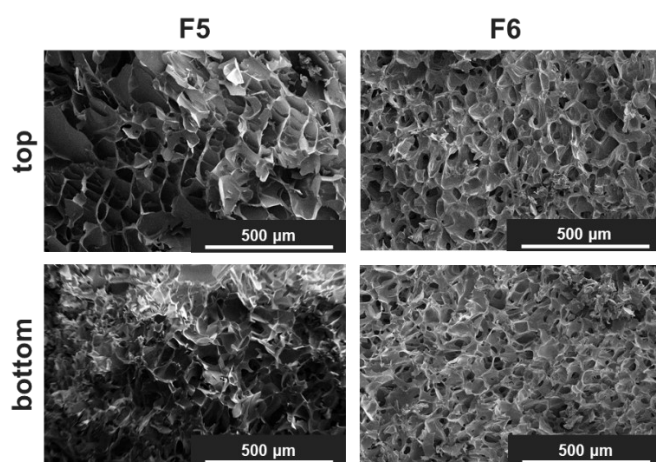

Figure IV.S2 Scanning electron microscopy images from top and bottom of the cakes of F5 and F6 at 175-fold magnification.
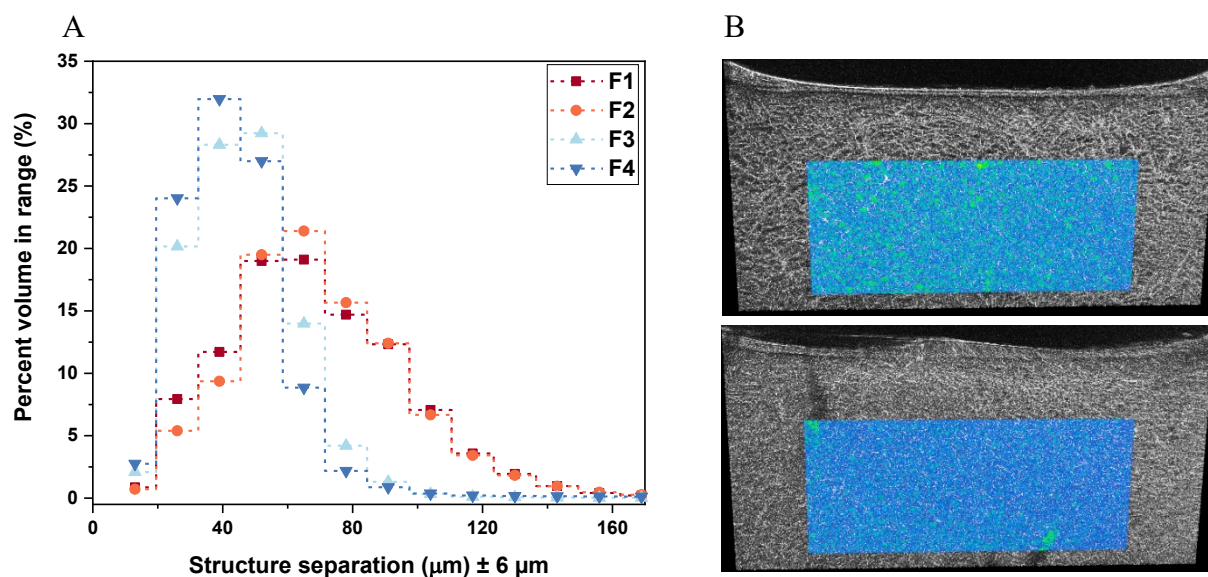
A

B

Figure IV.S3 Characterization of the cake structure with micro-computed tomography (µCT). (A) Average pore size is indicated by the structure separation. (B) Representative µCT pictures of F1 and F3. The rectangular box indicates the analyzed volume of interest (VOI) and the color scale represents the respective pore sizes (dark blue to green, 6 µm to 170 µm ± 6 µm, respectively).
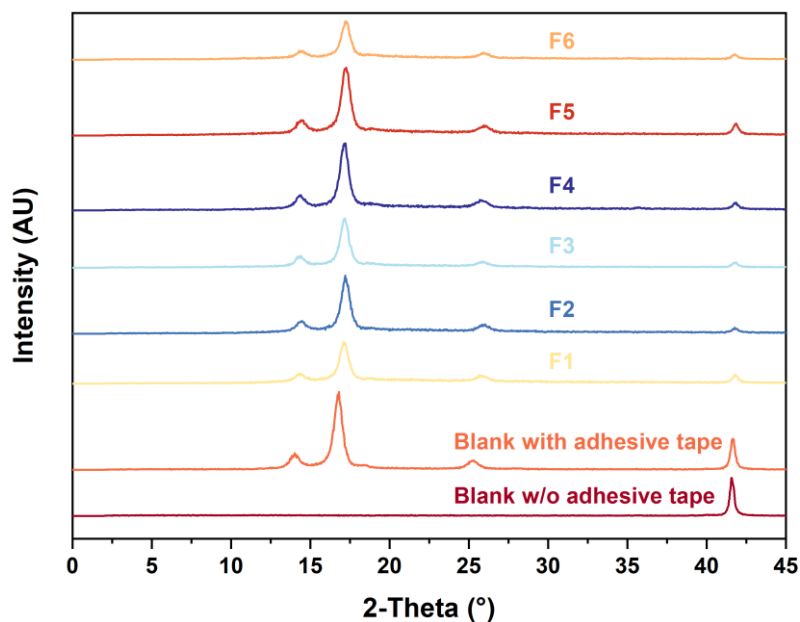

Figure IV.S4 Representative X-ray powder diffractograms of the investigated formulations after MFD. Adhesive tape was used to seal the sample holders immediately after sample mounting in order to protect the moisture sensitive powders from surrounding air. AU, arbitrary units.
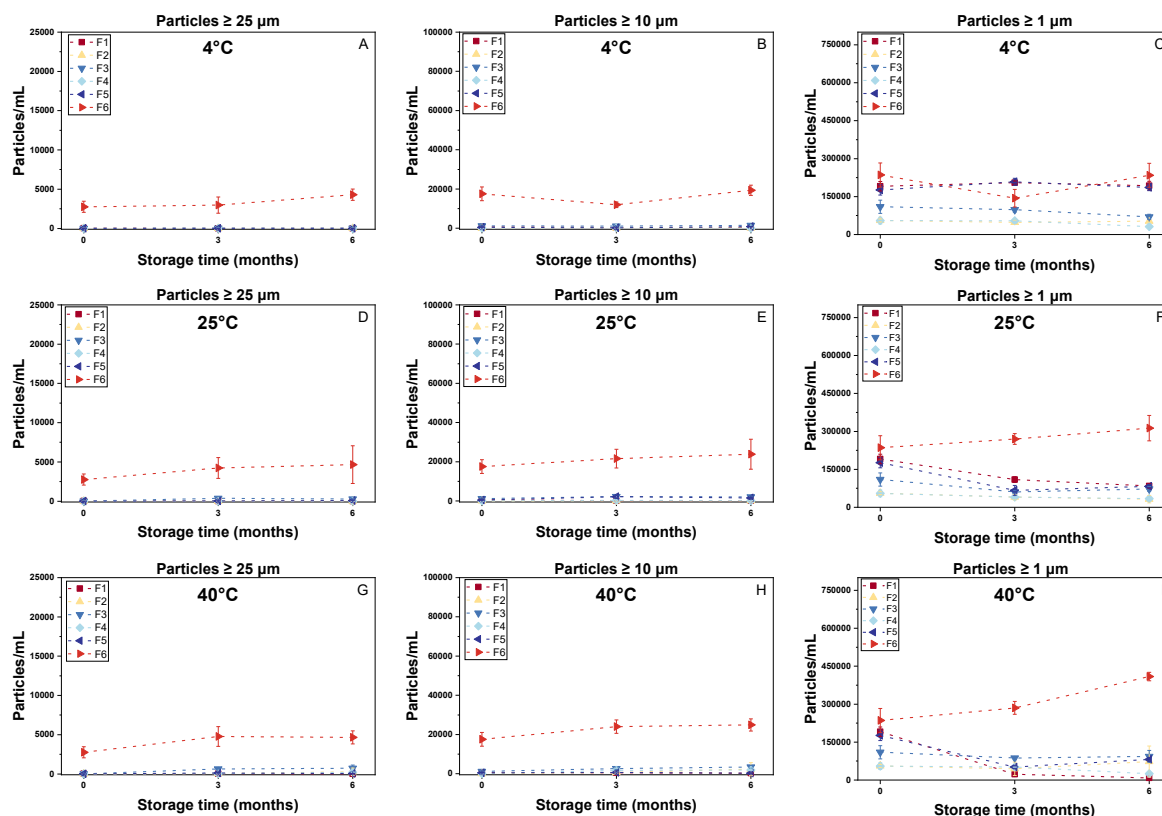
Figure IV.S5 Subvisible particle counts for the investigated formulations after MFD and storage at 4 °C (A), (B), (C) and 25 °C (D), (E), (F) as well as 40 °C (G), (H), (I). The values are means (n = 3 and technical duplicates per vial) ± standard deviation.

IV.7 Acknowledgements

IV.8 References

1. Chen, Y.; Mutukuri, T.T.; Wilson, N.E.; Zhou, Q. (Tony) Pharmaceutical protein solids: Drying technology, solid-state characterization and stability. *Adv. Drug Deliv. Rev.* **2021**, *172*, 211–233. https://doi.org/10.1016/j.addr.2021.02.016.

2. Kasper, J.C.; Winter, G.; Friess, W. Recent advances and further challenges in lyophilization. *Eur. J. Pharm. Biopharm.* **2013**, *85*, 162–169. https://doi.org/10.1016/j.ejpb.2013.05.019.

3.   Patel, S.M.; Doen, T.; Pikal, M.J. Determination of End Point of Primary Drying in Freeze-Drying Process Control. *AAPS PharmSciTech* **2010**, *11*, 73–84. https://doi.org/10.1208/s12249-009-9362-7.

4.   Tang, X.C.; Pikal, M.J. Design of Freeze-Drying Processes for Pharmaceuticals: Practical Advice. *Pharm. Res.* **2004**, *21*, 191–200. https://doi.org/10.1023/B:PHAM.0000016234.73023.75.

5.   Patient-centered drug manufacture. *Nat. Biotechnol.* **2017**, *35*, 485–485. https://doi.org/10.1038/nbt.3901.

6.   Langford, A.; Bhatnagar, B.; Walters, R.; Tchessalov, S.; Ohtake, S. Drying technologies for biopharmaceutical applications: Recent developments and future direction. *Dry. Technol.* **2018**, *36*, 677–684. https://doi.org/10.1080/07373937.2017.1355318.

7.   Langford, A.; Bhatnagar, B.; Walters, R.; Tchessalov, S.; Ohtake, S. Drying of biopharmaceuticals: Recent developments, new technologies and future direction. *Japan J. Food Eng.* **2018**, *19*, 15–24. https://doi.org/10.11301/jsfe.18514.

8.   Sharma, A.; Khamar, D.; Cullen, S.; Hayden, A.; Hughes, H. Innovative Drying Technologies for Biopharmaceuticals. *Int. J. Pharm.* **2021**, *609*, 121115. https://doi.org/10.1016/j.ijpharm.2021.121115.

9.   Emami, F.; Keihan Shokooh, M.; Mostafavi Yazdi, S.J. Recent progress in drying technologies for improving the stability and delivery efficiency of biopharmaceuticals. *J. Pharm. Investig.* **2023**, *53*, 35–57. https://doi.org/10.1007/s40005-022-00610-x.

10.   Haeuser, C.; Goldbach, P.; Huwyler, J.; Friess, W.; Allmendinger, A. Be Aggressive! Amorphous Excipients Enabling Single-Step Freeze-Drying of Monoclonal Antibody Formulations. *Pharmaceutics* **2019**, *11*, 616. https://doi.org/10.3390/pharmaceutics11110616.

11.   Haeuser, C.; Goldbach, P.; Huwyler, J.; Friess, W.; Allmendinger, A. Excipients for Room Temperature Stable Freeze-Dried Monoclonal Antibody Formulations. *J. Pharm. Sci.* **2020**, *109*, 807–817. https://doi.org/10.1016/j.xphs.2019.10.016.

12.   Pansare, S.K.; Patel, S.M. Lyophilization Process Design and Development: A Single-Step Drying Approach. *J. Pharm. Sci.* **2019**, *108*, 1423–1433. https://doi.org/10.1016/j.xphs.2018.11.021.

13.   Kasraian, K.; DeLuca, P.P. The Effect of Tertiary Butyl Alcohol on the Resistance of the Dry Product Layer During Primary Drying. *Pharm. Res. An Off. J. Am. Assoc. Pharm. Sci.* **1995**, *12*, 491–495. https://doi.org/10.1023/A:1016285425670.

14.   Teagarden, D.L.; Baker, D.S. Practical aspects of lyophilization using non-aqueous co-solvent systems. *Eur. J. Pharm. Sci.* **2002**, *15*, 115–133. https://doi.org/10.1016/S0928-098700221-4.

15.   Teagarden, D.L.; Wang, W.; Baker, D.S. Practical Aspects of Freeze-Drying of Pharmaceutical and Biological Products Using Nonaqueous Cosolvent Systems. In *Freeze-Drying/Lyophilization of Pharmaceutical and Biological Products*; Rey, L., May, J.C., Eds.; CRC Press: Boca Raton, FL, USA, 2010; pp. 254–287; ISBN 0429151853.

16.   De Meyer, L.; Van Bockstal, P.J.; Corver, J.; Vervaet, C.; Remon, J.P.; De Beer, T. Evaluation of spin freezing versus conventional freezing as part of a continuous pharmaceutical freeze-drying concept for unit doses. *Int. J. Pharm.* **2015**, *496*, 75–85. https://doi.org/10.1016/j.ijpharm.2015.05.025.

17.   Capozzi, L.C.; Trout, B.L.; Pisano, R. From Batch to Continuous: Freeze-Drying of Suspended Vials for Pharmaceuticals in Unit-Doses. *Ind. Eng. Chem. Res.* **2019**, *58*, 1635–1649. https://doi.org/10.1021/acs.iecr.8b02886.

18.   Thostenson, E.T.; Chou, T.W. Microwave processing: Fundamentals and applications. *Compos. Part A Appl. Sci. Manuf.* **1999**, *30*, 1055–1071. https://doi.org/10.1016/S1359-835X(99)00020-2.

19.   Franks, F.; Auffret, T. The Process Sequence in Summary. In *Freeze-Drying of Pharmaceuticals and Biopharmaceuticals: Principles and Practice*; The Royal Society of Chemistry: Cambridge, UK, 2007; pp. 13–19; ISBN 978-0-85404-268-5.

20.   Durance, T.; Noorbakhsh, R.; Sandberg, G.; Sáenz-Garza, N. Microwave Drying of Pharmaceuticals.

In *Drying Technologies for Biotechnologies and Pharmaceutical Applications*; Ohtake, S., Izutsu, K.-I., Lechuga-Ballesteros, D., Eds.; Wiley-VCH Verlag GmbH & Co. KGaA: Weinheim, Germany, 2020; pp. 239–255; ISBN 9783527341122.

21. Fan, K.; Zhang, M.; Mujumdar, A.S. Recent developments in high efficient freeze-drying of fruits and vegetables assisted by microwave: A review. *Crit. Rev. Food Sci. Nutr.* **2019**, *59*, 1357–1366. https://doi.org/10.1080/10408398.2017.1420624.

22. Chandrasekaran, S.; Ramanathan, S.; Basak, T. Microwave food processing—A review. *Food Res. Int.* **2013**, *52*, 243–261. https://doi.org/10.1016/J.FOODRES.2013.02.033.

23. Ambros, S.; Bauer, S.A.W.; Shylkina, L.; Foerst, P.; Kulozik, U. Microwave-Vacuum Drying of Lactic Acid Bacteria: Influence of Process Parameters on Survival and Acidification Activity. *Food Bioprocess Technol.* **2016**, *9*, 1901–1911. https://doi.org/10.1007/s11947-016-1768-0.

24. Bhambhani, A.; Stanbro, J.; Roth, D.; Sullivan, E.; Jones, M.; Evans, R.; Blue, J. Evaluation of Microwave Vacuum Drying as an Alternative to Freeze-Drying of Biologics and Vaccines: The Power of Simple Modeling to Identify a Mechanism for Faster Drying Times Achieved with Microwave. *AAPS PharmSciTech* **2021**, *22*, 52. https://doi.org/10.1208/s12249-020-01912-9.

25. Abdelraheem, A.; Tukra, R.; Kazarin, P.; Sinanis, M.D.; Topp, E.M.; Alexeenko, A.; Peroulis, D. Statistical electromagnetics for industrial pharmaceutical lyophilization. *PNAS Nexus* **2022**, 1–13. https://doi.org/10.1093/pnasnexus/pgac052.

26. Gitter, J.H.; Geidobler, R.; Presser, I.; Winter, G. Significant Drying Time Reduction Using Microwave-Assisted Freeze-Drying for a Monoclonal Antibody. *J. Pharm. Sci.* **2018**, *107*, 2538–2543. https://doi.org/10.1016/J.XPHS.2018.05.023.

27. Gitter, J.H.; Geidobler, R.; Presser, I.; Winter, G. Microwave-Assisted Freeze-Drying of Monoclonal Antibodies: Product Quality Aspects and Storage Stability. *Pharmaceutics* **2019**, *11*, 674. https://doi.org/10.3390/pharmaceutics11120674.

28. Evans, R.K. Applications of Microwave Vacuum Drying and Lyospheres to Freeze-Drying of Vaccines and Biologics. In Proceedings of the CPPR: Freeze-Drying of Pharmaceuticals and Biologicals ConferenceFreeze-Drying of Pharmaceuticals and Biologicals Conference; Garmisch-Partenkirchen, Germany, 23–26 September 2014.

29. Park, J.; Cho, J.H.; Braatz, R.D. Mathematical modeling and analysis of microwave-assisted freeze-drying in biopharmaceutical applications. *Comput. Chem. Eng.* **2021**, *153*, 107412. https://doi.org/10.1016/j.compchemeng.2021.107412.

30. Meredith, R.J. *Engineers' Handbook of Industrial Microwave Heating*; The Institution of Electrical Engineers: London, UK, 1998.

31. Nail, S.; Tchessalov, S.; Shalaev, E.; Ganguly, A.; Renzi, E.; Dimarco, F.; Wegiel, L.; Ferris, S.; Kessler, W.; Pikal, M.; et al. Recommended Best Practices for Process Monitoring Instrumentation in Pharmaceutical Freeze Drying—2017. *AAPS PharmSciTech* **2017**, *18*, 2379–2393. https://doi.org/10.1208/s12249-017-0733-1.

32. Svilenov, H.; Winter, G. The ReFOLD assay for protein formulation studies and prediction of protein aggregation during long-term storage. *Eur. J. Pharm. Biopharm.* **2019**, *137*, 131–139. https://doi.org/10.1016/j.ejpb.2019.02.018.

33. Cook, I.A.; Ward, K.R. Headspace moisture mapping and the information that can be gained about freeze-dried materials and processes. *PDA J. Pharm. Sci. Technol.* **2011**, *65*, 457–467. https://doi.org/10.5731/pdajpst.2011.00760.

34. Rambhatla, S.; Pikal, M.J. Heat and mass transfer scale-up issues during freeze-drying, I: Atypical radiation and the edge vial effect. *AAPS PharmSciTech* **2003**, *4*, 22–31. https://doi.org/10.1208/pt040214.

35. Ehlers, S.; Schroeder, R.; Friess, W. Trouble with the Neighbor During Freeze-Drying: Rivalry About

Energy. *J. Pharm. Sci.* **2021**, *110*, 1219–1226. https://doi.org/10.1016/j.xphs.2020.10.024.

36. Ryynänen, S. The electromagnetic properties of food materials: A review of the basic principles. *J. Food Eng.* **1995**, *26*, 409–429. https://doi.org/10.1016/0260-877400063-F.

37. Fernández, D.P.; Mulev, Y.; Goodwin, A.R.H.; Sengers, J.M.H.L. A Database for the Static Dielectric Constant of Water and Steam. *J. Phys. Chem. Ref. Data* **1995**, *24*, 33–70. https://doi.org/10.1063/1.555977.

38. Koh, G. Complex dielectric constant of ice at 1.8 GHz. *Cold Reg. Sci. Technol.* **1997**, *25*, 119–121. https://doi.org/10.1016/s0165-232x(96)00021-3.

39. Depaz, R.A.; Pansare, S.; Patel, S.M. Freeze-Drying above the Glass Transition Temperature in Amorphous Protein Formulations while Maintaining Product Quality and Improving Process Efficiency. *J. Pharm. Sci.* **2016**, *105*, 40–49. https://doi.org/10.1002/jps.24705.

40. Colandene, J.D.; Maldonado, L.M.; Creagh, A.T.; Vrettos, J.S.; Goad, K.G.; Spitznagel, T.M. Lyophilization Cycle Development for a High-Concentration Monoclonal Antibody Formulation Lacking a Crystalline Bulking Agent. *J. Pharm. Sci.* **2007**, *96*, 1598–1608. https://doi.org/10.1002/jps.20812.

41. Bosch, T. Aggressive Freeze-Drying—A Fast and Suitable Method to Stabilize Biopharmaceuticals. Ph.D. Thesis, Ludwig-Maximilians-Universität, München, Germany, 2014.

42. Wang, W. Lyophilization and development of solid protein pharmaceuticals. *Int. J. Pharm.* **2000**, *203*, 1–60. https://doi.org/10.1016/S0378-517300423-3.

43. Nail, S.L.; Jiang, S.; Chongprasert, S.; Knopp, S.A. Fundamentals of Freeze-Drying. In *Development and Manufacture of Protein Pharmaceuticals*; Nail, S.L., Akers, M.J., Eds.; Springer US: Boston, MA, USA, 2002; pp. 281–360; ISBN 978-1-4615-0549-5.

44. Hatley, R.H.M.; Mant, A. Determination of the unfrozen water content of maximally freeze-concentrated carbohydrate solutions. *Int. J. Biol. Macromol.* **1993**, *15*, 227–232. https://doi.org/10.1016/0141-813090042-K.

45. Wong, J.; Kipp, J.E.; Miller, R.L.; Nair, L.M.; Joseph Ray, G. Mechanism of 2-hydropropyl-beta-cyclodextrin in the stabilization of frozen formulations. *Eur. J. Pharm. Sci.* **2014**, *62*, 281–292. https://doi.org/10.1016/j.ejps.2014.05.024.

46. Meister, E.; Šašić, S.; Gieseler, H. Freeze-dry microscopy: Impact of nucleation temperature and excipient concentration on collapse temperature data. *AAPS PharmSciTech* **2009**, *10*, 582–588. https://doi.org/10.1208/s12249-009-9245-y.

47. Serno, T.; Geidobler, R.; Winter, G. Protein stabilization by cyclodextrins in the liquid and dried state. *Adv. Drug Deliv. Rev.* **2011**, *63*, 1086–1106. https://doi.org/10.1016/j.addr.2011.08.003.

48. Fitch, C.A.; Platzer, G.; Okon, M.; Garcia-Moreno, B.E.; McIntosh, L.P. Arginine: Its pKa value revisited. *Protein Sci.* **2015**, *24*, 752–761. https://doi.org/10.1002/pro.2647.

49. Stärtzel, P. Arginine as an Excipient for Protein Freeze-Drying: A Mini Review. *J. Pharm. Sci.* **2018**, *107*, 960–967. https://doi.org/10.1016/J.XPHS.2017.11.015.

50. Izutsu, K.I.; Kadoya, S.; Yomota, C.; Kawanishi, T.; Yonemochi, E.; Terada, K. Freeze-drying of proteins in glass solids formed by basic amino acids and dicarboxylic acids. *Chem. Pharm. Bull.* **2009**, *57*, 43–48. https://doi.org/10.1248/cpb.57.43.

51. Crowe, L.M.; Reid, D.S.; Crowe, J.H. Is trehalose special for preserving dry biomaterials? *Biophys. J.* **1996**, *71*, 2087–2093. https://doi.org/10.1016/S0006-349579407-9.

52. Izutsu, K.I.; Fujimaki, Y.; Kuwabara, A.; Aoyagi, N. Effect of counterions on the physical properties of L-arginine in frozen solutions and freeze-dried solids. *Int. J. Pharm.* **2005**, *301*, 161–169. https://doi.org/10.1016/j.ijpharm.2005.05.019.

53. Störtzel, P.; Gieseler, H.; Gieseler, M.; Abdul-Fattah, A.M.; Adler, M.; Mahler, H.-C.; Goldbach, P. Freeze Drying of l -Arginine/Sucrose-Based Protein Formulations, Part I: Influence of Formulation and Arginine Counter Ion on the Critical Formulation Temperature, Product Performance and Protein Stability. *J. Pharm. Sci.* **2015**, *104*, 2345–2358. https://doi.org/10.1002/jps.24501.

54. Yoshioka, S.; Aso, Y.; Kojima, S. Determination of molecular mobility of lyophilized bovine serum albumin and γ-globulin by solid-state 1H NMR and relation to aggregation-susceptibility. *Pharm. Res.* 1996, *13*, 926–930. https://doi.org/10.1023/A:1016069532204.

55. Costantino, H.R.; Langer, R.; Klibanov, A.M. Solid-phase aggregation of proteins under pharmaceutically relevant conditions. *J. Pharm. Sci.* **1994**, *83*, 1662–1669. https://doi.org/10.1002/jps.2600831205.

56. Bell, L.N.; Hageman, M.J.; Muraoka, L.M. Thermally induced denaturation of lyophilized bovine somatotropin and lysozyme as impacted by moisture and excipients. *J. Pharm. Sci.* **1995**, *84*, 707–712. https://doi.org/10.1002/jps.2600840608.

Chapter V   Microwave-Assisted Freeze-Drying: Impact of Microwave Radiation on the Quality of High-Concentration Antibody Formulations

This chapter is published as:

Author contributions:

N.H., R.G., I.P. and G.W. conceptualized the idea and planned the experiments. N.H. conducted the experiments and evaluated the data. N.H. wrote the manuscript. R.G., I.P. and G.W. provided scientific guidance, and reviewed and edited the manuscript.

The published article can be accessed online:

https://doi.org/10.3390/pharmaceutics15122783

Note from the authors:

The numbering of the subchapters, figures and tables was changed in comparison to the submitted version of the article, to fit the consecutive numbering of this thesis.

V.1 Abstract

Microwave-assisted freeze-drying (MFD) offers significant time savings compared to conventional freeze-drying (CFD). While a few studies have investigated the stability of biopharmaceuticals with low protein concentrations after MFD and storage, the impact of MFD on high-concentration monoclonal antibody (mAb) formulations remains unclear. In this study, we systematically examined the effect of protein concentration in MFD and assessed protein stability following MFD, CFD, and subsequent storage using seven protein formulations with various stabilizers and concentrations. We demonstrated that microwaves directly interact with the active pharmaceutical ingredient (API), leading to decreased physical stability, specifically aggregation, in high-concentration antibody formulations.

Furthermore, typically used sugar:protein ratios from CFD were insufficient for stabilizing mAbs when applying microwaves. We identified the intermediate drying phase as the most critical for particle formation, and cooling the samples provided some protection for the mAb. Our findings suggest that MFD technology may not be universally applicable to formulations well tested in CFD and could be particularly beneficial for formulations with low API concentrations requiring substantial amounts of glass-forming excipients, such as vaccines and RNA-based products.

Keywords: freeze-drying; lyophilization; microwave; protein; monoclonal antibody; stability; aggregation

V.2 Introduction

Although antibody therapeutics are now preferably formulated as liquid formulations, offering greater flexibility for patients, such as self-administration through pen devices [1,2], lyophilization remains the standard method when a particular molecule is facing stability issues [3]. Numerous reviews have been provided on the rational design of robust and optimized freeze-drying processes [4–7], as well as ideas for speeding up the typically lengthy process [8–11]. More recently, microwave-assisted freeze-drying (MFD) has gained attention due to its potential for significant time savings while maintaining the product quality of probiotics [12], vaccines, and proteins [13,14] and, more specifically, monoclonal antibodies (mAbs) [15–17]. While heat transfer in conventional freeze-drying (CFD) is primarily limited to convection, with some conduction and radiation, microwaves directly interact with the dipolar molecules of the formulation [18]. Energy is mainly transferred due to dipole rotation for permanent dipoles, i.e., in most biological materials [18]. The dielectric properties of a pharmaceutical formulation strongly depend on the concentration of buffer salts and disaccharides, typically used for cryo- and lyoprotection, as well as the amount of unfrozen water. Residual water great affects heat transfer because of the much higher effective loss factor of water compared to ice [19]. We hypothesized that microwaves excite the unfrozen water, and this causes the glass transition temperature T_g' to increase during drying [17]. As a result, drying processes become more robust and can be conducted very fast without impairing cake appearance. Interested readers should refer to works [19–21] for more information on microwave heating.

We recently introduced a new MFD setup that overcomes the drawbacks of previous machines, as it enables in-chamber freezing and stoppering [17]. This setup combines the advantages of a conventional lyophilizer, which was designed with good manufacturing practice (GMP) processes in mind, with microwave radiation. It employs flat, solid microwave modules that can be flexibly incorporated into the process. For details on the new setup, readers are referred to [17]. Additionally, we assessed mAb stability following MFD and found it to be comparable to mAb stability following CFD. Recent studies have focused on low-concentration protein formulations [13–15], with 50 mg/mL being the highest mAb concentration investigated [16]. However, in recent years, high-concentration antibody formulations have become immensely popular and successful [22], with 46 approved products ≥100 mg/mL in the US [1]. One of the major challenges in developing these formulations is protein aggregation, as it can increase at higher concentrations [23].

This work aims to explore the microwave-assisted freeze-drying of such high-concentration antibody formulations. We sequentially replaced sugar with antibodies to study their effect on the MFD process and protein stability. While drying times varied slightly, we observed reduced stability in the mAb when less stabilizing sugar was present in the formulation. These results prompted us to compare the stability profiles of high-concentration formulations directly after production with MFD and CFD, and after storage for up to six months at 4 °C, 25 °C, and 40 °C. When we found increased aggregate formation following MFD, we tried to identify the critical timeframe for degradation during the MFD process. Further studies using a microwave oven were then carried out to investigate whether microwave radiation directly interacts with the mAb, and how different levels of molecular mobility in the cake may affect this.

V.3 Materials and Methods

V.3.1 Proteins and Chemicals

In this study, two monoclonal IgG type-1 antibodies (mAbs) were used: one sourced from the laboratory's stock (LMU1, Munich, Germany), and the other (LMU2) generously provided by Boehringer Ingelheim Pharma GmbH & Co. KG (Ingelheim am Rhein, Germany). Further, G-CSF (filgrastim) was used as a model protein. L-histidine (cell culture reagent) and L-histidine monohydrochloride monohydrate (99% purity) were purchased from Alfa Aesar (Ward Hill, MA, USA). EMPROVE® exp sucrose, EMPROVE® exp

di-sodium hydrogen phosphate dihydrate, EMPROVE® bio sodium chloride, sodium citrate dihydrate (≥99.0%), and L-methionine were purchased from Merck KGaA (Darmstadt, Germany). D(+)-trehalose dihydrate (97.0–102.0% purity) Ph. Eur., NF certified, and D(−)-mannitol (97.0–102.0% purity) Ph. Eur., USP certified were purchased from VWR International (Radnor, PA, USA). Sodium dihydrogen phosphate dihydrate (99%) was purchased from Grüssing GmbH (Filsum, Germany). Trizma® base and Trizma® hydrochloride (both in BioXtra grade), anhydrous citric acid BioUltra grade (≥99.5%), and sodium azide (≥99.5%) were purchased from Sigma Aldrich (Burlington, MA, USA). Super Refined™ Polysorbate 20-LQ-(MH) was purchased from Croda (Edison, NJ, USA). All solutions were prepared using ultrapure water from a Sartorius Lab Instruments GmbH Arium® system (Goettingen, Germany).

V.3.2 Preparation of the Formulations

We used seven different verum formulations (Table 1). For F1–F5, we dialyzed and concentrated the mAb bulk solution using a Minimate™ Tangential Flow Filtration (TFF) capsule (MWCO 30 kDa; Pall Corporation, New York, NY, USA). A sevenfold excess of 10 mM histidine buffer (pH 5.5) was used for thorough dialysis, resulting in a final buffer mixture that contained 10 mM histidine and 0.04% (w/v) polysorbate 20. We determined the mAb concentration using a Nanodrop 2000 UV spectrophotometer (Thermo Fisher Scientific, Waltham, MA, USA) at 280 nm, based on the molar extinction coefficient. Excipient stock solutions were prepared in 10 mM histidine buffer and combined with the protein solution according to the target composition (Table 1). Formulation F6 was already provided in the final composition. For F7, the protein bulk solution underwent buffer exchange at 2–8 °C using Slide-A-Lyzer™ 2000 molecular weight cut-off dialysis cassettes (Thermo Fisher Scientific, Waltham, MA, USA). The sample-to-buffer ratio was 1:100, and buffer exchange was performed after 3 and 6 h, following dialysis overnight. All excipients were already added to the dialysis buffer, except for the surfactant, which was introduced after dialysis as a stock solution in 20 mM sodium citrate buffer. Following this, protein concentration was determined with a Nanodrop 2000 UV spectrophotometer (Thermo Fisher Scientific, Waltham, MA, USA) at 280 nm, and the formulation buffer was combined with the dialyzed protein solution. All formulations were sterile-filtered prior to lyophilization using 0.22 μm Sartolab® RF polyether sulfone vacuum filtration units (Sartorius AG, Goettingen, Germany).

Table V.1 Formulations investigated in the study.

Formulation Number	Protein Conc. (g/L)			Sucrose (%)	Trehalose (%)	Mannitol (%)	Methionine (mM)	PS 20 (%)	pH
	LMU1	LMU2	G-CSF						
F1	10			8				0.040	5.5
F2	30			6				0.040	5.5
F3	50			4				0.040	5.5
F4	70			2				0.040	5.5
F5	100			8				0.040	5.5
F6		21			1.9			0.009	6.0
F7			0.5	1		4	20	0.010	4.0

Conc., concentration; PS 20, polysorbate 20.

V.3.3 Freeze-Drying Process

Four distinct lyophilization cycle protocols were used (Table 2), with references to the respective processes provided in the text. For all processes, formulations were poured into 63 10R FIOLAX vials (MGlas AG, Muennerstadt, Germany) and placed on the middle of the shelf in a hexagonal array. Shelves were then cooled to −50 °C and held at the respective temperature until the product was completely frozen. For formulation F7, an additional annealing step was performed at −20 °C for 4 h, to enable the crystallization of mannitol.

Processes P1, P3, and P4 were conducted using a laboratory-scale freeze-dryer from OPTIMA Pharma GmbH (Schwäbisch Hall, Germany), which was equipped with flat, emitting semiconductor microwave modules. The vials were organized in a hexagonal pattern (180 mm × 190 mm) at the center of a shelf (486 mm × 440 mm). The microwave modules were attached to the underside of the shelf above the vials, covering an antenna area of approximately 26 cm × 26 cm. The modules were operated at 2.43–2.48 Ghz and exhibited exceptional mechanical stability, which enabled the stoppering of the vials following the drying process. Experiments were conducted in the machine manufacturer's technical workshop. As thermocouples and resistance temperature detectors would not work in the given electromagnetic environment, fiberoptic temperature sensors (Weidmann Technologies Deutschland GmbH, Dresden, Germany) were utilized for product temperature recording. A mass spectrometer (Pfeiffer Vacuum GmbH, Asslar, Germany) was employed, in conjunction with comparative pressure measurement via a Pirani and capacitance gauge, to monitor the drying process. Process P1 was designed to adhere to the typical format of primary and secondary drying steps, enabling a detailed study of protein concentration effects on MFD processes. Processes P3 and P4 aimed to compete with

aggressive CFD processes and were used to investigate the impact of the duration of microwave radiation on highly concentrated mAb formulations.

Process P2 was used to apply a comparable thermal history to CFD samples, as for those dried with microwave assistance. It was performed either on an FTS LyoStar™ 3 (SP Scientific, Stone Ridge, NY, USA) or a Christ ε2-6D (Martin Christ, Osterode am Harz, Germany) laboratory-scale freeze-dryer.

Once the drying processes were completed, the vials were stoppered under vacuum within the chamber of the lyophilizers in a nitrogen atmosphere, followed by capping with Flip-Off® seals (West Pharmaceutical Services, Inc., Exton, PA, USA). Subsequently, they were stored at 2–8 °C upon further processing.

Table V.2 Applied drying protocols in the study.

Drying Process	Step	T_s (°C)	P_c (mbar)	Hold Time (h)	Ramp Toward Step (K/min)	MW Application (W)
P1	1	−15	0.05	*	1.0	2 × 90**
	2	30	0.05	6	1.0	2 × 90**/†
P2	1	30	0.05	*	0.2	
P3	1	30	0.05	*	0.2	2 × 90‡
P4	1	10	0.05	*	0.2	2 × 90§
	2	30	0.05	4	1.0	-

* Maintained until Pirani signal equaled capacitance, and mass spectrometer revealed water vapor concentration $c_{H2O} < 10\%$. ** In case of MFD. † Applied continuously until the shelf temperature reached 0°C to not overheat the samples. ‡ Microwave module was stopped after 5h, 6h, and 8h respectively. In case of MFD of F7, 2 × 90W were applied until Pirani signal equaled capacitance sensor output, and mass spectrometer revealed water vapor concentration $c_{H2O} < 10\%$. § Microwave module was stopped after 10h and 13h, respectively. MW, microwave.

V.3.4 Karl–Fischer Titration

The lyophilizates' residual moisture content was measured using coulometric Karl–Fischer titration. In a controlled-humidity environment (relative humidity (rH) <10%), the lyophilized cakes were carefully crushed, and portions weighing 40–90 mg were transferred into 2R vials. These samples were then heated at 100 °C in an oven, and the extracted water was carried to the coulometric titration cell using a dry gas flow (Aqua 40.00 Vario Plus, ECH Elektrochemie Halle GmbH, Halle (Saale), Germany). The Apura® water standard oven 1% (Merck KGaA, Darmstadt, Germany) was used in triplicate to confirm the equipment's performance before analyzing the samples. The relative residual moisture content was calculated considering the cake mass (*w/w*).

V.3.5 Brunauer–Emmet–Teller (BET) Krypton Gas Adsorption

The Brunauer–Emmet–Teller (BET) method was employed to measure the specific surface area of the lyophilizates. Under controlled-humidity conditions (relative humidity < 10%), at least 100 mg of gently crushed samples was placed into 9 mm sample cells. The sample cells were cooled in a liquid nitrogen bath (77 K), and quantity of absorbed krypton gas was measured with an Autosorb 1 (Quantachrome, Boynton Beach, FL, USA). Krypton adsorption was determined over a p/p_0 ratio of 0.05–0.30 (11-point BET). An outgassing procedure was carried out at ambient temperature for a minimum of 2 h prior to the analysis. The Autosorb 1.55 software was used to calculate the specific surface area, applying the multipoint BET method fit.

V.3.6 Scanning Electron Microscopy (SEM)

The morphology of the lyophilizates was investigated using a Helios NanoLab G3 UC (FEI, Hillsboro, OR, USA) scanning electron microscope (SEM) at an acceleration voltage of 2 kV. Fragments from the top and bottom layers of the cakes were extracted in a glove box with a relative humidity of less than 10%. The samples were then sputtered with a 10 nm carbon layer using a CCU-010 HV sputterer (Safematic GmbH, Zizers, Switzerland). Images were captured at 175-fold magnification.

V.3.7 Experiments with the Microwave Oven

A Bosch HMT84M421 microwave oven (Robert Bosch Hausgeräte GmbH, München, Germany) was used to study the effect of microwave radiation on mAb stability. Prior to the experiments, flip-off seals were removed, and a single vial was positioned at the center of the rotating plate. A stainless steel cylinder, measuring approximately 5 cm × 3 cm, was pre-chilled at -70°C for one hour and subsequently used intermittently to cool the samples during irradiation. Microwave power levels of 180 W, 360 W, and 600 W were applied for specific time intervals. Afterward, the samples were reconstituted and subjected to analysis. To monitor the sample temperature, an Ebro TLC 750i thermometer (Xylem Analytics Germany GmbH, Weilheim, Germany) was used. To discern the effects of microwave radiation on the mAb from mere sample heating, the samples were placed in a Heraeus UT 20P drying cabinet (Thermo Fisher Scientific, Waltham, MA, USA).

V.3.8 Reconstitution of the Lyophilizates

The lyophilizates were reconstituted via the addition of ultrapure water. The necessary volume was individually determined for each formulation to correspond with the volume of water removed during the lyophilization process.

V.3.9 Size-Exclusion Chromatography (SEC)

A Thermo Scientific™ Dionex™ UltiMate™ 3000 UHPLC system was used in conjunction with a VWD-3400RS UV/Vis absorbance detection unit from Thermo Fisher Scientific (Waltham, MA, USA) to measure monomer yield and protein aggregates. First, 100 µg of LMU1 and LMU2 was injected onto a TSKgel G3000SWxl, 7.8 × 300 mm, 5 µm column (Tosoh Bioscience, Tokyo, Japan). The running buffer consisted of 100 mM sodium phosphate, 300 mM sodium chloride, and 0.05% (w/v) sodium azide at pH 7.0. For F7, 15 µg of G-CSF were injected onto a Superdex™ 75 Increase 10/300 GL, 10 × 300 mm column (GE Healthcare Bio-Sciences AB, Uppsala, Sweden). The mobile phase was composed of 100 mM sodium phosphate and 0.05% (w/v) sodium azide at pH 7.0. Both columns were operated at a flow rate of 1 mL/min. Absorption at 280 nm was used to detect elution, and the resulting chromatograms were integrated using Chromeleon™ 7.2.7 software (Thermo Fisher Scientific, Waltham, MA, USA). The monomer yield relative to the amount of monomer before freeze-drying the specific formulations was calculated. The method described in [25] was used to determine the relative number of high-molecular-weight species (HMWS).

V.3.10 Cation-Exchange Chromatography (IEX)

A Thermo Scientific™ Dionex™ UltiMate™ 3000 UHPLC system, featuring a VWD-3400RS UV/Vis absorbance detector and equipped with a ProPac™ WCX-10G BioLC™ analytical column (4 × 250 mm) together with a ProPac™ WCX-10G BioLC™ guard column (4 × 50 mm), all from Thermo Fisher Scientific (Waltham, MA, USA), was utilized to examine the chemical stability of LMU1. Mobile phase A was composed of 20 mM TRIS (pH 8.0), while mobile phase B consisted of 20 mM TRIS and 300 mM sodium chloride (pH 8.0). A linear salt gradient mode was used for elution, ranging from 0% B to 20% B over 30 minutes at a flow rate of 1 mL/min. Prior to analysis, samples were diluted 1:100 using mobile phase A, and the injection volume was 10 µL or 100 µL depending on the mAb concentration. Detection of elution occurred at 280 nm, and chromatogram integration was carried out using Chromeleon™ 7.2.7 software (Thermo Fisher Scientific, Waltham, MA, USA). The integrated chromatograms were categorized into three components: the main peak, acidic variants associated with each peak that eluted prior to the main peak, and basic variants linked to each peak that eluted after the main peak.

V.3.11 Flow imaging microscopy

The analysis of subvisible particle formation was conducted using a FlowCam 8100 (Fluid Imaging Technologies, Inc., Scarborough, ME, USA). The instrument was outfitted with a 10× magnification flow cell (80 μm × 700 μm) and was operated via VisualSpreadsheet® 4.7.6 software. A sample of 150 μL was analyzed at a flow rate of 0.15 mL/min, with particle images captured at an automatic frame rate of 28 frames/second. Parameters for particle identification were 3 μm distance to the nearest neighbor and particle thresholds of 13 and 10 for dark and light pixels, respectively. Particle sizes were presented as equivalent spherical diameters.

V.4 Results and Discussion

V.4.1 Substitution of Sugar by an Antibody

From CFD, it is well established that increasing protein concentrations lead to more robust drying processes due to a rise in the difference between the glass transition temperature (T_g') and collapse temperature (T_c) [26]. Consequently, the occurrence of collapse becomes less likely; however, it is important to consider the substantial dry-layer resistances to mass flow associated with high protein concentrations. However, the relationship between microwave-assisted freeze-drying processes and protein concentrations remains unclear. Recent studies have demonstrated that increasing the solute concentrations of stabilizers, such as sucrose and trehalose, results in enhanced dielectric heating [13,17]. To further investigate the effect of protein concentration in microwave-assisted drying processes, we gradually substituted sucrose with mAb (F1–F4, Table 1) and applied drying process P1 (Table 2). The overall solid content in all these samples was kept constant at ca. 9.0% (w/v) = 90 mg/mL. We observed that the drying time increased only slightly with higher mAb concentrations. With microwave assistance, F1 was dried within 28.5 h, while F2, F3, and F4 took 28.8 h, 29.5 h, and 30.3 h, respectively.

The lyophilizates appeared elegant on a macroscopic scale and scanning electron microscopy revealed a cellular pore structure for F2–F4 on a microscopic scale, whereas F1 exhibited microcollapse (Figure S1). Due to the low T_g' of low-concentrated mAb formulations in combination with sucrose, microcollapse may not be avoided with harsh drying conditions regardless of the application of microwaves [27], and we likewise observed microcollapse for F1 following CFD (data not shown). For low-concentration

protein formulations, T_g' and T_c are interchangeable [26]. Therefore, when the product temperature during drying exceeds the glass transition temperature for such formulations, the microstructure of the cake undergoes viscous flow and eventually collapses. The cake morphology corresponded with the observed specific surface areas after lyophilization, and stability study data suggest that it was maintained throughout the study (Figure 1A). Moreover, the residual moisture in the lyophilizates correlated with the sucrose concentration, i.e., samples became drier when the protein content was increased at the cost of the sugar (Figure 1A).

Regarding the physical stability of the mAb, aggregate formation increased with decreasing sucrose concentrations, both immediately after lyophilization and after six months of storage (Figure 1B). The same trend was observed for the chemical stability of LMU1 (Figure 1C–D), with F4 showing the highest number of basic variants after storage at 40 °C. An increase in basic species could be attributed to various modifications, including oxidation, succinimide formation, or disulfide-mediated changes [35]. Moreover, when the formulation contained less stabilizing sugar, the water replacement during the drying process was inadequate. Consequently, the protein was not stabilized in its native state, leading to the formation of aggregates. Past research has shown that aggregates of an IgG1 have a high affinity for cation-exchange columns and, as a result, they elute in the basic variant region in IEX [35]. Therefore, it can be inferred that aggregate formation in formulations with less stabilizing sugar and a concurrent increase in basic species are related to each other. Previous research has indicated that the sugar:protein ratio is crucial for protein stabilization during drying and storage [24]. Consequently, it appears that the reduced protein stability with a decreasing sugar:protein ratio is not due to microwave application but is generally related to less protection against stresses during the lyophilization process. For F1, the molar ratio of disaccharide to protein was significantly above the proposed proportion [24], at approximately 3500:1, while it was 125:1 for F4.
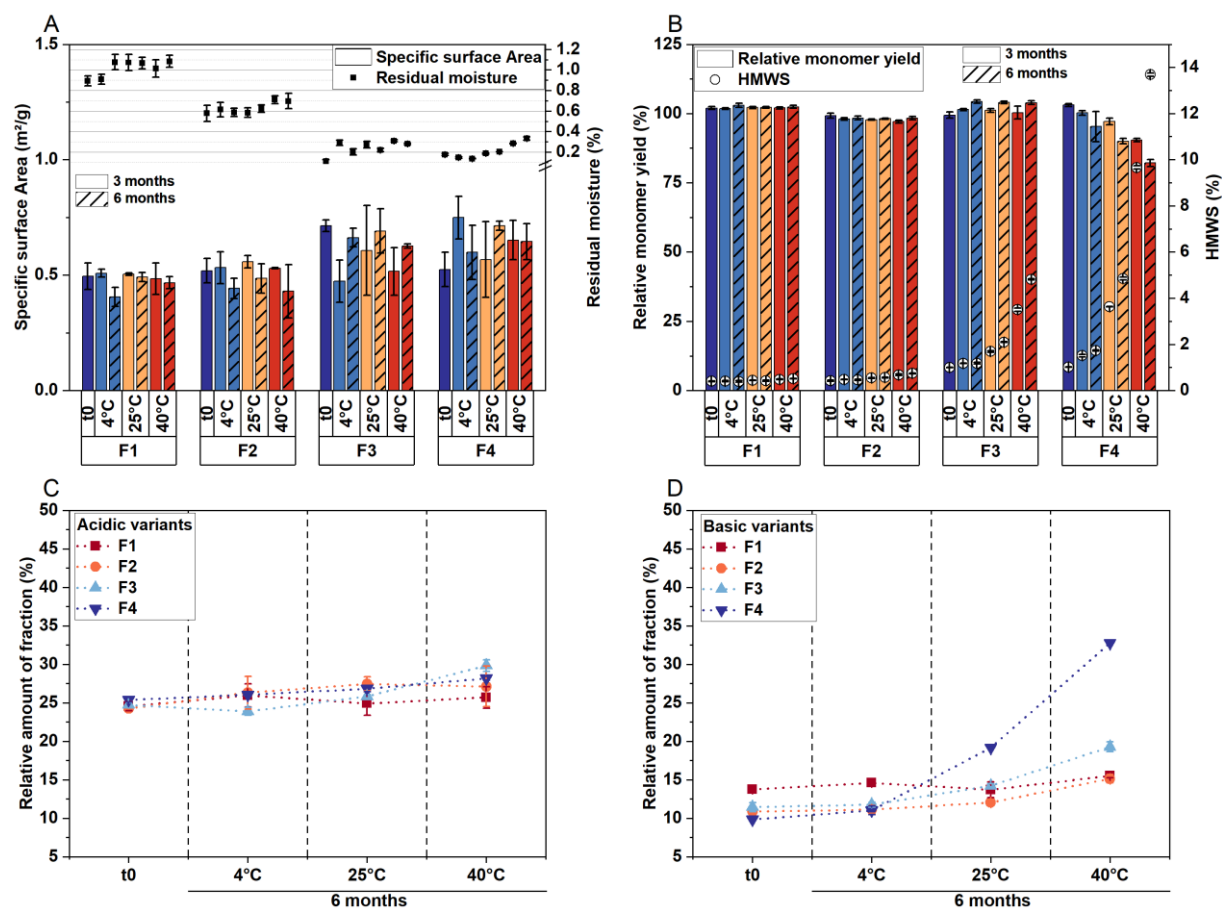
Figure V.1 The solid-state properties of the lyophilizates and storage stability of LMU1 when sugar was subsequently replaced with mAb. Samples were analyzed after MFD (t0) and storage at 4 °C, 25 °C, and 40 °C over 6 months. (**A**) Specific surface area (bars) and residual moisture (symbols). The relative monomer yields (bars) and percentages of soluble aggregates (HMWS, symbols) from SEC are shown in (**B**). (**C**) The relative number of acidic and (**D**) basic variants from IEX. All values are means ($n = 3$) ± standard deviation.

V.4.2 Comparison of Critical Quality Attributes of a Highly Concentrated mAb Formulation Following MFD and CFD

Based on the previous results, we aimed to directly compare the stability profiles of high-concentration mAb formulations following MFD and CFD. Consequently, we selected formulation F4, representing a worst-case scenario in terms of stabilizer concentration, and F5, which comprises a typically used sugar:protein ratio (350:1) sufficient for stabilizing monoclonal antibodies [24]. Furthermore, F5 comprises the same proportion of lyoprotectant to mAb as F3, but with twice the overall solute content. With microwave assistance, F5 was dried within 29.9 hours, while it took 59.6 hours with CFD. Moreover, it took 56.3 hours to lyophilize F4 without microwaves, compared to 30.3 hours using MFD. Samples were analyzed immediately after lyophilization (Process P1, Table V.2) and following storage at 4°C, 25°C, and 40°C over 6 months. The results are shown in Figure V.2.

The solid-state properties of the lyophilizates were very similar, irrespective of whether MFD or CFD was applied (Figure V.2A). However, given that the same drying protocol (Process P1, Table V.2) was used for both MFD and CFD, and the formulations consisted of high protein concentrations, the drying process was anticipated to be highly robust (i.e., with a high T_c). When comparing the relative number of acidic and basic variants, we observed no relevant differences between the two drying protocols (Figure V.2B). The monomer yields and aggregate formations exhibited the same trends during the stability study (Figure V.2C), with F4 demonstrating a lower capability in stabilizing the mAb compared to F5. However, this observation was independent of the application of microwave radiation.

Notably, subvisible particle analysis revealed increased particle formation following MFD compared to CFD across all size ranges (Figure V.2D, V.2E, and V.2F). Previous studies did not report this phenomenon, but most cases involved low concentrations [13–15,17] up to 50 mg/mL mAb [16]. To further investigate this observation, we sought to identify the root cause for the formation of subvisible particles following MFD.
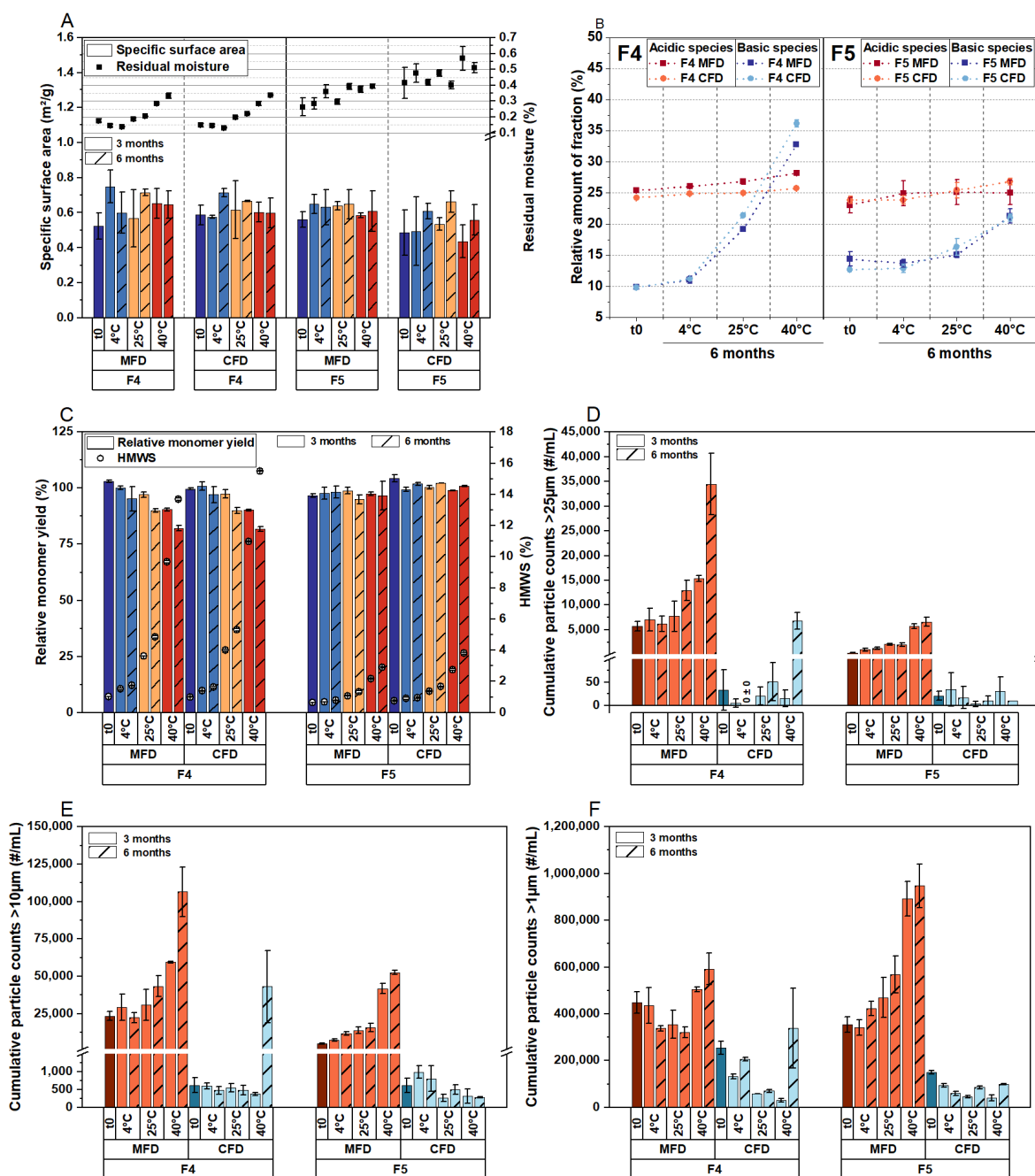
Figure V.2 The effect of the drying mechanism on critical quality attributes of highly concentrated LMU1 formulations. Following MFD and CFD (t0), the lyophilizates were stored at 4 °C, 25 °C, and 40 °C for 6 months. (A) The specific surface area (bars) and residual moisture (symbols) of the cakes. (B) The relative number of acidic and basic variants for F4 (left) and F5 (right) from IEX. (C) The relative monomer yield and the relative number of high-molecular-weight species (HMWS) was determined using SEC. Subvisible particles (SvP) detected with flow imaging microscopy: (D) > 25 µm, (E) > 10 µm, and (F) > 1 µm. All values are means ($n = 3$) ± standard deviation. SvP measurements were conducted in technical duplicates.

V.4.3 Effect of Thermal History and Investigation of Two Other Proteins in MFD

Considering these findings, we aimed to determine if the particle formation for LMU1 is a consequence of higher product temperatures during the MFD process compared to CFD.

To investigate this, we conducted a single-step CFD cycle (Process P2, Table 2) using formulation F5 to simulate the thermal history during the corresponding MFD process. The respective readouts are presented in Figure S2. The residual moisture was found to be comparable following both drying processes ($0.34\% \pm 0.02\%$ after CFD and $0.23\% \pm 0.06\%$ following MFD). Subvisible particle counts (given in #/mL cumulatively) were detected using flow imaging microscopy. We observed low subvisible particle counts after the aggressive CFD cycle with 10 ± 11, 110 ± 55, and 3444 ± 1017 for particles ≥ 25 µm, ≥ 10 µm, and ≥ 1 µm in size, respectively. After 7 months of storage at 40 °C, the subvisible particle counts were close to the initial amounts with 13 ± 13, 64 ± 35, and 4658 ± 428 for the respective sizes. Consequently, we concluded that high product temperatures during drying are not responsible for particle formation following MFD.

Next, we examined another mAb (Formulation F6, Table 1) to assess whether particle formation is specific to LMU1. To compare stability profiles, LMU2 was dried with and without microwaves using process P1. For F6, the molar sugar:protein ratio was approximately 360:1. Samples were analyzed immediately after lyophilization and after storage. Again, the residual moisture was found to be comparable following the drying processes ($0.18\% \pm 0.01\%$ after CFD and $0.20\% \pm 0.15\%$ following MFD). No differences were detected in the monomer yield and the formation of high-molecular-weight species in SEC (Figure 3A). However, as with LMU1, the subvisible particle counts revealed a significant increase in protein aggregation following MFD compared to CFD (Figure 3B).
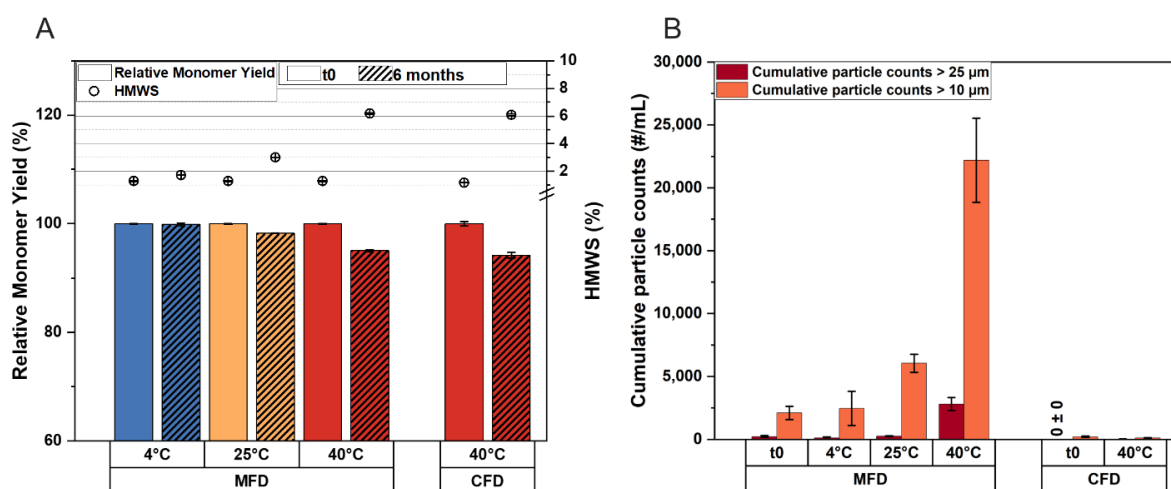

Figure V.3 Physical stability of LMU2 (formulation F6) following MFD and CFD. Samples were analyzed after lyophilization (t0) and storage at 4 °C, 25 °C, and 40 °C (MFD samples) and 40 °C (CFD samples). (A) The relative monomer yield and the relative number of high-molecular-weight species (HMWS). (B) Subvisible protein aggregates. All values are means ($n = 3$) ± standard deviation. Subvisible particle measurements were conducted in technical duplicates.

In a published study, we had investigated the stability of an IgG1 at low concentration in different formulations after MFD and storage. We had observed similar stability profiles following MFD and CFD [17]. These findings contrast with the results from this study on high-concentration antibody formulations, prompting us to examine the quality of another low-concentration protein, G-CSF (formulation F7) after MFD. Following the MFD process (Process P3, Table V.2), the monomer yield was $96.70\% \pm 0.70\%$. Protein aggregates detected with SEC ($0.27\% \pm 0.30\%$ high-molecular-weight species) and flow imaging microscopy (0 ± 0 >25 μm, 45 ± 33 >10 μm, and 1128 ± 498 >1 μm) were low. Based on these data, we consider that aggregation triggered by microwave radiation is directly related to protein concentration. Since microwaves directly interact with dipolar structures [21], we conclude that electromagnetic radiation excites not only the excipients but also the protein. As a result, the higher the protein concentration in the formulation, the greater the likelihood of inducing damage.

V.4.4 The Critical Timeframe that Leads to Protein Aggregation During MFD

To investigate the mechanism of particle formation in MFD processes, we used formulations F1 and F5 and the corresponding placebo. We temporarily activated the microwave modules during drying to determine: (A) whether the mAb is initially damaged when microwave radiation is started, or (B) if particle formation inversely correlates with residual water content. We concentrated on analyzing subvisible particles, as they proved to be a reliable degradation indicator in our previous experiments. First, using lyophilization cycle P3 (Table 2), microwaves were applied either in the first 5 h of the drying phase (Figure 4A) or toward the end of the drying process (Figure 4B). When microwave radiation was applied initially, subvisible particle counts were at the placebo level regardless of the mAb concentration (Figure 4C). However, we observed a significant increase in protein aggregates in F5 compared to F1 and the placebo formulation when microwaves were applied late in the drying process. The reason why the number of small subvisible particles, between 1μm and 10μm, increased in the placebo formulation as well, when microwaves were applied later in the process, merits further study.

Based on these findings, we conducted four additional runs and subsequently extended the microwave radiation time. The microwave modules were activated at the beginning of the drying process and ran continuously for 6 h, 8 h, 10 h, and 13 h (Figure S3A–D). To prevent sample overheating during MFD, cycles with 10 and 13 h microwave runtime were conducted using process P4 (Table 2), while runs with 6 and 8 h of microwave radiation

used process P3. This resulted in differences in product temperature across different runs (Figure 4D); however, the residual moisture and associated glass transition temperature of the cakes was similar for F5 (Figure S4). Due to the aggressive drying conditions, scanning electron microscopy revealed a microcollapsed morphology in F1 for all processes, while cellular pore structures were observed for F5 (Figure S5). Moreover, the point of termination of microwave radiation is clearly visible in all curves (Figure 4D).

Although product temperature during drying did not increase with longer microwave runtime due to the chosen settings (Figure 4D), aggregate formation clearly correlated with radiation time for F5 (Figure 4E). While the low-concentration formulation F1 equaled the placebo irrespective of runtime, we observed a gradual increase in subvisible particle counts in the high-concentration mAb formulation F5.

Since ice exhibits a low dielectric loss factor [21], microwaves most likely excite highly polarizable unfrozen water [28] and other excitable formulation components. We therefore hypothesize that protein preservation occurs as long as heat may be dissipated throughout the matrix; otherwise, damage takes place. As the dielectric properties of formulations change during drying [29], the very late stage of the drying process is considered particularly problematic concerning the physicochemical stability of active compounds [21]. However, our studies uncovered that high-concentration mAb formulations are susceptible to degradation much earlier; this occurs after just a few hours of drying when sublimation is still high.
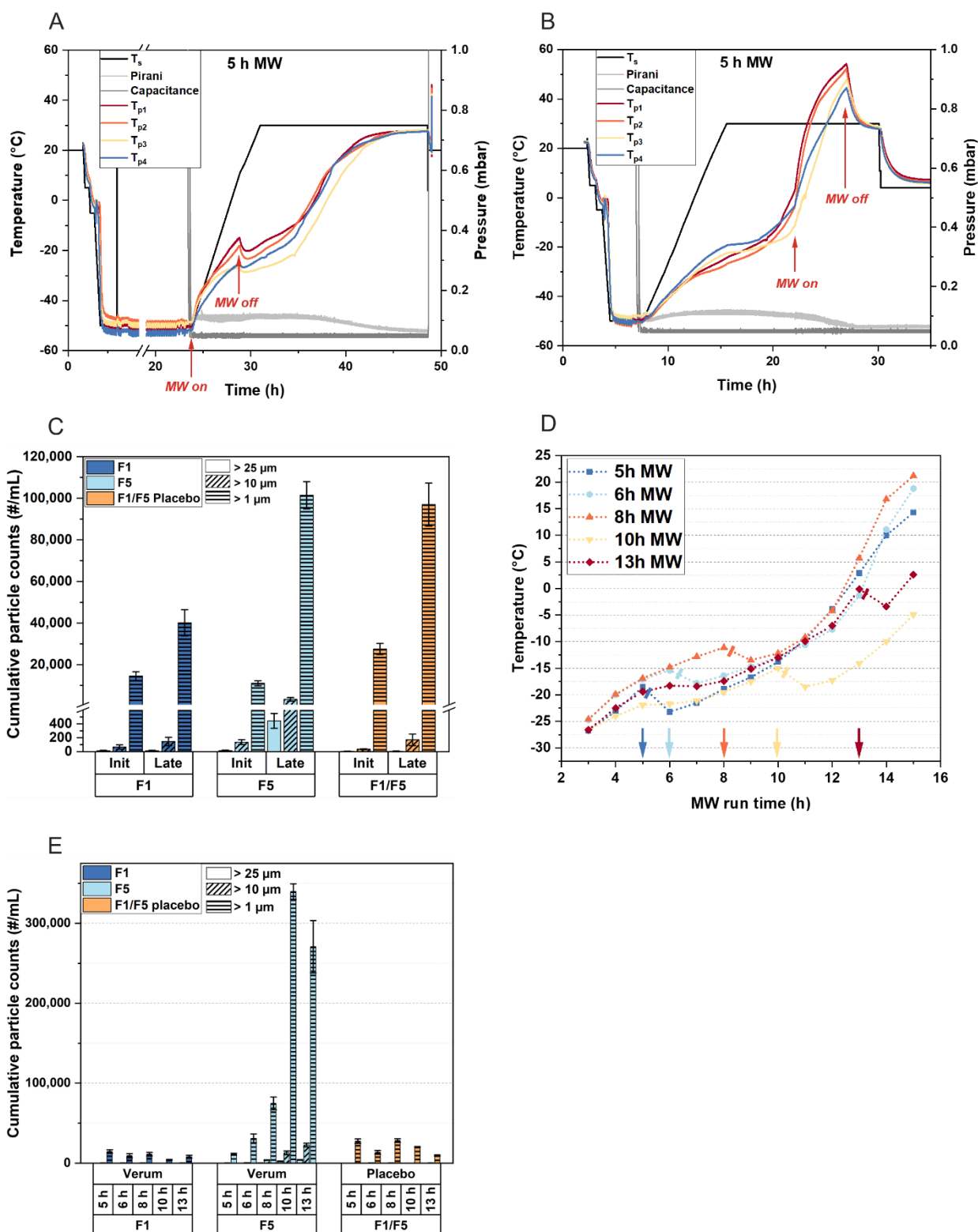
Figure V.4 The impact of the microwave run time on protein aggregation during MFD. (A) Graphical overview of the lyophilization process readouts for P3. Microwave radiation was started immediately after the desired vacuum for primary drying was established and ran for 5 hours. T_s denotes the shelf temperature; the chamber pressure is monitored via a Pirani gauge (Pirani) and capacitance gauge (Capacitance); T_p is the reading from the fiber-optic temperature sensors. (B) Process readouts for P3 when microwave radiation was applied for 5 hours toward the end of the process. (C) Comparison of subvisible particle formation in the F1, F5, and placebo formulations, as detected via flow imaging microscopy, when microwave radiation was applied during the initial 5 hours of drying (init) and for 5 hours later in the process (late), using process P3. (D) Product temperature profiles recorded for P3 and P4 with the different microwave module run times. The arrows

represent the switch off of microwave radiation. All temperature sensors shown in the process graphs (V.4A, V.4B, and V.4D) were placed in formulation F5. (E) Subvisible particle formation in the F1, F5, and placebo formulations when subjected to increasing microwave run times. The reported numbers of subvisible particles are means (n = 3 and technical duplicates per vial) ± standard deviation. MW, microwave irradiation.

V.4.5 Effect of Residual Moisture, Cooling, and the Source of Energy

The previous experiments raised the question of whether there is a potential tipping point during the MFD of highly concentrated protein formulations that leads to aggregation. To explore this, we conventionally lyophilized F5 (Process P2) and used the dried cakes to conduct experiments in a microwave oven.

Initially, we applied 360 W to the lyophilizates without cooling the vials during the experiment, using a polymeric vial for the insulation of the samples from the glass plate (Figure 5A). No relevant increase in subvisible particle counts was detected even after 180 min of irradiation. These results led us to conclude that the dried cake does not represent a worst-case scenario for aggregate formation during MFD, as the antibody is immobilized in a rigid matrix.

We then increased the residual moisture in the cakes to examine whether the moisture content and associated mobility comprise a dominant factor affecting aggregation. Different moisture levels were adapted according to the technique from [30], and we observed a significant increase in subvisible particle counts at an intermediate moisture level of 15% (m/m) (Figure 5B), which corresponds to the typical moisture content at the end of primary drying in a CFD process [31]. This confirmed our hypothesis that a certain degree of residual water and anti-plasticization is a prerequisite for aggregate formation.

Considering these findings, we adjusted the residual moisture to 15% (m/m) for all subsequent samples (except t0) and compared subvisible particle counts following different treatments (Figure 5C). Samples exposed to convective heat transfer at 80 °C in a drying cabinet showed low particle counts (light-blue bars). To mimic freeze-dryer shelf conditions, we placed a sample on a precooled stainless steel cylinder during microwave irradiation. Interestingly, cooling the sample protected the mAb from degradation, as no increase in protein aggregates was detected after 25 min in the microwave oven (red bars), contrasting with the uncooled sample that exhibited significant particle counts (hatched red bars). In another treatment, the sample was placed in the microwave oven for 5 min, followed by 20

min in the drying cabinet, resulting in slightly increased particle counts compared to convective heat application alone (orange bars).

To investigate differences in heating with microwaves versus other heat transfer methods, we exposed samples to microwaves, infrared radiation, and convective heat in a drying cabinet, aligning the temperature profiles for comparability (Figure 5D). We observed a significant increase in subvisible particle counts following microwave irradiation compared to other heating methods (Figure 5E), concluding that microwave radiation directly excites polar groups in the antibody structure, leading to protein aggregate formation.

It has been demonstrated that the intermediate, rubbery state during drying processes, characterized by considerable moisture content and low glass transition temperatures (T_g'), is the most detrimental phase for protein stability [32]. Increased concentrations of the protein in the viscous glassy matrix still allowing for notable mobility, as water is not sufficiently removed, make protein degradation more likely. This is consistent with our findings in MFD. We found that cooling the sample can provide some protection for the mAb (Figure 5C). However, this presents a deadlock in the drying process, as complete drying while maintaining cold temperatures is unattainable. Moreover, the need for cooling to preserve protein stability prevents the full exploitation of MFD technology. Our findings show that high product temperatures are only problematic for the stability of the mAb when microwave radiation is applied.

The preservation of a protein's native structure during lyophilization via adding an adequate ratio of lyoprotectant has been well documented [4,24]. With growing interest in high-concentration mAb formulations [33], e.g., for subcutaneous injections, high disaccharide concentrations are often required, and the reconstitution time is directly influenced by the sugar:protein ratio [34]. Our studies revealed the importance of sugar:protein ratios regarding stabilization in MFD technology. MFD is a competitive technology for low-concentration protein formulations; however, for high-concentration mAb formulations, water replacement via the classical approach [4,24] was insufficient. Additional research is required to determine whether an optimized sugar:protein ratio or other formulation compositions could provide enhanced protection for high-concentration protein formulations during microwave-assisted freeze-drying.
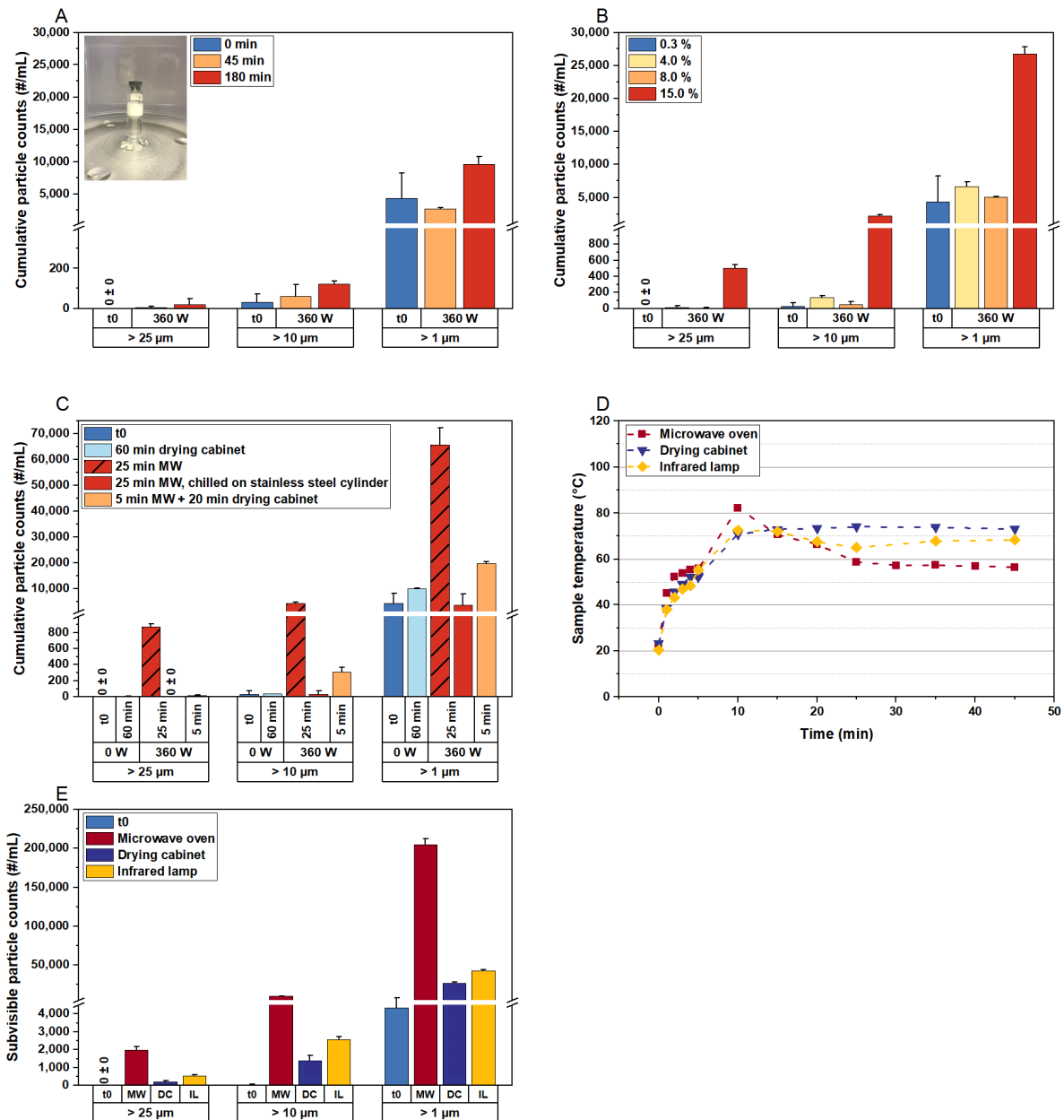
Figure V.5 The impact of microwave radiation on protein aggregate formation in lyophilized formulation F5. Initial subvisible particle counts (t0) were determined immediately after conventional freeze-drying. (A) Samples were exposed to 360 W for different durations, without chilling during exposure to microwave radiation. A polymeric vial was used as a spacer to insulate the samples from the rotating glass plate in the microwave oven. This setup was used for the following experiments, with the data shown in (B–E). (B) The formation of subvisible particles with increased residual moisture. The residual moisture content of 15% was adjusted in all processed samples shown in (C–E). (C) Comparison of convective heat transfer and microwave heating, with the drying cabinet temperature set to 80°C. To mimic freeze-drying conditions, the vial was placed on a precooled stainless steel cylinder inside the microwave oven (red bars, without pattern). (D, E) Lyophilizates were subjected to three different energy sources. (D) The temperature within the cakes and (E) the corresponding formation of protein aggregates. The subvisible particle data represent the mean values of technical duplicates per vial ± standard deviation. MW, microwave irradiation.

V.5 Conclusions

These studies are connected to previous work on a novel microwave-assisted freeze-drying setup [17] and provide a first design space for the use of this technology. While the applicability of MFD for low-concentration protein formulations is reaffirmed, we observed particle formation with high-concentration antibody formulations, which were not observed for conventional freeze-drying controls. We demonstrated that microwaves directly interact with the active pharmaceutical ingredient (API), and the higher the API concentration, the more protein could be excited by the microwaves. This interaction resulted in decreased physical stability in the investigated high-concentration antibody formulations, manifesting as the formation of subvisible protein aggregates. Additionally, we showed that particle formation does not occur immediately after starting MFD, but during the intermediate drying phase. However, since the collapse temperature significantly increases with higher protein concentrations, reduced drying times for high-concentration protein formulations can be also achieved using aggressive CFD conditions [26]. In this configuration, the potential benefit of MFD regarding reduced process times is anyway limited. Based on our findings, we believe that MFD technology is particularly beneficial for low-concentration formulations requiring substantial amounts of glass-forming excipients, which normally limit time savings in CFD. Here, one could, of course, envision the fast, mass production of, e.g., vaccines that typically contain a relatively low-to-very-low amount of protein or another antigen. Furthermore, modern RNA-based products and vaccines, as well as virus and virus-like particle (VLP) formulations, etc., also containing a rather-low-to-very-low total amount of active ingredient in the matrix and can potentially benefit from MFD.
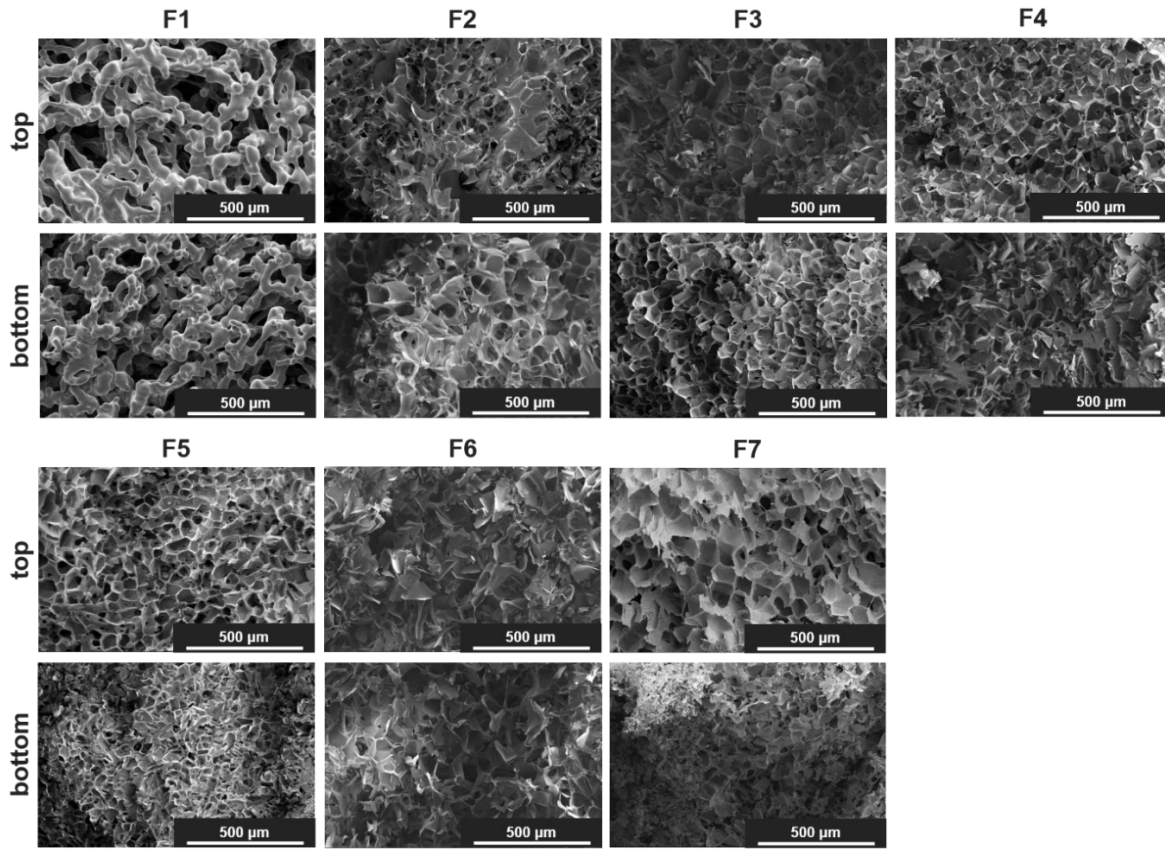
V.6 Supplementary materials

Figure V.S1 Representative SEM pictures of the top and bottom of the lyophilizates of F1–F7 after MFD, captured at 175-fold magnification.
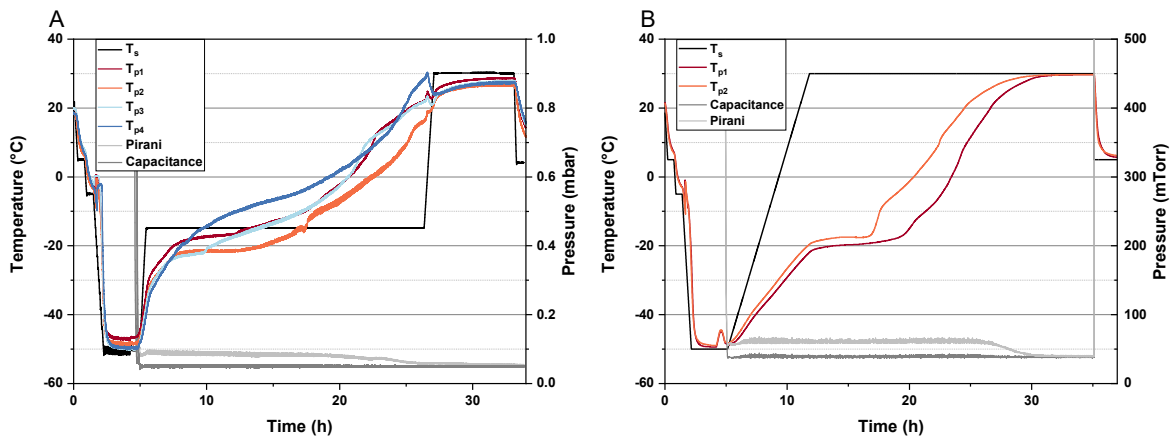

Figure V.S2 Readouts from drying processes of F5. T_s represents the shelf temperature; the chamber pressure is monitored via a Pirani gauge (Pirani) and capacitance gauge (Capacitance); T_p refers to the readouts of the temperature sensors. (A) Formulation F5 underwent MFD according to process P1. (B) To mimic the temperature profiles of (A), process P2 was applied to F5 (i.e., without microwave radiation).
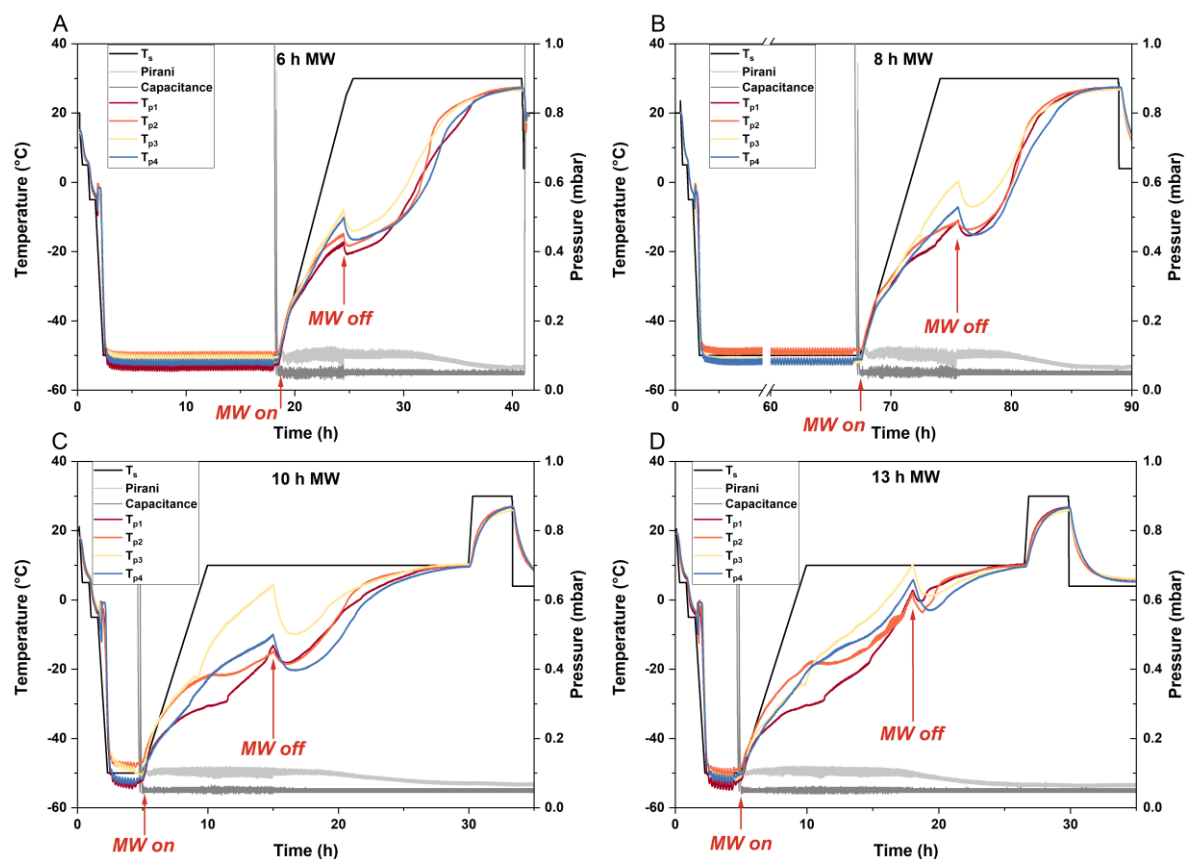
Figure V.S3 Readouts from the MFD processes with varying microwave run times. T_s represents the shelf temperature; the chamber pressure is monitored via a Pirani gauge (Pirani) and capacitance gauge (Capacitance); T_p refers to the readouts of the fiber optic temperature sensors. Microwave modules were manually started (MW on) and automatically terminated (MW off) after (A) 6 hours, (B) 8 hours, (C) 10 hours, and (D) 13 hours. MW, microwave irradiation.
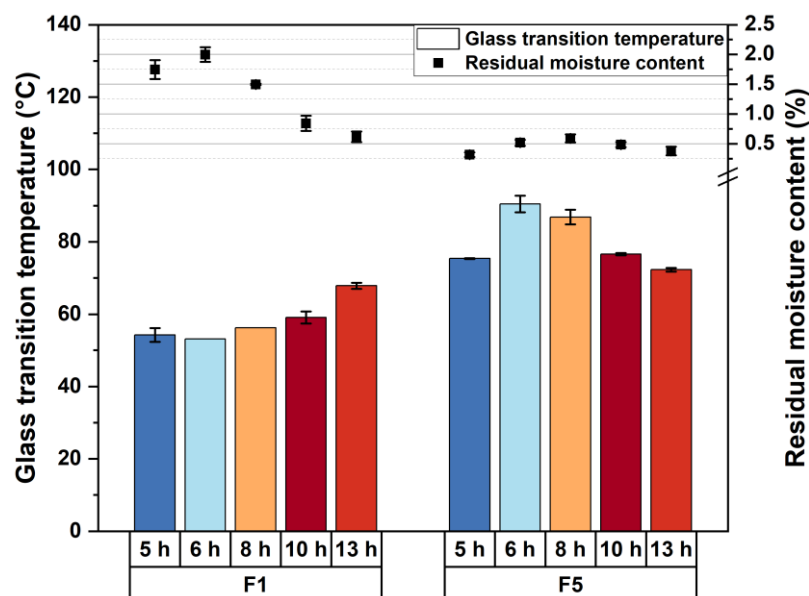

Figure V.S4 Solid-state properties of F1 and F5 lyophilizates after cycles with various microwave run times. Glass transition temperature (bars) and residual moisture (symbols) were measured immediately following lyophilization. The values represent the means (n = 3, except for T_g of F1 6h and 8h where n = 1) ± standard deviation.
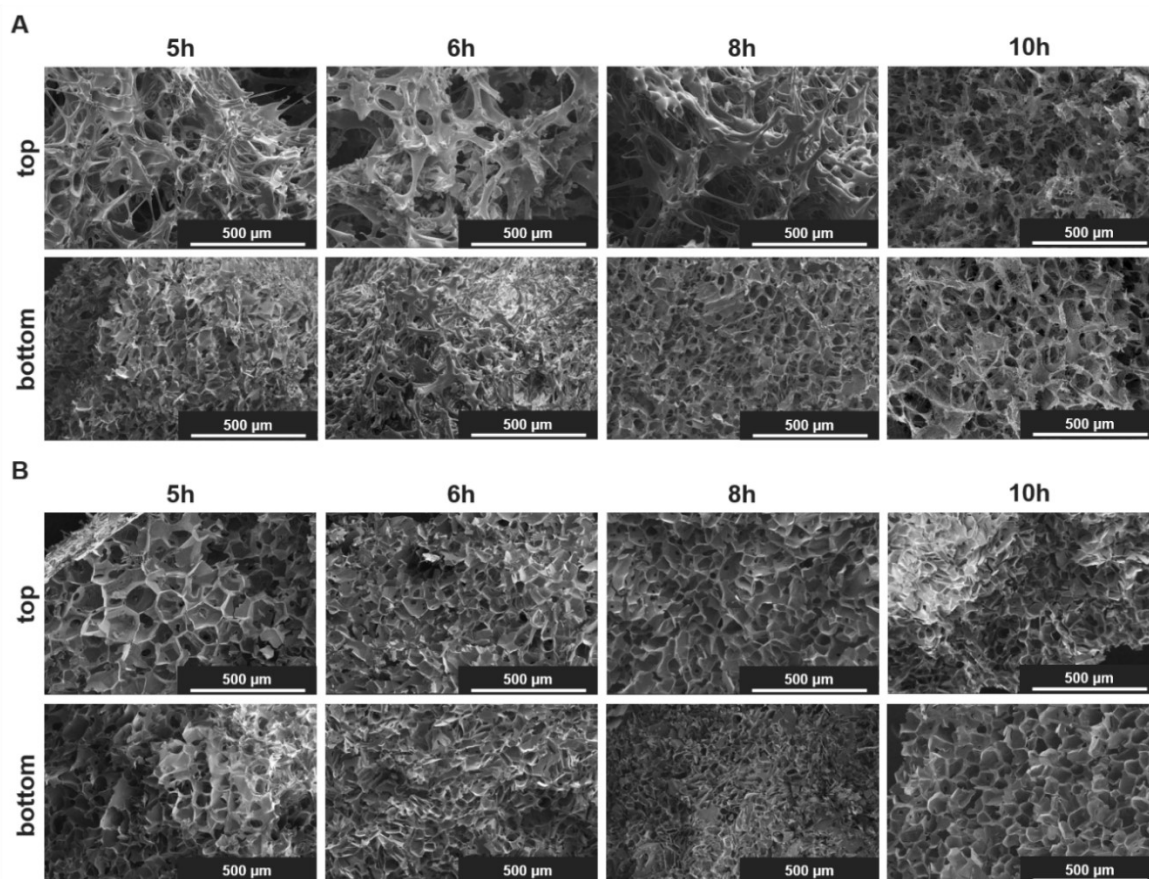
Figure V.S5 Representative SEM pictures of the top and bottom of the lyophilizates of (A) F1 and (B) F5 after different microwave runtimes. Images were captured at 175-fold magnification.

V.7 Acknowledgements

V.8 References

1. Ghosh, I.; Gutka, H.; Krause, M.E.; Clemens, R.; Kashi, R.S. A systematic review of commercial high concentration antibody drug products approved in the US: formulation composition, dosage form design and primary packaging considerations. *MAbs* **2023**, *15*, 2205540, https://doi.org/10.1080/19420862.2023.2205540.

2. Mieczkowski, C.A. The Evolution of Commercial Antibody Formulations. *J. Pharm. Sci.* **2023**. *112*, 1801–1810, https://doi.org/10.1016/j.xphs.2023.03.026.

3. Wang, W.; Singh, S.; Zeng, D.L.; King, K.; Nema, S. Antibody Structure, Instability, and Formulation.

J. Pharm. Sci. **2007**, *96*, 1–26, https://doi.org/10.1002/jps.20727.

4. Carpenter, J.F.; Pikal, M.J.; Chang, B.S.; Randolph, T.W. Rational Design of Stable Lyophilized Protein Formulations: Some Practical Advice. *Pharm. Res.* **1997**, *14*, 969–975, https://doi.org/10.1023/A:1012180707283.

5. Wang, W. Lyophilization and development of solid protein pharmaceuticals. *Int. J. Pharm.* **2000**, *203*, 1–60, https://doi.org/10.1016/S0378-5173(00)00423-3.

6. Patel, S.M.; Pikal, M.J. Lyophilization process design space. *J. Pharm. Sci.* **2013**, *102*, 3883–3887, https://doi.org/10.1002/jps.23703.

7. Kasper, J.C.; Winter, G.; Friess, W. Recent advances and further challenges in lyophilization. *Eur. J. Pharm. Biopharm.* **2013**, *85*, 162–169, https://doi.org/10.1016/j.ejpb.2013.05.019.

8. Haeuser, C.; Goldbach, P.; Huwyler, J.; Friess, W.; Allmendinger, A. Be Aggressive! Amorphous Excipients Enabling Single-Step Freeze-Drying of Monoclonal Antibody Formulations. *Pharmaceutics* **2019**, *11*, 616, https://doi.org/10.3390/pharmaceutics11110616.

9. Teagarden, D.L.; Baker, D.S. Practical aspects of lyophilization using non-aqueous co-solvent systems. *Eur. J. Pharm. Sci.* **2002**, *15*, 115–133, https://doi.org/10.1016/S0928-0987(01)00221-4.

10. De Meyer, L.; Van Bockstal, P.J.; Corver, J.; Vervaet, C.; Remon, J.P.; De Beer, T. Evaluation of spin freezing versus conventional freezing as part of a continuous pharmaceutical freeze-drying concept for unit doses. *Int. J. Pharm.* **2015**, *496*, 75–85, https://doi.org/10.1016/j.ijpharm.2015.05.025.

11. Capozzi, L.C.; Trout, B.L.; Pisano, R. From Batch to Continuous: Freeze-Drying of Suspended Vials for Pharmaceuticals in Unit-Doses. *Ind. Eng. Chem. Res.* **2019**, *58*, 1635–1649, https://doi.org/10.1021/acs.iecr.8b02886.

12. Ambros, S.; Bauer, S.A.W.; Shylkina, L.; Foerst, P.; Kulozik, U. Microwave-Vacuum Drying of Lactic Acid Bacteria: Influence of Process Parameters on Survival and Acidification Activity. *Food Bioprocess Technol.* **2016**, *9*, 1901–1911, https://doi.org/10.1007/s11947-016-1768-0.

13. Bhambhani, A.; Stanbro, J.; Roth, D.; Sullivan, E.; Jones, M.; Evans, R.; Blue, J. Evaluation of Microwave Vacuum Drying as an Alternative to Freeze-Drying of Biologics and Vaccines: the Power of Simple Modeling to Identify a Mechanism for Faster Drying Times Achieved with Microwave. *AAPS PharmSciTech* **2021**, *22*, 52, https://doi.org/10.1208/s12249-020-01912-9.

14. Abdelraheem, A.; Tukra, R.; Kazarin, P.; Sinanis, M.D.; Topp, E.M.; Alexeenko, A.; Peroulis, D. Statistical electromagnetics for industrial pharmaceutical lyophilization. *PNAS Nexus* **2022**, *1*, pgac052. https://doi.org/10.1093/pnasnexus/pgac052.

15. Gitter, J.H.; Geidobler, R.; Presser, I.; Winter, G. Significant Drying Time Reduction Using Microwave-Assisted Freeze-Drying for a Monoclonal Antibody. *J. Pharm. Sci.* **2018**, *107*, 2538–2543, https://doi.org/10.1016/j.xphs.2018.05.023.

16. Gitter, J.H.; Geidobler, R.; Presser, I.; Winter, G. Microwave-Assisted Freeze-Drying of Monoclonal Antibodies: Product Quality Aspects and Storage Stability. *Pharmaceutics* **2019**, *11*, 674, https://doi.org/10.3390/pharmaceutics11120674.

17. Härdter, N.; Geidobler, R.; Presser, I.; Winter, G. Accelerated Production of Biopharmaceuticals via Microwave-Assisted Freeze-Drying (MFD). *Pharmaceutics* **2023**, *15*, 1342, https://doi.org/10.3390/pharmaceutics15051342.

18. Thostenson, E.T.; Chou, T.W. Microwave processing: fundamentals and applications. *Compos. Part A Appl. Sci. Manuf.* **1999**, *30*, 1055–1071, https://doi.org/10.1016/S1359-835X(99)00020-2.

19. Metaxas, A.C. Microwave heating. *Power Eng. J.* **1991**, *5*, 237–247, https://doi.org/10.1049/pe:19910047.

20. Meredith, R.J. *Engineers' handbook of industrial microwave heating*; The Institution of Electrical Engineers: London, UK, 1998.

21. Durance, T.; Noorbakhsh, R.; Sandberg, G.; Sáenz-Garza, N. Microwave Drying of Pharmaceuticals. In *Drying technologies for biotechnologies and pharmaceutical applications*; Ohtake, S., Izutsu, K.-I., Lechuga-Ballesteros, D., Eds.; Wiley-VCH Verlag GmbH & Co. KGaA: Weinheim, Germany, 2020; pp. 239–255. ISBN 9783527341122.

22. Wang, S.S.; Yan, Y.; Ho, K. US FDA-approved therapeutic antibodies with high-concentration formulation: summaries and perspectives. *Antib. Ther.* **2021**, *4*, 262–272, https://doi.org/10.1093/abt/tbab027.

23. Shire, S.J.; Shahrokh, Z.; Liu, J. Challenges in the development of high protein concentration formulations. *J. Pharm. Sci.* **2004**, *93*, 1390–1402, https://doi.org/10.1002/jps.20079.

24. Cleland, J.L.; Lam, X.; Kendrick, B.; Yang, J.; Yang, T.H.; Overcashier, D.; Brooks, D.; Hsu, C.; Carpenter, J.F. A specific molar ratio of stabilizer to protein is required for storage stability of a lyophilized monoclonal antibody. *J. Pharm. Sci.* **2001**, *90*, 310–321, https://doi.org/10.1002/1520-6017(200103)90:3<310::AID-JPS6>3.0.CO;2-R.

25. Svilenov, H.; Winter, G. The ReFOLD assay for protein formulation studies and prediction of protein aggregation during long-term storage. *Eur. J. Pharm. Biopharm.* **2019**, *137*, 131–139, https://doi.org/10.1016/j.ejpb.2019.02.018.

26. Depaz, R.A.; Pansare, S.; Patel, S.M. Freeze-Drying above the Glass Transition Temperature in Amorphous Protein Formulations while Maintaining Product Quality and Improving Process Efficiency. *J. Pharm. Sci.* **2016**, *105*, 40–49, https://doi.org/10.1002/jps.24705.

27. Haeuser, C.; Goldbach, P.; Huwyler, J.; Friess, W.; Allmendinger, A. Excipients for Room Temperature Stable Freeze-Dried Monoclonal Antibody Formulations. *J. Pharm. Sci.* **2020**, *109*, 807–817, https://doi.org/10.1016/j.xphs.2019.10.016.

28. Park, J.; Cho, J.H.; Braatz, R.D. Mathematical modeling and analysis of microwave-assisted freeze-drying in biopharmaceutical applications. *Comput. Chem. Eng.* **2021**, *153*, 107412, https://doi.org/10.1016/j.compchemeng.2021.107412.

29. Kelen, Á.; Ress, S.; Nagy, T.; Pallai, E.; Pintye-Hódi, K. Mapping of temperature distribution in pharmaceutical microwave vacuum drying. *Powder Technol.* **2006**, *162*, 133–137, https://doi.org/10.1016/j.powtec.2005.12.001.

30. Lo Presti, K.; Frieß, W. Adjustment of specific residual moisture levels in completely freeze-dried protein formulations by controlled spiking of small water volumes. *Eur. J. Pharm. Biopharm.* **2021**, *169*, 292–296, https://doi.org/10.1016/j.ejpb.2021.10.011.

31. Patel, S.M.; Doen, T.; Pikal, M.J. Determination of End Point of Primary Drying in Freeze-Drying Process Control. *AAPS PharmSciTech* **2010**, *11*, 73–84, https://doi.org/10.1208/s12249-009-9362-7.

32. Willmann, M. Stabilisierung von pharmazeutischen Proteinlösungen durch Vakuumtrocknung; Verfahrenstechnische Optimierung verschiedener Vakuumtrocknungsverfahren, Untersuchung von Aggregations-Phänomenen und Evaluierung von Hilfsstoffen. Ph.D. Thesis, Ludwig-Maximilians-Universität München, München, Germany, 2003.

33. Jiskoot, W.; Hawe, A.; Menzen, T.; Volkin, D.B.; Crommelin, D.J.A. Ongoing Challenges to Develop High Concentration Monoclonal Antibody-based Formulations for Subcutaneous Administration: Quo Vadis? *J. Pharm. Sci.* **2022**, *111*, 681–867, https://doi.org/10.1016/j.xphs.2021.11.008.

34. Kulkarni, S.S.; Patel, S.M.; Bogner, R.H. Reconstitution Time for Highly Concentrated Lyophilized Proteins: Role of Formulation and Protein. *J. Pharm. Sci.* **2020**, *109*, 2975–2985, https://doi.org/10.1016/j.xphs.2020.05.029.

35. Khawli, L.A.; Goswami, S.; Hutchinson, R.; Kwong, Z.W.; Yang, J.; Wang, X.; Yao, Z.; Sreedhara, A.; Cano, T.; Tesar, D.; et al. Charge variants in IgG1: Isolation, characterization, in vitro binding properties and pharmacokinetics in rats. *MAbs* **2010**, *2*, 613–624, doi:10.4161/mabs.2.6.13333.

Chapter VI   Summary of the thesis

The thesis focused on two main topics in the field of lyophilization. The first objective was to develop a secondary packaging configuration for lyophilizates in polymer vials, designed to overcome permeability issues associated with the material and to protect protein pharmaceuticals. The second objective was to investigate a new microwave-assisted freeze-drying (MFD) setup and gain insights into the drying behavior and effects of formulation parameters.

Chapter I provides a brief overview of the topics assessed, highlighting the motivation behind the thesis. Typical degradation pathways, particularly oxidation, and the opportunities and challenges associated with different packaging materials are discussed. Moreover, emerging technologies advancing the lyophilization process are shortly presented and MFD is introduced.

In *Chapter II*, a secondary packaging approach for lyophilizates in vials made of cyclic olefin polymer (COP) was investigated. Each vial was heat-sealed in an aluminum pouch together with a combined oxygen and moisture absorber. This configuration was compared to polymer vials without secondary packaging (serving as a positive control) and glass vials, which are the current gold standard for primary packaging of lyophilizates. The stability of two monoclonal IgG1 type antibodies was assessed over 12 months. The amount of fully oxidized mAb for the lyophilizates stored in the COP vials within the secondary packaging was comparable to that in the glass vials. This was attributed to the presence of the absorber, which played a crucial role in maintaining low levels of oxygen in the headspace and ensuring stable moisture levels within the lyophilized cakes.

Based on the previous results, in *Chapter III*, further studies on the permeability of polymer vials were conducted. Limited literature is available on that topic, bridging the intersection between packaging material manufacturers and pharmaceutical development. Various configurations were investigated aiming to assess the effect of pressure in the vial, the capability of the absorbers, and diffusion behavior. The findings revealed that the typically applied reduced pressure within the vial, intended to ensure proper stopper location and container closure integrity (CCI), leads to slower nitrogen permeation from inside to outside the vial and less oxygen ingress compared to atmospheric headspace pressure. This is beneficial for maintaining drug product quality during storage in COP. Moreover, the absorbers' capability in actively removing oxygen from the vial headspaces was demonstrated. Additionally, the solid absorber sachets were found to be as effective as liquid scavengers.

Chapter IV introduces the first part of the studies on microwave-assisted freeze-drying using a new machinery setup. Unlike previously described machines, the investigated setup is based on a rectangular, standard lyophilizer that may be used for GMP processes, and the microwave modules can be retrofitted and added to the process on demand. The impact of several excipients commonly used as cryo- and lyoprotectants at different concentrations on drying behavior and monoclonal antibody (mAb) stability was tested, including sugars and amino acids. A key finding was the unique drying mechanism in MFD, as separated primary and secondary drying do not exist. By this, aggressive drying of formulations that are typically deemed difficult to dry can be lyophilized fast and without impairing cake appearance. The chapter concludes with a stability study that reveals comparable mAb stability of a low-concentration mAb formulation (10 g/L) following MFD and CFD.

Chapter V describes the second part of the studies on MFD and the effect of microwave radiation on high-concentration protein formulations. Data on such formulations were lacking, and the effect of protein concentration in the MFD process and concurrent information on protein stability needed clarification. To study this, sugar was subsequently replaced by a mAb and protein stability was assessed. While the drying time differed only slightly, inferior stability was found with less stabilizing sugar following MFD, resulting in further studies on high-concentration protein formulations (i.e., 100 g/L and 70 g/L mAb and 80 g/L and 20 g/L sucrose, respectively). Protein stability was found to be inferior following MFD compared to conventional freeze-drying (CFD), manifesting in the formation of subvisible particles. Moreover, the intermediate, rubber phase of drying was identified as the phase where damage to the mAb occurs (i.e., aggregation), while cooling provided some protection. However, the suitability of MFD for low-concentration formulations was reaffirmed.

In conclusion, this thesis provides guidance for appropriate secondary packaging for lyophilizates in COP vials, leveraging the use of polymer vials in freeze-drying by overcoming the material's drawbacks. Moreover, studies on the permeability of the COP vials and capability of the oxygen absorbers were presented. It is important to note that if different pouch/blister volumes, or absorbers are used, slight adjustments might be necessary to ensure complete removal of oxygen from the surrounding air in the pouch. However, if the capability is chosen appropriately, the presented approach can be universally applied to prevent protein oxidation in polymer vials, utilizing the permeability of the material.

Furthermore, a new, advanced setup for MFD was presented and understanding of the underlying drying mechanism was broadened. Additionally, a first design space for the use

of the technology was provided, which can support scientists in future application of MFD in the pharmaceutical field. While MFD appears particularly beneficial for low-concentration formulations (i.e., proteins, vaccines, virus-like-particle formulations, etc.), requiring substantial amounts of excipients for water replacement, high protein API concentrations limit the application of the technology, as protein stability is impeded.

Lastly, several aspects need to be evaluated further regarding the application of MFD in a GMP environment. From a technical point of few, the resistance of the microwave modules to clean in place (CIP) and sterilize in place (SIP) procedures needs to be proven. Moreover, the homogeneity of the microwave field, scalability, and the associated impact of running microwave modules simultaneously on various shelves in a freeze-dryer needs to be studied. If applicable, computational simulations may assist in investigating and visualizing the electromagnetic field and drying behavior.

Appendix 1: Publications associated with this thesis

Härdter, N.; Menzen, T.; Winter, G. Minimizing Oxidation of Freeze-Dried Monoclonal Antibodies in Polymeric Vials Using a Smart Packaging Approach. *Pharmaceutics* **2021**, *13*, 1695. https://doi.org/10.3390/pharmaceutics13101695

Härdter, N.; Geidobler, R.; Presser, I.; Winter, G. Accelerated Production of Biopharmaceuticals via Microwave-Assisted Freeze-Drying (MFD). *Pharmaceutics* **2023**, *15*, 1342. https://doi.org/10.3390/pharmaceutics15051342

Härdter, N.; Geidobler, R.; Presser, I.; Winter, G. Microwave-Assisted Freeze-Drying: Impact of Microwave Radiation on the Quality of High-Concentration Antibody Formulations. *Pharmaceutics* **2023**, *15*, x. https://doi.org/10.3390/xxxxx

Appendix 2: Presentations associated with this thesis

Oral presentations:

Härdter, N.; Geidobler, R.; Presser, I.; Winter, G. Microwave-assisted freeze-drying of biologicals, GMP–PHARMA CONGRESS, 24th Conference and Expo, Pharma Manufacturing & Technology, May 31 – June 1, 2022, Düsseldorf/Neuss

Härdter, N.; Menzen, T.; Winter, G. Preventing oxidation of a lyophilized monoclonal antibody by smart polymer packaging, 2021 PDA Pharmaceutical Lyophilization Conference, September 14 – 15, 2021, Online Conference

Härdter, N.; Menzen, T.; Winter, G. Creating Highest Quality Lyophilisates With Low Oxygen and Water Content by Smart Polymer Packaging, 12th World Meeting on Pharmaceutics, Biopharmaceutics and Pharmaceutical Technology, May 11 – 14, 2021, Online Conference

Poster presentations:

Härdter, N.; Geidobler, R.; Presser, I.; Winter, G. Systematic evaluation of microwave-assisted freeze-drying of antibody formulations, 13th World Meeting on Pharmaceutics, Biopharmaceutics and Pharmaceutical Technology, March 28 – 31, 2022, Rotterdam